



CAFFEINE BIOSYNTHESIS AND PURINE METABOLISM IN LEAVES OF MASCAROCOFFEA SPECIES

Wei-Wei Deng,^[a] Jean-Jacques Rakotomalala,^[b] Chifumi Nagai,^[c] and Hiroshi Ashihara ^{[d]*}

Keywords: *Coffea canephora*, *Coffea millotii*, *Coffea perrieri*, *Mascarocoffea*, caffeine, trigonelline, adenine, purine salvage, biosynthesis, metabolism

Caffeine, a purine alkaloid, was not detected in leaves of two *Mascarocoffea* species, *Coffea millotii* and *Coffea perrieri*. Trigonelline, a pyridine alkaloid, occurred in these species, but the levels (3–4 $\mu\text{mol g}^{-1}$ fresh weight) were much lower than that of Robusta coffee (*Coffea canephora*) (36 $\mu\text{mol g}^{-1}$ fresh weight). Feeding experiments with [8-¹⁴C]adenine indicated that purine alkaloid biosynthesis was terminated at 7-methylxanthine formation and as a consequence theobromine and caffeine were not produced in *Coffea millotii* and *Coffea perrieri*. The adenine salvage activity was lower, but its degradation activity was higher in leaves of these *Mascarocoffea* species than those in *Coffea canephora*. The metabolic fate of the purine nucleosides, [8-¹⁴C]inosine, [8-¹⁴C]guanosine and [8-¹⁴C]xanthosine was investigated in leaves of *Coffea millotii*. The biosynthesis of 7-methylxanthine, but not theobromine or caffeine, from these precursors was detected. Large amounts of these purine nucleosides were catabolized via allantoin. Limited amounts of [8-¹⁴C]inosine and [8-¹⁴C]guanosine were salvaged and utilized for RNA synthesis, however, no [8-¹⁴C]xanthosine salvage was observed. Little or no ¹⁴C-metabolites were observed when [8-¹⁴C]theobromine and [8-¹⁴C]caffeine were applied to leaf disks of *Coffea millotii*. From the results obtained in this study, possible metabolic pathways of purines in *Mascarocoffea* species are discussed.

*Corresponding Authors

Fax: +81-3-5700-4225

E-Mail: ashihara.hiroshi@ocha.ac.jp

- [a] School of Tea and Food Science and Technology, Anhui Agricultural University, Hefei 230036, Anhui, China
 [b] Centre National de la Recherche Appliquée au développement Rural (FOFIFA), Ambatobe, Antananarivo, Madagascar
 [c] Hawaii Agriculture Research Center, Kunia, HI, 96759, USA
 [d] Department of Biology, Faculty of Science, Ochanomizu University, Tokyo, 112-8610, Japan

In the present studies, we used two *Mascarocoffea* species, *C. millotii* (Fig. 1) and *C. perrieri* and the level of caffeine and trigonelline and the activity of caffeine biosynthesis are compared with those in caffeine-accumulating *C. canephora*. As expected, caffeine was found only in *C. canephora*. In contrast, trigonelline occurred in all three *Coffea* samples examined. Since purine and purine alkaloid metabolism have not yet been investigated in *Mascarocoffea* species, we examined by the feeding experiments with ¹⁴C-labelled adenine, inosine, guanosine, xanthosine, theobromine and caffeine. Possible pathways of purine metabolism in *Mascarocoffea* species is discussed.

Introduction

Coffee plants accumulate two types of alkaloids, caffeine and trigonelline which are derived from purine and pyridine nucleotides, respectively.¹⁻⁴ Caffeine-free species in the genus *Coffea* have been screened by several investigators and reviewed by Hamon et al.⁵ Most wild coffee species belonging to the *Mascarocoffea* section grown in Madagascar and neighboring islands are caffeine free, although the occurrence of theobromine and caffeine has been reported in a few *Mascarocoffea* species.⁵⁻⁸

In Arabica coffee (*Coffea arabica*) and Robusta coffee (*C. canephora*) plants which are used for coffee beverages, rapid biosynthesis of caffeine have been demonstrated in young leaf and fruit tissues, but the degradation of caffeine is very slow, as a result, caffeine is accumulated in mature leaves and seeds.⁹ The activity of biosynthesis and degradation of caffeine in leaves of low-caffeine-containing *Coffea* species, *C. salvatrix*, *C. eugenioides*, and *C. bengalensis* has been investigated by Ashihara and Crozier.¹⁰ The biosynthesis of caffeine is less pronounced in leaves of these *Coffea* species than in *C. arabica*. Degradation of caffeine was slow in both of high- and low caffeine coffee species, except in *C. eugenioides* which rapidly catabolises caffeine.^{10, 11}



Figure 1. A tree (A) and fruits (B) of *Coffea millotii*.

Materials and methods

Plant materials

Leaves of *Coffea millotii* (A950), *C. perrieri* (A305) and *C. canephora* (K28) used in this study were obtained at the FOFIFA Experimental Stations, Kianjavato, Madagascar.

Determination of purine alkaloids and trigonelline

Endogenous levels of purine alkaloids and trigonelline were determined according to Zheng and Ashihara¹². Samples were ground with 80% methanol in a mortar and pestle. After incubation at 60°C for 30 min, the homogenates were centrifuged and the supernatant was collected. After complete evaporation of the methanol, the extracts were dissolved in distilled water. The aliquots (10–50 µL) of water-soluble fraction were used for determination by HPLC after centrifugation.

HPLC was carried out with a Shimadzu CLASS-VP HPLC system, Type LC 10A (Shimadzu Corporation, Kyoto, Japan) on a ferrule-less column (250 mm x 4.6 mm i.d.) packed with a 5 µm ODS Hypersil support (Thermo Electron Corporation, Waltham, MA, USA), eluting a flow rate of 1 mL min⁻¹ with a 35 min, 0–70 % gradient of methanol in 50 mM sodium acetate, pH 5.0 (0–10 min: 0 % methanol; 10–20 min: 0–10 % linear gradient; 20–35 min: 10–70 % linear gradient). The absorbance at 190–370 nm was monitored using a Shimadzu Diode Array Detector, type SPD-M10A. The purine alkaloid and trigonelline contents were estimated from the absorption of 270 nm of standards obtained from Sigma-Aldrich Co., St. Louis, MO, USA.

¹⁴C-Feeding experiments

All radiochemicals used were obtained from Moravек Biochemicals Inc, Brea, CA, USA. The labeled compounds were administered essentially as described in previous reports.^{11, 13, 14} In brief, leaves were sterilized with 1 % sodium hypochlorite solution and then washed with sterilized distilled water, and leaf disks (~4 mm x 4 mm) were prepared aseptically. Samples (~100 mg f.w.), and 2.0 mL of 30 mM potassium phosphate buffer (pH 5.6) containing 10 mM sucrose and 1 % sodium ascorbate, were placed in the main compartment of a 30 mL Erlenmeyer flask fitted with a glass tube containing a piece of filter paper impregnated with 0.1 mL of 20 % KOH in the centre well. Each reaction was started by addition of ¹⁴C-labelled purine compounds.

The flasks were incubated in an oscillating water bath at 27°C. After incubation, the glass tube was removed from the center well and placed in a 50 mL Erlenmeyer flask containing 10 mL of distilled water. At the same time, the leaf disks were separated from the incubation medium by filtering through a tea strainer. The samples were washed with distilled water and then frozen with liquid N₂ and stored at -80° C. The KH¹⁴CO₃ that had been absorbed by the filter paper was allowed to diffuse overnight into the distilled water, and 0.5 mL aliquots of the resulting solution were used for the determination of radioactivity incorporated into CO₂.

Metabolites from ¹⁴C-labelled purine bases and nucleosides were extracted successively with 4 mL of cold 6 % perchloric acid solution. Lipids in the insoluble materials were removed with a mixture of ethanol and diethyl ether (1:1, v/v) at 50°C for 15 min. The precipitate was washed with the same mixture, then with distilled water. RNA in the insoluble fraction was hydrolysed with 0.3 M KOH at 37°C for 18 h, and RNA hydrolysates was obtained.¹⁴

The perchloric acid-soluble metabolites and the RNA hydrolysates were neutralized with KOH and radioactive metabolites were separated by TLC using cellulose plates and the solvent systems shown in a previous paper.¹⁴ Radioactivity of liquid samples and on the TLC plates was determined using a multipurpose scintillation counter (Beckman, LS 6500) and a bio-imaging analyzer (Type FLA-2000, Fuji Photo Film Co. Ltd.), respectively.

Results and discussion

Endogenous levels of caffeine and trigonelline

Table 1 shows the leaf sizes and fresh weights of two species of *Mascarocoffea* and *Coffea canephora*. We used well-developed young leaves in this study. Accumulation of caffeine was found only in *C. canephora* while caffeine could not be detected in *C. millotii* and *C. perrieri*. In contrast, trigonelline was found in the leaves of all samples. The level of trigonelline in *C. perrieri* and *C. millotii* leaves were respectively 8- and 12-fold lower than the level in *C. canephora* leaves.

Comparison of purine alkaloid biosynthesis

Among exogenously administered purine precursors, it has been known that adenine is the most effective precursor for the biosynthesis of caffeine.¹⁵ Therefore, we first examined the metabolic fate of [8-¹⁴C]adenine in two *Mascarocoffea* species, *C. millotii* and *C. perrieri* and compared with the metabolism in *C. canephora*. As shown in Table 2, a limited amount of radioactivity from [8-¹⁴C]adenine accumulated as methylxanthines (purine alkaloids). Although radioactivity was found in 7-methylxanthine in all three species, incorporation into theobromine and caffeine was found only in *C. canephora*. In *C. canephora*, more radioactivity was found in 7-methylxanthine and theobromine than in caffeine. This is probably due to the fact that the precursors could not be transformed into caffeine during the incubation period, although caffeine is the end-product.

In *C. arabica* and *C. canephora*, three *N*-methyltransferases for caffeine biosynthesis occur. The first enzyme, 7-methylxanthosine synthase (EC 2.1.1.158) catalyzes the conversion of xanthosine to 7-methylxanthosine (step 11 in Fig. 2).¹⁶ The product, 7-methylxanthosine is hydrolysed to 7-methylxanthine (step 12) by *N*-methylnucleosidase (EC 3.2.2.25).¹⁷ Thus, all three species possess the machinery up to 7-methylxanthine.

Table 1. Leaf sizes (length and width) and purine alkaloid contents in three different *Coffea* species used in this research. nd, not detected.

Species	FOFIFA accession number	Leaf size (l x w, mm)	Leaf weight (f.w., g)	Caffeine ($\mu\text{mol g f.w.}^{-1}$)	Trigonelline ($\mu\text{mol g f.w.}^{-1}$)
<i>C. millotii</i>	A950	105 x 57	1.05 \pm 0.07	nd	2.89 \pm 0.03
<i>C. perrieri</i>	A305	127 x 33	0.68 \pm 0.01	nd	4.37 \pm 0.29
<i>C. canephora</i>	K28	229 x 98	2.52 \pm 0.06	25.3 \pm 0.79	36.0 \pm 2.1

Table 2. Comparison of adenine metabolism in leaf segments of *Coffea millotii*, *C. perrieri*, and *C. canephora*.

Metabolites	<i>C. millotii</i>	<i>C. perrieri</i>	<i>C. canephora</i>
Nucleotides	23.8 \pm 2.1	34.7 \pm 0.73	12.1 \pm 3.8
RNA	14.6 \pm 0.27	16.5 \pm 1.6	61.0 \pm 6.4
Nucleosides and bases			
Adenine	1.52 \pm 0.09	6.27 \pm 1.28	8.46 \pm 0.90
Hypoxanthine	2.53 \pm 0.24	nd	nd
Xanthosine	7.09 \pm 0.93	7.95 \pm 0.70	3.35 \pm 1.99
Xanthine	12.4 \pm 0.20	5.68 \pm 1.30	2.73 \pm 1.68
Purine alkaloids			
7-Methyl-xanthine	1.13 \pm 0.61	4.18 \pm 0.43	2.45 \pm 0.22
Theobromine	nd	nd	2.49 \pm 1.53
Theophylline	nd	nd	0.26 \pm 0.01
Caffeine	nd	nd	0.31 \pm 0.03
Degradation products			
Ureides (allantoin and allantoic acid)	21.1 \pm 0.67	20.8 \pm 1.0	4.14 \pm 2.11
Carbon dioxide	15.9 \pm 0.94	4.02 \pm 0.93	2.72 \pm 2.03
Total uptake	39.4 \pm 1.7	20.8 \pm 0.58	8.95 \pm 4.05

[8-¹⁴C]Adenine (10 μM , specific activity 1.9 GBq mol⁻¹) was administered for 18 h. The mean incorporation of radioactivity into individual metabolites is expressed as the percentage of total radioactivity taken up by the segments \pm SD. Total uptake is expressed as kBq 100 mg f.w.⁻¹, nd, not detected

However, it seems likely that *Mascarocoffea* species lack the enzyme(s) which catalyze the conversion of 7-methylxanthine to caffeine (steps 13 and 14). In *C. arabica* and *C. canephora*, plural *N*-methyltransferases, namely dual functional caffeine synthase (EC 2.1.1.160) and theobromine synthase (EC 2.1.1.159) catalyze this step^{18, 19}. In *C. canephora*, in addition to theobromine, very small amounts (<0.3 %) of radioactivity were detected in theophylline (Table 2). It might be produced by a minor pathway of purine alkaloid biosynthesis as has been observed in tea leaves.¹⁴

Comparison of adenine salvage and degradation

In addition to purine alkaloids, the radioactivity from [8-¹⁴C]adenine was distributed in various metabolites (Table 2). Since only small amounts of [8-¹⁴C]adenine (2–8 % of total radioactivity) were detected in the leaf disks, exogenously supplied [8-¹⁴C]adenine was not retained as adenine, but rapidly metabolized to other compounds. Substantial amounts of radioactivity from [8-¹⁴C]adenine was incorporated into the salvage products, namely, nucleotides and RNA. However, compared with *C. canephora* (73 % of total radioactivity), the rate of adenine salvage (38–51 %) was low in *Mascarocoffea* species.

As shown in other plants, adenine was converted to AMP by adenine phosphoribosyltransferase (EC 2.4.2.7, step 1 in Fig. 2) and then entered the adenine nucleotide pool comprising AMP, ADP and ATP. Some ATP was utilized for RNA synthesis.¹⁰ In addition to the methylxanthines shown above, radioactivity was also found in xanthosine, hypoxanthine and xanthine. In *C. millotii* and *C. perrieri*, significant amounts of radioactivity (25–37 %) were incorporated in the purine degradation products, ureides (allantoin and allantoic acid) and CO₂.

Unlike in bacteria and animals, no adenosine deaminase or adenine deaminase is present in plants,^{20, 21} deamination of adenine molecules is performed by AMP deaminase (step 5).^{22, 23} The product, IMP, is converted to inosine and hypoxanthine (steps 8 and 9). Hypoxanthine is oxidized yielding xanthine (step 15) and then catabolised by the purine degradation pathway (steps 17–22). Compared to *Mascarocoffea* species, the catabolic activity of [8-¹⁴C]adenine is much lower (7 % of total radioactivity) in *C. canephora*.

Purine nucleoside metabolism in *C. millotii*

Metabolic fate of [8-¹⁴C]inosine, [8-¹⁴C]guanosine and [8-¹⁴C]xanthosine applied to the leaf disks of *C. millotii* is presented in Table 3. As the same as [8-¹⁴C]adenine, radioactivity from these precursors was incorporated into 7-methylxanthine, but not into theobromine and caffeine. The radioactivity from [8-¹⁴C]inosine and [8-¹⁴C]guanosine (16 % and 23 % of total radioactivity, respectively) was incorporated into free nucleotides and RNA, but [8-¹⁴C]xanthosine was not salvaged. Inosine and guanosine appear to be converted to IMP and GMP by inosine-guanosine kinase (EC 2.7.1.73) and/or nucleoside phosphotransferase (EC 2.7.1.77) and converted to GTP (steps 25 and 6–7 or step 24) and then incorporated into RNA (step 2–4).

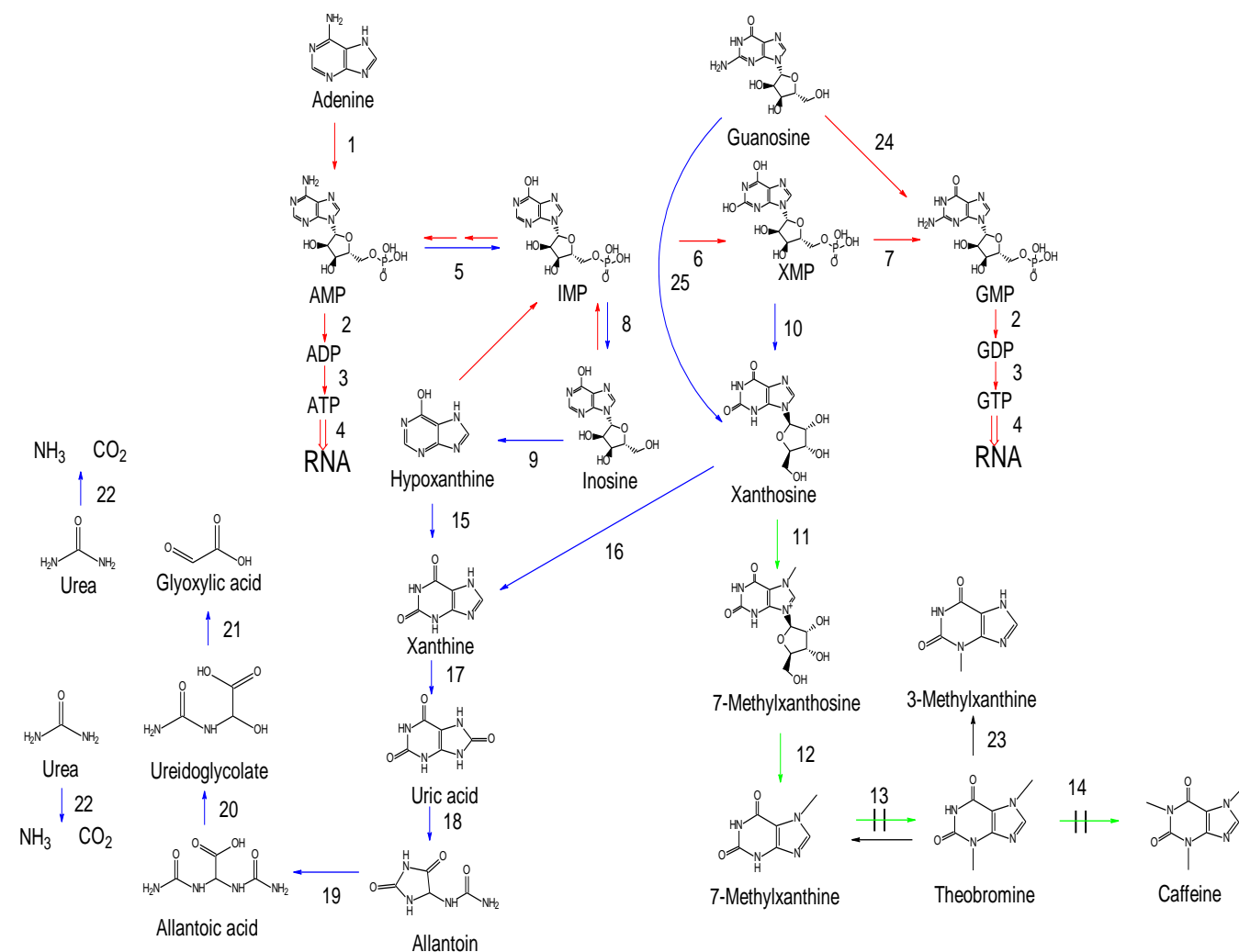


Figure 2. Possible metabolic routes of adenine, inosine, guanosine and xanthosine in *Coffea canephora* and *Mascarocoffea* species. → (red), salvage pathways; → (green), purine alkaloid biosynthesis; → (blue), degradation pathway.

Substantial amounts of inosine (68%), guanosine (55%) and xanthosine (84%) were degraded to allantoin, allantoic acid and CO₂. There are several possible routes of the formation of xanthine, a key starting metabolite for purine catabolism. From the results obtained from other plant sources,^{14, 24} the following routes are the most likely: inosine → hypoxanthine → xanthine (steps 9 and 15); guanosine → xanthosine → xanthine (steps 25 and 16); xanthosine → xanthine (step 16). Although the metabolic profile of these purine nucleosides has not reported in *Coffea* plants, the results are essentially the same as the profile reported to operate in other plants.^{14, 24-26}

Purine alkaloid metabolism

Metabolic fate of exogenously supplied [8-¹⁴C]theobromine and [8-¹⁴C]caffeine in the disks of *C. millotii* is presented in Table 4. In contrast to purine bases and nucleosides, these methylxanthines were not actively metabolized; 93% of theobromine and 99% of caffeine were retained unmetabolized. In the case of [8-¹⁴C]theobromine, small amounts of radioactivity was detected in 3-

methylxanthine (3.5%), 7-methylxanthine (1.9%), xanthine (0.6%) and CO₂ (1.4%). Thus, *C. millotii* leaves seem to have machinery, i.e., enzymes of theobromine catabolism, although its activity is low. Theobromine is a direct precursor of caffeine biosynthesis in *C. arabica* and *C. canephora*, but no conversion of theobromine to caffeine was detected in *C. millotii*.

Comparison of purine metabolism in caffeine reduced *Coffea* plants

Biosynthesis and degradation of caffeine occur in low caffeine *Coffea* plants including native and transgenic plants.⁹ In most cases, the activity of *N*-methyltransferase is reduced. There are at least two distinct *N*-methyltransferases, 7-methylxanthosine synthase and dual functional caffeine synthase which catalyzes the last two steps, namely, 7-methylxanthine → theobromine → caffeine (steps 13 and 14 in Fig. 2).⁹ The reduction of activity of *N*-methyltransferase activity was suggested in all cases. In addition, a few species including *C. eugenioides* and *C. dewevrei* catabolize caffeine and this may also cause reduction of the caffeine level.^{10, 27-29}

In the present study, we found that the purine alkaloid synthesis was stopped at 7-methylxanthine, thus dual functional caffeine synthase activity appeared to be missing in *Mascarocoffea* species.

Table 3. Metabolism of inosine, guanosine and xanthosine in *Coffea mellotii* leaf segments.

Metabolites	[8- ¹⁴ C]-labelled		
	Inosine	Guanosine	Xanthosine
Nucleotides	7.16 ± 4.15	6.33 ± 1.05	nd
RNA	9.15 ± 0.74	16.8 ± 0.29	nd
Nucleosides and bases			
Inosine	4.17 ± 0.36	nd	nd
Hypoxanthine	2.45 ± 0.14	nd	nd
Guanosine and guanine	nd	11.3 ± 0.63	nd
Xanthosine	8.43 ± 0.92	9.16 ± 0.86	10.5 ± 0.93
Xanthine	nd	nd	4.03 ± 0.20
Purine alkaloids			
7-Methylxanthine	0.86 ± 0.07	0.67 ± 0.08	1.39 ± 0.71
3-Methylxanthine	nd	nd	nd
Theobromine	nd	nd	nd
Caffeine	nd	nd	nd
Degradation products			
Ureides	20.8 ± 1.3	15.9 ± 1.71	20.7 ± 2.3
Carbon dioxide	46.9 ± 3.5	38.7 ± 0.68	63.4 ± 1.9
Unidentified	nd	1.03 ± 0.15	nd
Total uptake	25.4 ± 0.5	24.6 ± 1.2	4.73 ± 0.10

[8-¹⁴C]Inosine (10 μM, specific activity 1.9 GBq mmol⁻¹), [8-¹⁴C]guanosine (10 μM, specific activity 1.9 GBq mmol⁻¹) and [8-¹⁴C]xanthosine (9 μM, specific activity 2.1 GBq mmol⁻¹) were administered for 18 h. The mean incorporation of radioactivity into individual metabolites is expressed as the percentage of total radioactivity taken up by the segments ± SD. Total uptake is expressed as kBq 100 mg f.w.⁻¹, nd, not detected.

In contrast, Silvarolla et al.³⁰ reported that theobromine was accumulated in a naturally decaffeinated *C. arabica* plant from Ethiopia designated "AC". They found that the leaves accumulated radioactivity in theobromine when [¹⁴C]adenine was fed to the "AC" plants, with none being incorporated into caffeine. In contrast, no difference was found in degradation of [¹⁴C]caffeine between in the "AC" plants and caffeine accumulating normal *C. arabica* plants. These results indicate that the low caffeine content in the "AC" plants is due to the lack of the activity of *N*-methyltransferase which catalyzes the last step in the caffeine biosynthesis pathway (step 14 in Fig. 2). Although no data was shown, they mentioned that no caffeine synthase activity was detected in the leaves, and concluded that the caffeine synthase gene had mutated in the AC plants. In this case, theobromine synthase which is distinct from a dual-functional caffeine synthase may be functional.

The reduction of caffeine synthase has also been suggested in low-caffeine hybrid coffee by ¹⁴C-feeding experiments, the hybrid named GCAs which are new tetraploid interspecific hybrids developed in Madagascar

from *C. eugenioides*, *C. canephora* and *C. arabica*. Selected GCA contained low caffeine (<0.4 % dry wt.) and no detectable theobromine in seeds. Low caffeine accumulation in GCA plants is due mainly to the low caffeine biosynthesis activity, possibly due to extremely weak *N*-methyltransferase reactions. No significant catabolic activity of caffeine was found in the GCA, in common with *C. arabica*.

Table 4. Metabolism of theobromine and caffeine in *Coffea mellotii* leaf segments.

Metabolites	[8- ¹⁴ C]Theobromine	[8- ¹⁴ C]Caffeine
Nucleotides	nd	nd
RNA	nd	nd
Nucleosides and bases		
Xanthine	0.60 ± 0.05	nd
Purine alkaloids		
7-Methylxanthine	1.89 ± 0.28	nd
3-Methylxanthine	3.54 ± 0.72	nd
Theobromine	92.5 ± 1.4	nd
Caffeine	nd	98.6 ± 0.01
Degradation products		
Ureides	nd	nd
Carbon dioxide	1.38 ± 0.25	0.43 ± 0.12
Total Uptake	13.2 ± 2.3	1.45 ± 0.21

[8-¹⁴C]Theobromine (9 μM, specific activity 2.0 GBq mmol⁻¹) and [8-¹⁴C] caffeine (10 μM, specific activity 2.0 GBq mmol⁻¹) were administered for 18 h. The mean incorporation of radioactivity into individual metabolites is expressed as the percentage of total radioactivity taken up by the segments ± SD. Total uptake is expressed as kBq 100 mg f.w.⁻¹, nd, not detected.

Similar results were also demonstrated in anti-sense and RNA interference transgenic plants of *C. canephora* in which the expression of an *N*-methyltransferase gene was suppressed. Compared with wild-type control plants, total purine alkaloid biosynthesis from adenine and conversion of theobromine to caffeine were both reduced in the transgenic plants. In the transgenic plants, metabolism of [8-¹⁴C]adenine shifted from purine alkaloid synthesis to purine catabolism or salvage for nucleotides.

From these results, we can speculate that in most caffeine-free *Coffea* plants including *Mascarocoffea* species, caffeine synthase-related genes are varied and, as a result, there is reduced the enzyme activity *in planta*. In these plants, the metabolic flow of purine metabolites to the purine alkaloids synthesis appeared to be shifted to the purine catabolism.

Acknowledgement

We thank the BEC (Biodiversité, Eco-valorisation et Caféiers) Association for supports of the maintenance of the Kianjavato collection since 2012 and the UCC (Ueshima Coffee Co., Ltd.), Japan for the sample collection in Madagascar.

References

- ¹Ashihara, H., *Nat. Prod. Commun.*, **2016**, *11*, 1047-1054.
- ²Ashihara, H., *Brazil. J. Plant Physiol.*, **2006**, *18*, 1-8.
- ³Ashihara, H., Yokota, T. and Crozier, A., *Adv. Bot. Res.*, **2013**, *68*, 111-138. <https://doi.org/10.1016/B978-0-12-408061-4.00004-3>
- ⁴Ashihara, H., Ludwig, I., Katahira, R., Yokota, T., Fujimura, T. and Crozier, A., *Phytochem. Rev.*, **2015**, *14*, 765-798. <https://doi.org/10.1007/s11101-014-9375-z>
- ⁵Hamon, P., Rakotomalala, J.J., Akaffou, S., Razafinarivo, N.J., Couturon, E., Guyot, R., Crouzillat, D., Hamon, S. and De Kochko, A., in *Coffee in Health and Disease Prevention*, ed. Preedy, V.R., Academic Press, London, **2014**, pp. 39-44.
- ⁶Rakotomalala, J.J., Cros, E., Clifford, M.N. and Charrier, A., *Phytochemistry*, **1992**, *31*, 1271-1272. [https://doi.org/10.1016/0031-9422\(92\)80275-J](https://doi.org/10.1016/0031-9422(92)80275-J)
- ⁷Clifford, M.N., Gibson, C.L., Rakotomalala, J.J.R., Cros, E. and Charrier, A., *Phytochemistry*, **1991**, *30*, 4039-4040. [https://doi.org/10.1016/0031-9422\(91\)83461-S](https://doi.org/10.1016/0031-9422(91)83461-S)
- ⁸Rakotomalala, J.-J.R., Kumamoto, T., Aburatani, T., Rabemifara, A., Nagai, C., Kawashima, Y. and Rabenatoandro, Y.N., *Proc. ASIC Conf.* **2004**, *20*, 154-160.
- ⁹Ashihara, H., Mizuno, K., Yokota, T. and Crozier, A., in *Progress in the Chemistry of Organic Natural Products 105*, eds. Kinghorn, A.D., Falk, H., Gibbons, S. and Kobayashi, J., Springer, Cham, Switzerland, **2017**, pp. 1-88.
- ¹⁰Ashihara, H. and Crozier, A., *J. Agric. Food Chem.*, **1999**, *47*, 3425-3431. <https://doi.org/10.1021/jf981209n>
- ¹¹Ashihara, H., Monteiro, A.M., Moritz, T., Gillies, F.M. and Crozier, A., *Planta*, **1996**, *198*, 334-339. <https://doi.org/10.1007/BF00620048>
- ¹²Zheng, X.Q. and Ashihara, H., *Plant Sci.*, **2004**, *166*, 807-813. <https://doi.org/10.1016/j.plantsci.2003.11.024>
- ¹³Ashihara, H., Monteiro, A.M., Gillies, F.M. and Crozier, A., *Plant Physiol.*, **1996**, *111*, 747-753. <https://doi.org/10.1104/pp.111.3.747>
- ¹⁴Deng, W.-W. and Ashihara, H., *Plant Cell Physiol.*, **2010**, *51*, 2105-2118. <https://doi.org/10.1093/pcp/pcq175>
- ¹⁵Suzuki, T., Ashihara, H. and Waller, G.R., *Phytochemistry*, **1992**, *31*, 2575-2584. [https://doi.org/10.1016/0031-9422\(92\)83590-U](https://doi.org/10.1016/0031-9422(92)83590-U)
- ¹⁶Mizuno, K., Kato, M., Irino, F., Yoneyama, N., Fujimura, T. and Ashihara, H., *FEBS Lett.*, **2003**, *547*, 56-60. [https://doi.org/10.1016/S0014-5793\(03\)00670-7](https://doi.org/10.1016/S0014-5793(03)00670-7)
- ¹⁷Negishi, O., Ozawa, T. and Imagawa, H., *Agric. Biol. Chem.*, **1988**, *52*, 169-175.
- ¹⁸Mizuno, K., Okuda, A., Kato, M., Yoneyama, N., Tanaka, H., Ashihara, H. and Fujimura, T., *FEBS Lett.*, **2003**, *534*, 75-81. [https://doi.org/10.1016/S0014-5793\(02\)03781-X](https://doi.org/10.1016/S0014-5793(02)03781-X)
- ¹⁹Uefuji, H., Ogita, S., Yamaguchi, Y., Koizumi, N. and Sano, H., *Plant Physiol.*, **2003**, *132*, 372-380. <https://doi.org/10.1104/pp.102.019679>
- ²⁰Stasolla, C., Katahira, R., Thorpe, T.A. and Ashihara, H., *J. Plant Physiol.*, **2003**, *160*, 1271-1295. <https://doi.org/10.1078/0176-1617-01169>
- ²¹Zrenner, R., Stitt, M., Sonnewald, U. and Boldt, R., *Annu. Rev. Plant Biol.*, **2006**, *57*, 805-836. <https://doi.org/10.1146/annurev.arplant.57.032905.105421>
- ²²Yabuki, N. and Ashihara, H., *Biochim. Biophys. Acta*, **1991**, *1073*, 474-480. [https://doi.org/10.1016/0304-4165\(91\)90218-6](https://doi.org/10.1016/0304-4165(91)90218-6)
- ²³Koshiishi, C., Kato, A., Yama, S., Crozier, A. and Ashihara, H., *FEBS Lett.*, **2001**, *499*, 50-54. [https://doi.org/10.1016/S0014-5793\(01\)02512-1](https://doi.org/10.1016/S0014-5793(01)02512-1)
- ²⁴Katahira, R. and Ashihara, H., *Planta*, **2006**, *225*, 115-126. <https://doi.org/10.1007/s00425-006-0334-9>
- ²⁵Yin, Y., Katahira, R. and Ashihara, H., *Eur. Chem. Bull.*, **2014**, *3*, 925-934. DOI: 10.17628/ecb.2014.3.925-934
- ²⁶Koyama, Y., Tomoda, Y., Kato, M. and Ashihara, H., *Plant Physiol. Biochem.*, **2003**, *41*, 977-984. <https://doi.org/10.1016/j.plaphy.2003.07.002>
- ²⁷Mazzafera, P., Crozier, A. and Magalhães, A.C., *Phytochemistry*, **1991**, *30*, 3913-3916. [https://doi.org/10.1016/0031-9422\(91\)83433-L](https://doi.org/10.1016/0031-9422(91)83433-L)
- ²⁸Mazzafera, P., *J. Agric. Food Chem.*, **1993**, *41*, 1541-1543. <https://doi.org/10.1021/jf00034a002>
- ²⁹Mazzafera, P., Crozier, A. and Sandberg, G., *J. Agric. Food Chem.*, **1994**, *42*, 1423-1427. <https://doi.org/10.1021/jf00043a007>
- ³⁰Silvarolla, M.B., Mazzafera, P. and Fazuoli, L.C., *Nature*, **2004**, *429*, 826-826. <https://doi.org/10.1038/429826a>

Received: 06.06.2017.
Accepted: 27.06.2017.



LIGHT OPTICAL STUDY OF HUMAN BREAST CANCER TISSUE EMBEDDED IN EPOXY RESINS

Kukurtchyan, N. S.^[a] and Karapetyan, G. R.^[a]

Keywords: human breast cancer; angiogenesis; light optical microscopy; epoxy resins.

A new possibility is shown for the study of the microcirculatory bed of human breast cancer tissue embedded in Epoxy resins. Using current method - staining the material by Azur II - it becomes possible the obtaining 3D images of blood vessels of human breast cancer tissue which gives new opportunities for further study of this disease.

* Corresponding Authors: Karapetyan, G. R.

Fax: +374 -10-28 19 51

E-Mail: sapootraa_a@yahoo.com

[a] H. Buniatian Institute of Biochemistry, of National Academy of Sciences of Republic Armenia, Paruir Sevag str. 5/1, 0014, Yerevan, Republic of Armenia.

INTRODUCTION

Breast cancer is an increasing public health problem and usual combinations of local and systemic therapies are not always curative.⁴ Blood vessels deliver oxygen and nutrients to every part of the body, but also nourish diseases such as cancer.^{5,15}

It is well known that the most solid tumors has limited oxygen supply caused by lack of blood vessels as well as their destruction.¹¹ Extensive laboratory data suggest that angiogenesis plays an essential role in breast cancer development, invasion, and metastasis. Angiogenesis precedes transformation of mammary hyperplasia to malignancy.^{3,10}

In spite the fact that capillary net around the tumor formed by normal endothelial cells, it is quite different from capillaries which have normal morphology, density and penetration.²¹ The dense capillary net provides enough oxygen and necessary nutrients to developing tumor cells, as well as moves out the products of cells metabolism. The presence of capillary net leads to easier dissemination of metastatic tumor cells.²³

So, for increasing the thickness of malignant tumor cells, the high specialized capillary net is required.

The formation of new blood vessels (angiogenesis) is essential for the growth of most tumors. One of the most well-studied angiogenesis factors is called vascular endothelial derived growth factor (VEGF). VEGF or other angiogenesis factors produced by tumor cells or nearby cells can cause the development of blood vessels that feed the growing tumor.^{1,11,18,20} Hyperplastic murine breast papillomas and histologically normal lobules adjacent to cancerous breast tissue^{2,5,6} support angiogenesis in

preclinical models, suggesting that angiogenesis precedes transformation of mammary hyperplasia to malignancy. Our current knowledge of tumor angiogenesis is based mainly on experiments performed in tumor-transplanted mice, and it has become evident that these models are not representative of human cancer.¹⁴

The aim of this study is to show the new possibilities for the study of the microcirculatory bed of human breast cancer tissue embedded in Epoxy resins.

MATERIALS AND METHODS

Reagents: Powdered paraformaldehyde; OsO₄; sodium cacodylate trihydrate; 96 % ethyl alcohol, acetone, Epon 812, Epon Hardener MNA, Epon Hardener DDSA, Epon accelerator DNP-30, Azur II, sodium borate. All reagent used were of analytical grade and purchased from Sigma Chemical Co. (USA).

The biopate of tissue used in the current study were taken during Core biopsy (5 patients), as well as at surgical procedures before chemotherapy (5 patients).

All procedures involved human subject were approved by institutional review board/bioethical committee (Erevan State Medical University, RA) conformed to the Legal Aspects of Research Ethics and Science in European Community directive (2001/20/EC

Small pieces of tissue have immediately put in a cold mix of paraformaldehyde in a sodium cacodylate buffer and glutaraldehyde for 12 hours at 4 °C with following post fixation in 1 % OsO₄ solution for 2 h, then dehydration take place in ascending series of spirits; saturation in a mixture of acetone and Epoxy resins of different proportions to make gelatinous capsules were performed.

Observation under a light microscope: semithin epoxy sections with up to 1 μm thickness were made using ultracuts LKB (Swedish) and Reichert (Austria) stained with Azur II and studied under light microscope supplied with 40 x10 ocular lens.

RESULTS

The study of a 4- μm -thick section from each formalin-fixed and the paraffin-embedded tumor is generally accepted. Although the thickness of semithin epoxy slices is about 0.5–1 μm , while the paraffin-embedded ones thicknesses are 3–4 μm . It means, that the morphological results of tissues in semithin slices could be more informative than the paraffin embedded ones. Although the observation field of materials embedded in semithin epoxy slices under a light optical microscope is lesser than in case of the paraffin-embedded ones, however, the results are more informative.

As it can be seen from the results of our study, using Azure II staining method it becomes possible to obtain 3D images of blood vessels of human breast cancer tissue embedded in epoxy resins. So, we can say that this method is quite effective for the study of semithin slices of material taken at core biopsy as well as during surgical procedures (Fig.1, 2, 3, 4, 5) as it gives more opportunities for the study of human breast cancer by obtaining very informative images of blood vessels for their further study and analysis.

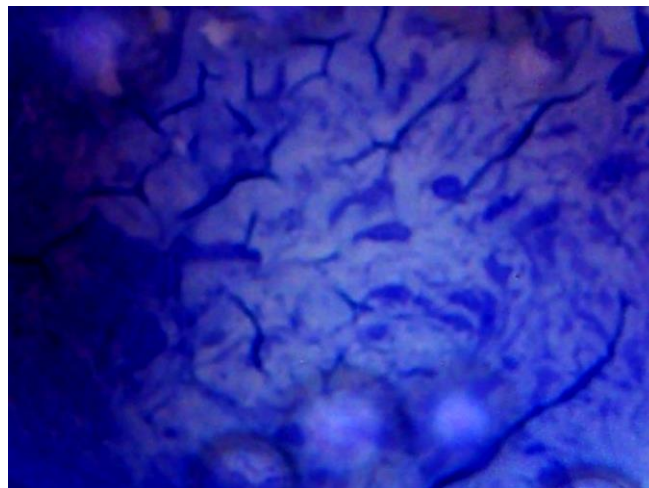


Figure 3. Blood vessels of human breast cancer tissue at core biopsy. 40 x10 ocular lens.

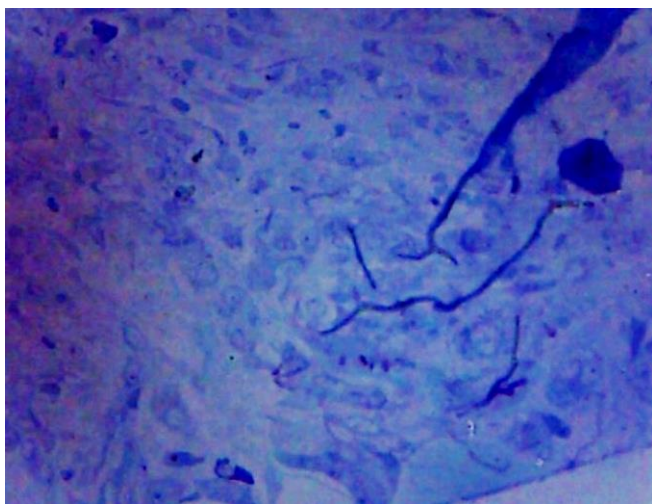


Figure 1. Blood vessels of human breast cancer tissue taken during surgical procedures. 40 x10 ocular lens.

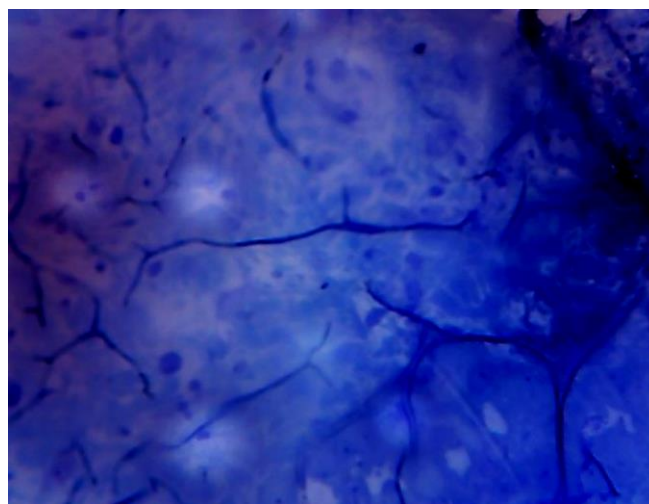


Figure 4. Blood vessels of human breast cancer tissue at core biopsy. 40 x10 ocular lens.

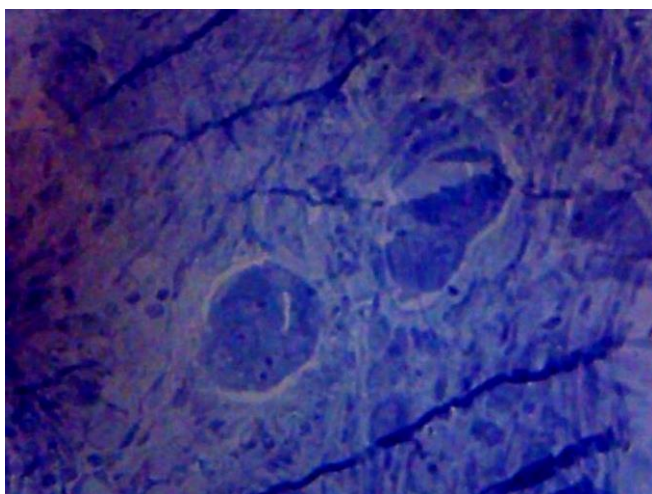


Figure 2. Blood vessels of human breast cancer tissue taken during surgical procedures. 40 x10 ocular lens.

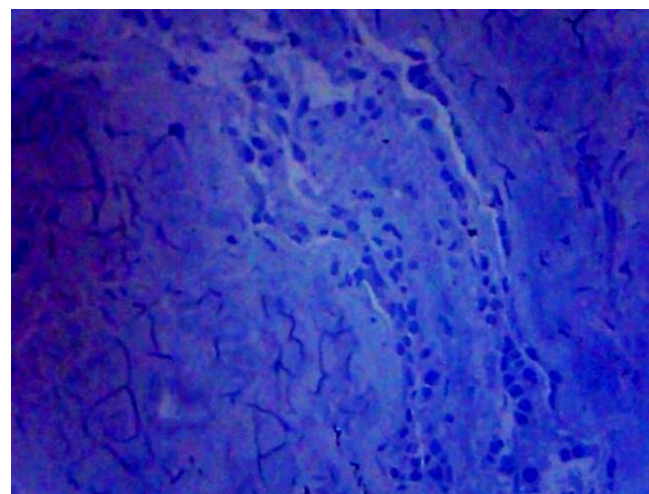


Figure 5. Blood vessels of human breast cancer tissue at core biopsy. 40 x10 ocular lens.

DISCUSSION

Recently, paraffin, celloidin and gelatin pouring of tissues have allowed to get histological specimens stained in different ways to carry out immunohistochemical investigations. However, the quality of tissue structures' preservation proved to be moderate.^{9,17} The best preservation of tissue structures could be reached with epoxy injection of tissues.

The tumor growth dependency on angiogenesis^{7,15} makes the hypothesis of angiogenesis as a prognosticator attractive. However, there is still uncertainty about angiogenesis as a prognosticator in breast cancer based on the publications contains conflicting results.⁸ Studies of the assessment of angiogenesis have mainly been based on the hot-spot approach, preferentially using the technique of counting microvessel profiles by all immunohistochemically stained distinct endothelial cells or cell clusters microscopically. The method of tissue staining by Azur II do not request using any specific markers, sources, or involving additional methods for obtaining of images vessels.¹³

A useful method of angiogenesis estimation in human tumors is the microvessels counting method in the primary tumor using specific markers of endothelial cells such as VIII-factor, CD31, CD34, as well as the standard immunoperoxidase technique of vessels staining.^{16,21,22} The studies on antibodies to CD31 factor was proved to be more sensitive method as the available panendothelial markers. This method recognizes more microvessels as other endothelial markers. CD34 and VIII-factor do not stain all vessels of the tumor, and antibodies to VIII-factor have reactions with lymphocytes as well. However, the specific characters of antibodies to CD31 are also not absolute, as they have a positive reaction with plasmatic cells. It must be mentioned that these markers stain normal, active/proliferating endothelium. Since different studies used different techniques, it would be relevant to re-evaluate the prognostic value of angiogenesis by Chalkley counting in a confirmative study design.¹⁹

The importance of the Chalkley counting as an independent prognostic factor in breast cancer diagnosis, together with age, axillaries metastatic nodal involvement, tumor size, and histological grade of malignancy is high.²⁰ But it must be mentioned that Chalkley counting method, as well as other original methods, have limited abilities. Our method developed let us obtain the 3D images of vessels in human breast cancer tissue, which let us find the relation between angiogenesis types and molecular biological basic of human breast precancer types. The relations between transformations between each form of angiogenesis can show how could become the transformation of angiogenesis type to be a prognostic factor for disease, its early relapse and metastasis phase.

CONCLUSION

Obtaining blood vessels images of human breast cancer on semithin epoxy slices gives new opportunities for studies of tissues and recognition of this disease.

REFERENCES

- ¹Areck, A., Ucuzian, A., Gassman, A., East, A. T. and Greisler, H. P., *J. Burn. Care Res.*, **2010**, *31(1)*, 158. doi:10.1097/BCR.0b013e3181c7ed82
- ²Brem, S. S., Gullino, P. M., Medina, D., *Science*, **1977**, *195*, 880-882. DOI: 10.1126/science.402692
- ³Bryan, P., Schneider, K. Miller, D., *J. Clin. Oncol.*, **2005**, *23(8)*, 1782-1790. DOI: 10.1200/JCO.2005.12.017
- ⁴Binns, C., Low, W. Lee, Y., *Pac. J. Public Health*, **2013**, *25(5)*, 364-7. doi: 10.1177/1010539513505050
- ⁵Carmeliet, P., Jain, R. K., *Nature*, **2011**, *473(7347)*, 298-307. doi: 10.1038/nature10144.
- ⁶Djonov, V., Andres, A. C., Ziemieski, A., *Microsc. Res. Tech.*, **2001**, *52(2)*, 182-9. DOI: 10.1200/JCO.2005.12.017
- ⁷Folkman, J., Mendelsohn, J., Howley, P. M., Israel, M. A., Liotta, L. A. Saunders, W. B., *The Molecular Basis of Cancer*, **1995**, 206-232.
- ⁸Fox, S. B. *Histopathology*, **1997**, *30*, 294-301
- ⁹Groos, S., Real, E., Luciano, J., *J. Histochem. Cytochem.*, **2001**, *49(3)*, 397-406. doi.org/10.1177/002215540104900313
- ¹⁰Schatten, H., *Cell Mol. Biol. Breast Cancer*, **2013**, DOI: 10.1007/978-1-62703-634-4
- ¹¹Jahroudi, N., Lvnch, D. C., *Mol. Cell. Biol.*, **1994**, *14*, 999.
- ¹²Jensen, H. M., Chen, I., DeVault, M. R. And Lewis, A. E.: *Science*, **1982**, *218*, 293-295, DOI: 10.1200/JCO.2005.05.098
- ¹³Kukurtchyan, N. S., Karapetyan, G. R., *Patent 2844 A, Rep. Armenia*, **2014**.
- ¹⁴Eklund, L., Bry, M., *Mol. Oncol.*, **2013**, *7(2)*, 259-282. https://doi.org/10.1016/j.molonc.2013.02.007
- ¹⁵Naoyo, N., Hirohisa, Y., Takashi, N., Toshihari, K. and Masamichi, K.. *Vask. Health Risk Manag.*, **2006**, *2(3)*, 213-219.
- ¹⁶Parums, D. V., Cordell, J. L., Micklem, K., *J. Clin. Pathol.*, **1990**, *43*, 752-7.
- ¹⁷Richardson, K.C ., Jarret, L., Finke, E. H. *Stain Technol.*, **1960**, *35*, 313. https://doi.org/10.3109/10520296009114754
- ¹⁸Salven, P., Ruotsalainen, T., Mattson, K., *Int. J. Cancer*, **1998**, *79*,144-146. DOI:10.1002/(SICI)1097-0215(19980417)79:2
- ¹⁹Simon, R., Altman, D. G. *Brit. J. Cancer*, **1994**, *69*, 979-985. DOI: 10.1038/bjc.1994.192
- ²⁰Takahashi, Y., Kitadai, Y., Bucana, C. D., Cleary, KR and Ellis, LM.: *Cancer Res.* **1995**, *55*, 3964-3968.
- ²¹Torry, R. G., Rongish, B. J. *Am. J. Reprod. Immunol.*, **1992**, *27(3-4)*, 171-9. DOI: 10.1111/j.1600-0897.1992.tb00746.x
- ²²Weidner, K. M., Arakaki, N., Hartmann, G., Vanderkeckhove, J., Birchmeier, W., *Proc. Nat. Acad. Sci. USA*, **1991**, *88*, 7001-7005. doi: 10.1073/pnas.88.16.7001
- ²³Zhukova, T. V. *Republic Scientific-Practical Center of Traumatology and Orthopedics, Minsk J Medical news*, **2011**, *11*.

Received: 01.05.2017

Accepted: 27.06.2017



INFLUENCE OF COFFEE ON THE CORROSION RESISTANCE OF ORTHODONTIC WIRES IN ARTIFICIAL SALIVA

A. Christy Catherine Mary,^[a] S. Rajendran^[b,c] and J. Jeyasundari^[d]

Keywords: artificial saliva; corrosion; metals; coffee; polarization study; AC impedance spectra.

Corrosion resistance of Ni-Ti, Thermoactive alloy, and SS 316 L alloy in artificial saliva (AS) in the absence and presence of coffee has been evaluated by electrochemical studies such as polarization study and AC impedance spectroscopy. The polarization and AC impedance spectroscopy studies lead to the conclusion that corrosion resistance of the alloys decreases in the following order: SS 316 L alloy > Thermoactive alloy > Ni-Ti alloy. In all the three cases, the corrosion resistance of the wires increases in the presence of coffee. Among the three orthodontic wires, SS316L alloy is the best candidate.

* Corresponding Author

E-Mail: chriscethi@gmail.com

[a] Department of Chemistry, Parvathy's Arts and Science College, Dindigul, India.

[b] Department of Chemistry, Corrosion Research Center, St. Antony's College of Arts and Sciences For Women, Dindigul.

[c] Department of Chemistry, AMET University, 135, East Coast road, Kanathur – 603112, Chennai, India.

[d] Department of Chemistry, SVN College, Madurai, India.

electrochemical studies such as polarization study and AC impedance spectroscopy in artificial saliva in presence and absence of coffee.

Materials and methods

Preparation of coffee test solution

The coffee test solution was prepared by heating 250 ml of milk to boil, and with added the 5 g of instant coffee powder (BRU Instant Coffee), the mixture was mixed with a teaspoon of sugar.

Corrosion behavior of Ni-Ti, Thermoactive alloy, and SS316L alloy have been investigated in various test solutions such as artificial saliva (AS), coffee, AS + coffee. The composition of AS is given in Table 1.

Table 1. The composition of artificial saliva

Content	Concentration, g L ⁻¹
NaCl	0.4
NaH ₂ PO ₄ .2H ₂ O	0.690
KCl	0.4
CaCl ₂ .2H ₂ O	0.906
Na ₂ S.9H ₂ O	0.005
Urea	1

The metal specimens were immersed in Fusayama-Meyer artificial saliva.²¹ The pH of the solution was 6.5. In electrochemical studies, the alloys were used as working electrodes. Artificial saliva was used as an electrolyte. The experiments were carried out at 64.5 ° C (temperature of the coffee drink).

Potentiodynamic polarization study

Polarization studies were carried out in a CHI-electrochemical workstation with impedance, Model 660A. A three-electrode cell assembly was used.

Introduction

Metallic materials such as Ag, Au, Ni-Ti, Ni-Cr, SS 316L, SS18/8, etc., are used as implants in regulative oral surgery to the array of teeth. The metals for complete and partial crowns and bridges should be hypoallergenic materials with good mechanical properties, corrosion resistant towards soft drinks, hot drinks, food items, and tablets. Titanium alloys are the most commonly used material for implantation of the teeth.¹ Corrosion of metallic implants has vital importance because it can adversely affect the biocompatibility and mechanical integrity of implants. The electrochemical behavior of orthodontic wires in artificial saliva has been investigated by polarization study and AC impedance spectra². The resistance to corrosion of the metallic orthodontic wires in simulated intra-oral environment has been evaluated by Ziebowicz et al.³ The effects of multilayered Ti/TiN or single-layered TiN film deposited by Pulse-Biased Arc Ion Plating (PBAIP) on the corrosion behavior of NiTi orthodontic wires in artificial saliva have also been investigated.⁴ Rajendran et al. have studied the corrosion behavior of SS 316L and AS in artificial saliva in the presence of electoral, spirulina powder, and glucose, respectively.^{5,6,7} A lot of studied have been published on the use of natural products as corrosion inhibitors.⁷⁻¹³ Corrosion behavior of Thermoactive super elastic shape memory alloy and Gold 22K has been investigated in artificial saliva in the presence of syzygium cumini fruit juice.¹⁵ The corrosion resistance of Ti depends on the passive film alloys formed on surface.¹⁶⁻²⁰

In the present study, the corrosion resistance of Ni-Ti, SS 316L, and Thermoactive alloys has been evaluated by

Table 2. Corrosion parameters of metals immersed in artificial saliva (AS) in the absence and the presence of coffee obtained by polarization study

Metal	System	E_{corr} , mV vs SCE	b_c , mV decade ⁻¹	b_a , mV decade ⁻¹	LPR , ohm cm ²	I_{corr} , A cm ⁻²
Ni-Ti alloy	AS	-395	178	302	3277970	1.488x10 ⁻⁸
	AS+Coffee	-778	126	335	5557295	7.170x10 ⁻⁹
SS316L alloy	AS	-454	164	317	4177473	1.127 x10 ⁻⁸
	AS+Coffee	-447	123	216	12072330	2.825x10 ⁻⁹
Thermoactive alloy	AS	-501	158	315	7936745	5.775x10 ⁻⁸
	AS+Coffee	-726	130	339	8025230	5.095x10 ⁻⁹

The working electrode was one of the three alloys. A saturated calomel electrode (SCE) was the reference electrode, and platinum was the counter electrode.

AC impedance spectra

The cell setup was the same as in the case of polarization study. The real part (Z') and imaginary part ($-Z''$) of the cell impedance were measured in ohms at various frequencies.

Result and Discussion

Analysis of polarization curves

Polarization analysis has been used for detection of the protective films formed on the metal surface during corrosion inhibition process.²² The corrosion parameters of Ni-Ti, Thermoactive alloy, and SS316L alloy in the test solutions are given in Table 2, and the potentiodynamic polarization curves are shown in Figures 1 and 2.

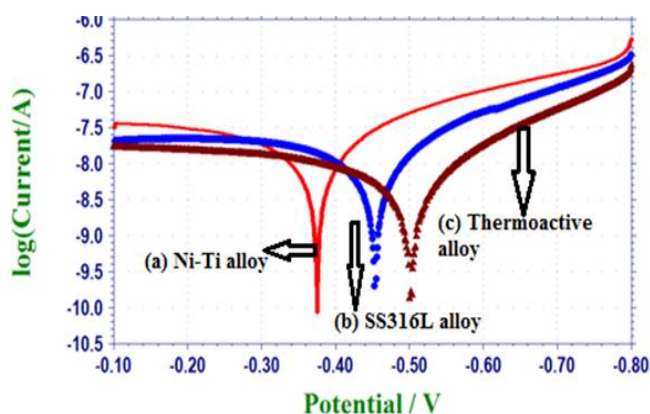


Figure 1. Polarization curve of Ni-Ti alloy, SS 316L alloy and Thermoactive alloy immersed in AS

As it is given in Table 2, when Ni-Ti alloy was immersed in AS, the corrosion potential is -375 mV vs. SCE (Figure 1a). The Linear Polarization Resistance (LPR) value was 3277970 ohm cm², and the corrosion current (I_{corr}) was 1.488 x 10⁻⁸ A cm⁻².

When the Thermoactive alloy was immersed in AS the E_{corr} value was -501 mV vs. SCE (Figure 1c). The LPR value was 7930745 ohm cm². This was found to be higher than in case of Ni-Ti alloy. The corrosion current (I_{corr}) was found to be 5.775 x 10⁻⁹ A cm⁻². This was found to be lower than in case of Ni-Ti alloy. These observations indicated that thermoactive alloy was more corrosion resistant than Ni-Ti alloy.

In the case of Thermoactive alloys, the cathodic Tafel slope was (b_c) 158 mV decade⁻¹, and the anodic Tafel slope was (b_a) 315 mV decade⁻¹. These values suggested that during anodic polarization, the rate of change of corrosion current with potential was high, and it was less during the cathodic polarization.

When the SS316L alloy was immersed in AS, the corrosion potential was -454 mV vs. SCE (Figure 1b). The LPR value was 12072330 ohm cm². The corrosion current was 1.127x10⁻⁸ A cm⁻². The values of Tafel slopes ($b_c = 164$; $b_a = 317$ mV decade⁻¹) indicated that the rate of change of current with potential increased in higher rate during the anodic polarization than during the cathodic polarization. A comparison of LPR values and corrosion current values of these alloys investigated revealed that SS316L was more corrosion resistance than other two alloys.

Corrosion behavior of alloys in AS containing coffee

Ni -Ti alloy

AS it can be seen in Table 2, when Ni-Ti alloy was immersed in AS containing coffee, the corrosion potential was -778 mV vs. SCE (Figure 2a). It was interesting to note that in the presence of coffee the LPR value increased (5557295 ohm cm²) and the corrosion current value decreased (7.170 x 10⁻⁹ A cm⁻²). It seemed that a protective layer was formed on the metal surface which controlled the rate of corrosion of Ni-Ti in AS in the presence of coffee. The values of Tafel slopes were $b_c = 130$ mV decade⁻¹; $b_a = 339$ mV decade⁻¹.

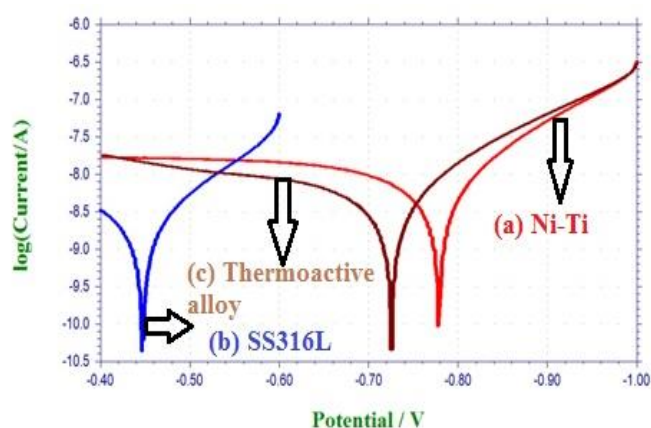
Thermoactive alloy

When the Thermoactive alloy was immersed in AS containing coffee the corrosion potential was -712 mV vs. SCE (Figure 2c). The Tafel slope were $b_c = 130$ mV decade⁻¹ and $b_a = 339$ mV decade⁻¹.

Table 3. Corrosion parameters of metals immersed in Artificial saliva (AS) in the absence and the presence of coffee obtained by AC impedance spectra

Metal	System	Nyquist plot, R_t ohm cm^2	C_{dl} , F cm^{-2}	Bode plot, impedance $\log(Z \text{ ohm}^{-1})$
Ni-Ti alloy	AS	12278	4.1538	4.203
	AS+coffee	3823.8	1.30759	4.4
SS316L alloy	AS	12468	4.0905	4.443
	AS+coffee	247279.52	2.0235	4.6
Thermoac-tive alloy	AS	27941	1.8253	4.344
	AS+coffee	88930	5.6224	4.393

The LPR value was increased from 7936745 ohm cm^2 to 8025230 ohm cm^2 , the corrosion current was decreased from 5.775×10^{-8} A cm^{-2} to 5.095×10^{-9} A cm^{-2} . That is, in the presence of coffee, the corrosion resistance of thermoactive alloy was increased.

**Figure 2.** Polarization curve of Ni-Ti alloy, SS316L alloy and Thermoactive alloy immersed in AS+Coffee

SS 316 L alloy

In the presence of coffee, the corrosion resistance of SS316L increased. This is revealed by the increase in LPR value (from 4177473 ohm cm^2 to 12072330 ohm cm^2) and decrease in corrosion current (from 1.127×10^{-8} to 2.825×10^{-9}) (Figure 2b). The value of Tafel slope were $b_c = 123$ mV decade $^{-1}$; $b_a = 216$ mV decade $^{-1}$. Thus polarization study leads to the conclusion that in the presence of coffee in AS the corrosion resistance of alloys decreased in the following order: SS316L alloy > Thermoactive alloy > Ni-Ti alloy. Polarization study reveals that the corrosion resistance of the three alloys in AS in absence and presence of coffee decreases in the following order; SS316L alloy > Thermoactive alloy > Ni-Ti alloy.

Implication

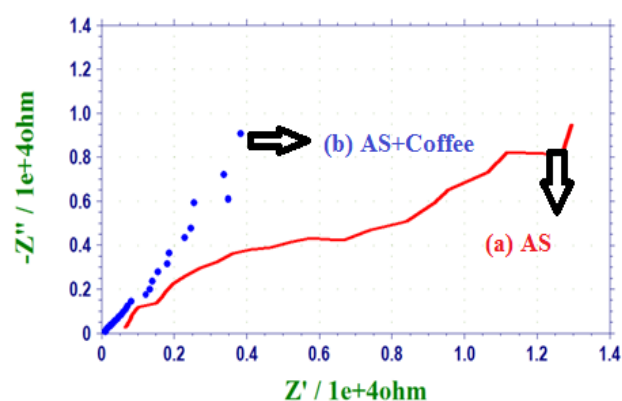
It implies that SS316L alloy is a better candidate for making orthodontic wire.

AC impedance spectra

AC impedance parameters such as charge transfer resistance (R_t), double layer capacitance (C_{dl}) (derived from Nyquist plots) and impedance value $\log(Z \text{ ohm}^{-1})$ (derived from Bode plots), of various alloys immersed in AS and AS containing coffee, are given in Table 3. AS impedance spectra are shown in Fig 3 to 5 (Nyquist Plots) and 6 to 11 (Bode plots).

Ni-Ti alloy

When Ni-Ti is immersed in AS (Figure 3a), the charge transfer resistance was 1227 ohm cm^2 . The double layer capacitance was 4.1538×10^{-10} F cm^{-2} . The impedance value [$\log(Z \text{ ohm}^{-1})$] was 4.20315 in the presence of coffee (Figure 3b), R_t value increased (from 12278 ohm cm^2 to 38238 ohm cm^2) and C_{dl} value was decreased. There was an increase in the value of impedance [$\log(Z \text{ ohm}^{-1})$] (Fig 7b). These observations indicated that in the presence of coffee in AS, the corrosion rate of Ni-Ti was reduced due to the formation of the protective film formed on the metal surface.

**Figure 3.** AC impedance spectra (Nyquist plot) of Ni-Ti alloy immersed in AS and AS+Coffee

Thermoactive alloy

When the Thermoactive alloy was immersed in AS (Figure 4a), the R_t value is 27941 ohm cm^2 . The double layer capacitance was 1.8253×10^{-10} F cm^{-2} . The impedance value [$\log(Z \text{ ohm}^{-1})$] was 3.82 (Figure 8).

When the R_t values were compared with the value of Ni-Ti, it was noted that Thermoactive alloy was more corrosion resistant in AS than Ni-Ti alloy. Similarly, when Thermoactive alloy was immersed in AS mixed with coffee (Figure 4b) the R_t value was increased from 27941 to 88930 ohm cm², the C_{dl} value decreased from 1.8253×10^{-10} F cm⁻² to 5.622×10^{-11} F cm⁻², and the impedance value increased from 3.871 to 4.393 (Figure 9). This observation concluded that the film formation on the metal surface in AS in the presence of coffee.

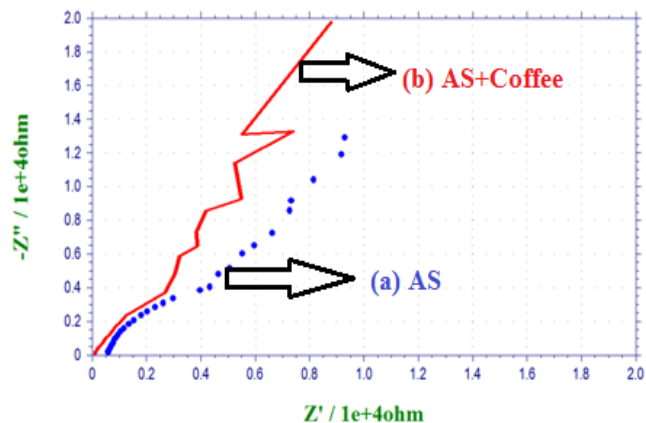


Figure 4. AC impedance spectra (Nyquist plot) of Thermoactive alloy immersed in AS and AS+Coffee

SS316L alloy

When SS316 L alloy was immersed in AS, the R_t value was 12468 ohm cm². The C_{dl} value was 4.0905×10^{-10} F cm⁻², and the impedance value [$\log(Z \text{ ohm}^{-1})$] was 4.443 (Figure 10). These observations suggest that the protective film formed on the SS316L alloy. SS316L was a better candidate in AS since it was more corrosion resistant than Ni-Ti and Thermoactive alloys.

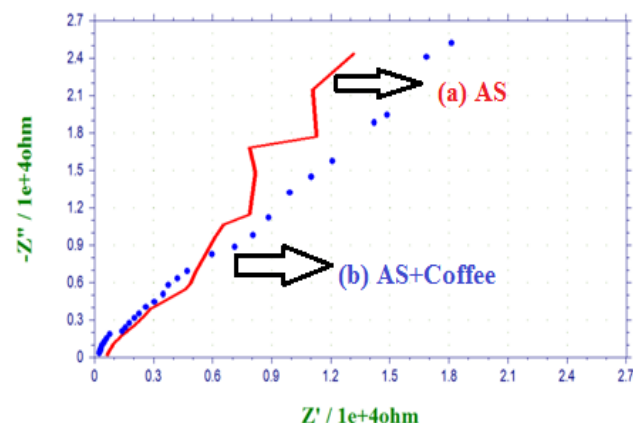


Figure 5. AC impedance spectra (Nyquist plot) of SS 316L alloy immersed in AS and AS+Coffee

When SS316L was immersed in AS in the presence of coffee the R_t value is increase from 12468 to 247279.52 ohm cm², the C_{dl} value is decreased from 4.0905×10^{-10} F cm⁻² to 2.0235×10^{-10} F cm⁻² and impedance value increased from 4.443 to 4.6 [$\log(Z \text{ ohm}^{-1})$] (Figure 11).

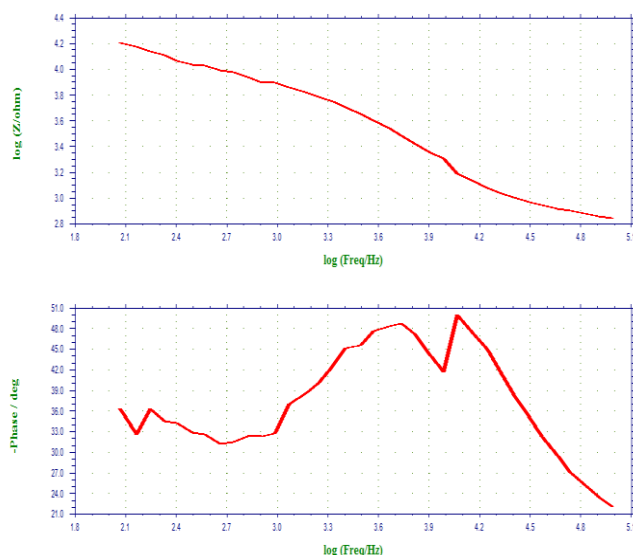


Figure 6. AC impedance spectra (Bode Plot) of Ni-Ti alloy immersed in AS

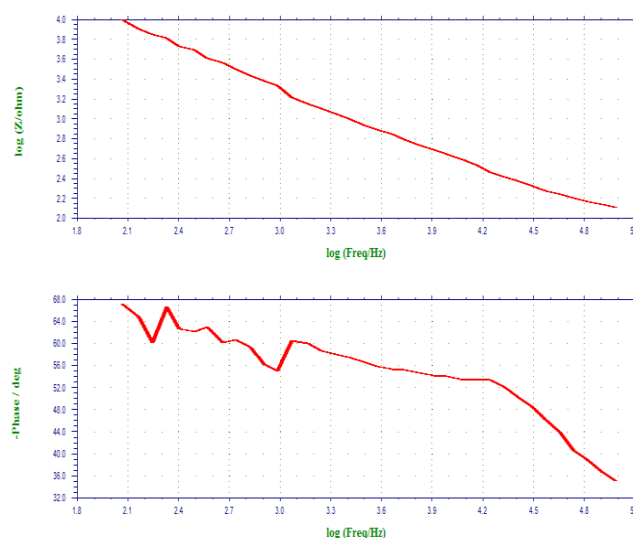


Figure 7. AC impedance spectra (Bode Plot) of Ni-Ti alloy immersed in AS +Coffee

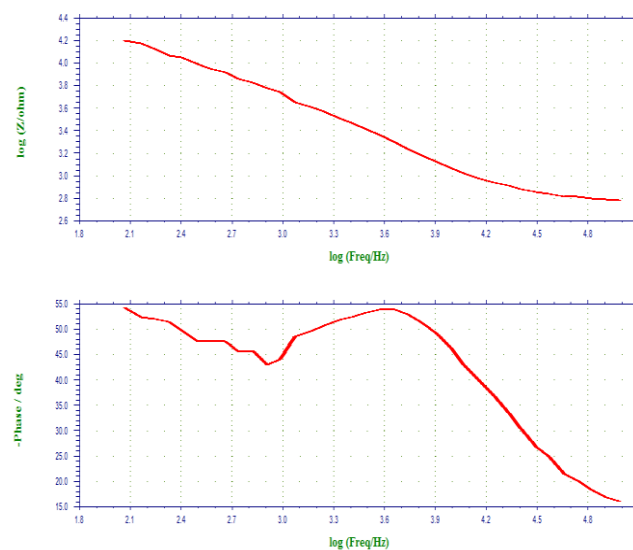


Figure 8. AC impedance spectra (Bode Plot) of Thermoactive alloy immersed in AS

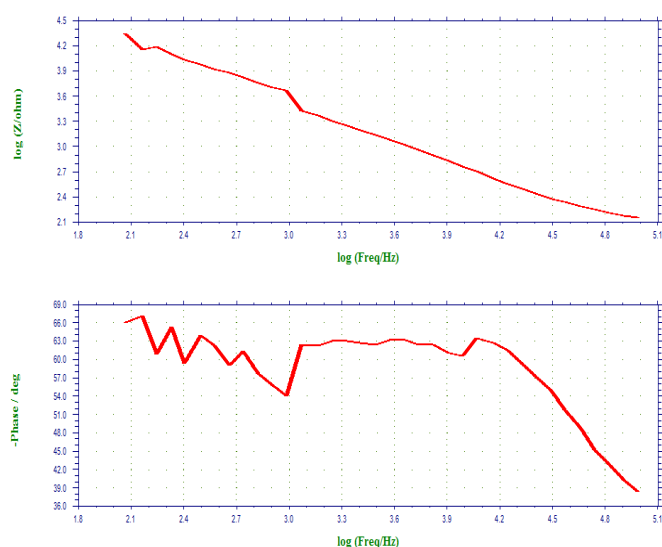


Figure 9. AC impedance spectra (Bode plot) of Thermoactive alloy immersed in AS+Coffee

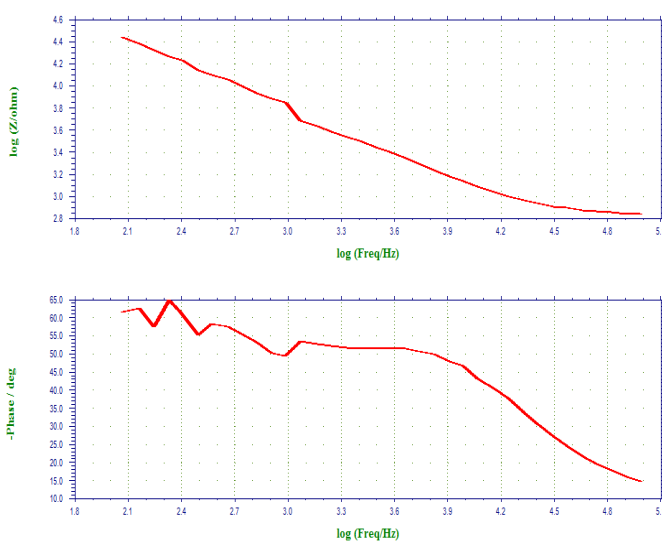


Figure 10. AC impedance spectra (Bode plot) of SS316L immersed in AS

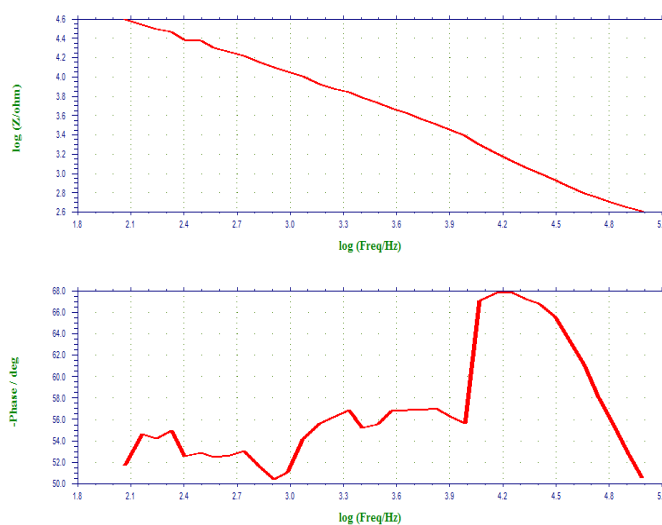


Figure 11. AC impedance spectra (Bode plot) of SS316L immersed in AS+Coffee

Conclusion

The present study led to the conclusion that in the presence of coffee in AS, the corrosion resistance of SS316L increased. In the presence of coffee in AS, the corrosion resistance of alloys decreased in the following order;

SS 316 L alloy > Thermoactive alloy > Ni-Ti alloy

Acknowledgement

The authors of thankful to their Managements.

References

- Saranya, R., Rajendran, S., Krishnaveni, A., Pandiyarajan, M., Nagalakshmi, R., *Eur. Chem. Bull.*, **2013**, 2(4), 163-170. DOI: 10.17628/ecb.2013.2.163-170
- Vieira, A. C., Ribeiro, A. R., Rocha, L. A., Celis, J. P., *WEAR*, **2006**, 261, 994. <https://doi.org/10.1016/j.wear.2006.03.031>
- Ziebowicz, A., Walke, W., Barucha Kepka, A., Kiel, M., *J. Achiev. Mater. Manuf. Engg.*, **2008**, 27, 151-154.
- Kiu, C. L., Chu, P. K., Lin, Q. Q., Yang, D. Z., *Corr. Sci.*, **2007**, 49, 3783. <https://doi.org/10.1016/j.corsci.2007.03.041>
- Rajendran, S., Chitra Devi, P., John Mary, S., Krishnaveni, A., Kanchana, S., Lidia Christy., Nagalakshmi, R., Narayana Samy, B., *Zastit. Mater.*, **2010**, 51(3), 149-158.
- Rajendran, S., Paul Raj, J., Regan, P., Jeyasundari, J., Manivanna, M., *J. Dent. Oral Hyg.*, **2009**, 1, 1-8.
- Rajendran, S., Uma, V., Krishnaveni, A., Jeyasundari, J., Shyamaladevi, B., Manivanna, M., *Arabian J. Sci. Engg.*, **2009**, 34(2), 147-158.
- Loto, C. A., Mohammed, A. Loto, I., *Corros. Prevent. Control*, **2003**, 50(3), 107-118.
- Loto, C. A., Mohammed, A. Loto., I., *Corros. Prevent. Control*, **2000**, 47(2), 50-56.
- Da Rocha, J. C., Da Cunha, P. G. J., Elia, E. D., *Corros. Sci.*, **2010**, 52(7), 2341-2348. <https://doi.org/10.1016/j.corsci.2010.03.033A>
- Okafor, P. C., Ebenso, E. E., *Pigment Resin Technol.*, **2007**, 36(3), 134-140. <https://doi.org/10.1108/03699420710748992>
- Priya, S. L., Chitra, A., Rajendran, S., Anuradha, K., *Surf. Engg.*, **2005**, 21(3), 229-231. <https://doi.org/10.1179/174329405X50073>
- Bouyanzer, A., Hammouti, B., *Bull. Electrochem.*, **2004**, 20(2), 63-65.
- Singh., A., Quraishi, M. A., *Res. Chem. Intermed.*, **2015**, 41(3), 2901-2914. <https://doi.org/10.1007/s11164-013-1398-3>
- Madhumitha, S., Priyadarshini, V., Sheela, A., Adithya, C., Sangeetha, M., Rajendran, S., *Int. J. Nano corr. Sci. Engg.*, **2016**, 3(4), 407-414.
- Lausmaa, J., Kasemo, J. B., Hansson, S., *Biomaterials*, **1985**, 6, 23-27. [https://doi.org/10.1016/0142-9612\(85\)90033-x](https://doi.org/10.1016/0142-9612(85)90033-x)
- Nakagawa, M., Malsuya, S., Shiraiishi, T., Ohta, M., *J. Dent. Res.*, **1999**, 78(9), 1568-1572. <https://doi.org/10.1177/00220345990780091201>
- Kononen., Mauno, Lavonius, H., Eeva, T., Kivilahti, K., *Dent. Mater.*, **1995**, 11, 269-272.

¹⁹Morshita, M., Chikuda, M., Astrida, Y., Morinaga, M., Yukawa, N., Adachi, H., *J. Japan Inst. Metals*, **1999**, *55*(6), 720-726. <https://doi.org/10.2320/jinstmet1952.55.6.720>

²⁰Watanabe, T., Narito, H., *J. Japan Inst. Metals*, **1988**, *52*(8), 780-785. <https://doi.org/10.2320/jinstmet1952.52.8.780>

²¹Kinani, L., Chtaini, A., *Leonardo J. Sci.*, **2007**, *11*, 33-40.

²²Saranya, R., Rajendran, S., Krishnaveni, A., Jayasundari, J., *Eur. Chem. Bull.* **2013**, *2*(6), 389-392. DOI: [10.17628/ecb.2013.2.389-392](https://doi.org/10.17628/ecb.2013.2.389-392)

Received: 13.05.2017.
Accepted: 27.06.2017.



NEW ENVIRONMENTALLY FRIENDLY METHOD FOR QUANTIFICATION OF CEFAZOLIN SODIUM

Bárbara Saú Rechelo,^[a] Felipe Hugo Alencar Fernandes,^[a] Ana Carolina Kogawa^{[a]*} and Hérica Regina Nunes Salgado^[a]

Keywords: Cefazolin sodium; quality control; visible spectrophotometry; green technique; eco-friendly method

Cefazolin sodium, a β -lactam antimicrobial agent belonging to the first generation cephalosporins, has a broad spectrum of action, acting against gram positive and gram negative bacteria. Stands out over other cephalosporins for its ability to also act against some species of *Enterobacter*, and have a long half-life, thus reducing the frequency of administrations. A simple, fast and reproducible method by visible spectrophotometry was developed and validated for quantification of cefazolin sodium in the lyophilized powder. This technique is widely used in the pharmaceutical industry due to its ease of execution, low cost, safety and high precision and accuracy. It has been employed in the quality control routine of numerous pharmaceuticals in order to identify them and quantify their active principles. The method was capable of detecting and quantifying the cefazolin sodium obtaining satisfactory results regarding selectivity, precision, accuracy and robustness, on linear range of 32.0 to 92.0 $\mu\text{g mL}^{-1}$, showing the correlation coefficient of 0.9993 when analyzed at 767 nm. Due to the environmental impacts caused by global economic development, green chemistry has come up with a proposal to minimize and/or eliminate the use of harmful solvents, which generate large amounts of toxic waste to the environment and the health of operators, as well as reducing expenses with costly processes. The proposed method does not use toxic solvent, proving to be effective, low cost, easy to apply and safe for the analyst and environment.

*Corresponding Authors

Fax: +55 16 3301 6967

E-Mail: ac_kogawa@yahoo.com.br

[a] ¹Department of Pharmaceutics, School of Pharmaceutical Sciences of Araraquara, Univ Estadual Paulista - UNESP, Araraquara, São Paulo, Brazil

Introduction

Cefazolin sodium (CFZ, Figure 1) is a β -lactam antimicrobial agent, belonging to the first generation of cephalosporins. It stands out because CFZ has activity against some species of *Enterobacter* and can be administered less frequently because of its longer half-life.¹⁻⁵ Its mechanism of action results from the inhibition of cell wall synthesis in Gram-negative and Gram-positive bacteria, preventing transpeptidases enzymes to form cross-links peptidoglycan in the bacterial cell wall.⁶⁻⁹

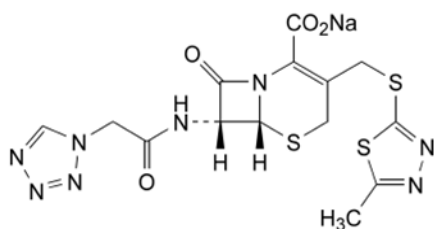


Figure 1. Chemical structure of cefazolin sodium (CAS 27164-46-1).

Considering the great importance of cefazolin sodium on the global scene in the treatment of infectious diseases, the development of practical, economical and reliable analytical methods, which can be used in the quality control of this drug, is essential and highly relevant, seeking the

therapeutic efficacy, patient's safety and also benefits for the pharmaceutical industries and compounding pharmacies.¹⁰

Cefazolin sodium has some analytical methods described in official compendia such as British,¹¹ European,¹² Japanese,¹³ Portuguese¹⁴ and US¹⁵ pharmacopeias. In the literature, several methods have been described for the qualitative¹⁶ and quantitative analysis of cefazolin sodium, included spectrophotometry,¹⁷⁻²⁹ high-performance liquid chromatography³⁰⁻⁴⁷ and voltammetry.⁴⁸ However, most of them were time-consuming and dedicated to sophisticated and expensive analytical instruments.

The methods found in the literature for the identification and quantification of sodium cefazolin use mostly mobile phases consisting of buffer solutions and solvents such as acetonitrile and trifluoroacetic acid, which, according to the concepts of green chemistry, are extremely aggressive to the environment.⁴⁹

The validation process is essential to set up a developed methodology is completely appropriate to the objectives which it is intended in order to obtain reliable results that can be satisfactorily interpreted. It involves the development of an analytical method, adaptation or implementation of a known method and an evaluation process to estimate its efficiency.⁵⁰

Looking for quality control and seeking to optimize processes in the industry, researches involving analytical methods are extremely important and highly relevant to improve analysis in the pharmaceutical industry and ensure the quality of the marketed product. As a complementary alternative to analytical methods existing to cefazolin sodium, this paper aimed to develop, validate and apply a low-cost analytical method, simple, fast, reproducible and safe to the environment and analyst by visible spectrophotometry for quantification of cefazolin sodium in powder for injection solution.

Experimentals

Material

Cefazolin sodium reference substance was a standard with a declared purity of 98.2 %, obtained from Sigma-Aldrich™. The samples were lyophilized powders in vials containing 1g, kindly supplied from ABL™.

Chemicals

Sodium carbonate was obtained from Synth™ and Folin-Ciocalteu reagent was obtained from Sigma-Aldrich™. Purified water was used to prepare all solutions. Was weighed 5.0g of sodium carbonate and transferred to 25 mL flask with water. It took to ultrasound for 30 minutes to complete solubilization and was completed the volume with purified water, yielding reagent with 5.0 % of final concentration.

Equipment

The method was performed in spectrophotometer UV-Vis Shimadzu, model UV 1800, using quartz cuvettes 1 cm optical path, under controlled temperature 25° C.

Ringbom's Curve

For the development of the visible spectrophotometric method, Ringbom's curve was constructed in order to establish the concentrations of work to which the drug has linearity. Aliquots of the standard stock solution of 200.0 µg mL⁻¹ were transferred using a micropipette to 10 mL volumetric flasks, and the volume was completed with purified water, in addition to sodium carbonate buffer and Folin-Ciocalteu reagent to obtain increasing concentrations 2.0-182.0 µg mL⁻¹.

Analytical Curve

For the development of the visible spectrophotometric method, the calibration curve was constructed to determine the range in which the drug has an increased linearity. Aliquots of stock solutions corresponding to 1.6, 2.2, 2.8, 3.4, 4.0 and 4.6 mL to 10.0 mL volumetric flasks. Were added to each volumetric flask aliquots of 300 µL of sodium carbonate buffer solution 5 % and 100 µL of Folin-Ciocalteu reagent. The volume was completed with purified water, for obtaining solutions with concentrations of 32.0, 44.0, 56.0, 68.0, 80.0 and 92.0 µg mL⁻¹, respectively.

Purified water, sodium carbonate buffer and Folin-Ciocalteu reagent were used as blank to reset the appliance.

Analytical Method Validation

On validation of analytical methods, as well in this research, the determined parameters was selectivity, linearity, precision, accuracy, robustness, limit of detection (LD) and limit of quantification (LQ).⁵⁰⁻⁵⁵

Linearity

The linearity of the method was obtained through the analysis of three analytical curves on three different days. The results obtained were analyzed to obtain the equation of the line by the least-squares method, and verification of the linearity was detected by Analysis of Variance (ANOVA).

Limits of detection (LD) and quantification (LQ)

The limit of detection (LD) and limit of quantification (LQ) were calculated by standard deviation of the intercept and the slope of the analytical curve. The equations are:

$$LD = \frac{3.3\sigma}{IC} \quad (1)$$

$$LQ = \frac{10\sigma}{IC} \quad (2)$$

Precision

The precision of the method was performed for repeatability and intermediate precision, which were evaluated by relative standard deviation (RSD).

Repeatability

The repeatability was determined by analysis of six solutions of cefazolin sodium at a concentration of 56.0 µg mL⁻¹ prepared on the same day. Thus, results were obtained using the same experimental conditions.

Intermediate precision

The intermediate precision was evaluated through analysis of six solutions of cefazolin sodium at a concentration of 56.0 µg mL⁻¹ were prepared and executed by different analysts in different days under the same experimental conditions.

Selectivity

Three scans on spectrophotometer were performed for the study of selectivity of the proposed method, both between 380-780 nm: the first scan was made with a standard solution of cefazolin sodium at 56.0 µg mL⁻¹, the second scan was made with a solution of cefazolin sodium in lyophilized powder at same concentration, and the third was made with a solution containing only the chosen solvent (purified water, sodium carbonate buffer and Folin-Ciocalteu reagent).

Accuracy

The solutions were prepared according to Table 1.

Table 1. Preparation of test solutions for accuracy parameter of the visible spectrophotometric method at 767 nm.

	Volume (mL) of CFZ solution (200.0 µg mL ⁻¹)		Theoretical concentration (µg mL ⁻¹)*
	sample	standard	
Sample	1.6	-	32.0
R ₁	1.6	0.6	44.0
R ₂	1.6	1.2	56.0
R ₃	1.6	1.8	68.0
Standard	-	1.6	32.0

* 10 mL volumetric flask

Robustness

The robustness of the method was determined by comparing the contents obtained by varying the wavelength and evaluated by the test F and Student's t test.

Determination of cefazolin sodium content in lyophilized powder

Solutions of 56.0 µg mL⁻¹CFZ were prepared in triplicate, on three different days and analyzed by spectrophotometer at 767 nm. The content of cefazolin sodium was calculated, according to Equation 3.

$$C_S = \frac{A_S C_{RS}}{A_{RS}} \quad (3)$$

where

C_S = concentration of the sample

A_S = absorbance of the sample

C_{RS} = concentration of the reference substance

A_{RS} = absorbance of the reference substance

Results

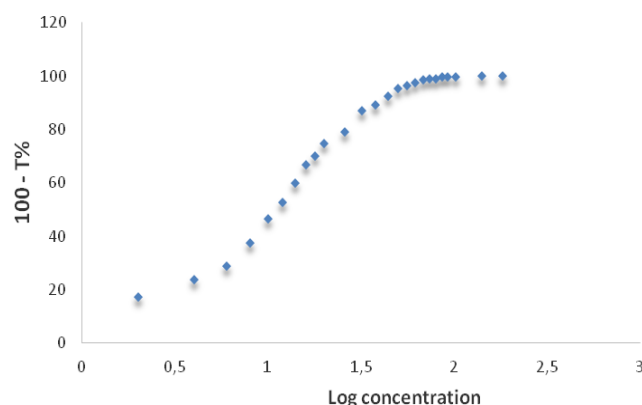
Cefazolin sodium reacts with Folin-Ciocalteu reagent to form a blue solution at 767 nm.

Ringbom's Curve

The absorbance of concentrations between 2.0 to 182.0 µg mL⁻¹ was converted to transmittance. These data were plotted on a graph of transmittance versus log concentration of cefazolin sodium reference substance as shown in Figure 2.

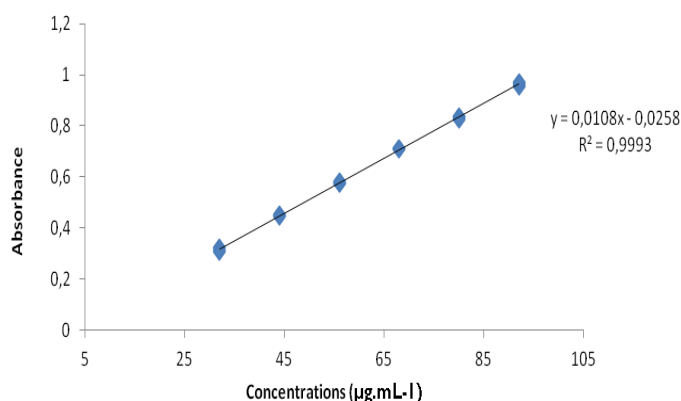
Analytical methods validation

The choice of cefazolin sodium study conducting in concentration of 56.0 µg mL⁻¹ to assays of precision (repeatability and intermediate precision), selectivity and determination of the content is justified as being the midpoint of the working range established by Ringbom's curve.

**Figure 2.** Ringbom's curve obtained by visible spectrophotometric method to cefazolin sodium standard.

Linearity

The analytical curve of cefazolin sodium was built with the average of the absorbance values of three analytical curves with concentrations from 32.0 to 92.0 µg mL⁻¹, obtained during the linearity test. Figure 3 shows the corresponding analytical curve.

**Figure 3.** Analytical curve of cefazolin sodium, at concentrations 32.0; 44.0; 56.0; 68.0; 80.0 e 92.0 µg mL⁻¹, obtained by visible spectrophotometric method.

The equation of line determined by the method of least squares was $y = 0.0108x - 0.0258$, with a coefficient of determination (R^2) equal to 0.9993 and correlation coefficient (r) equal to 0.9996 to cefazolin sodium standard.

The ANOVA calculated for the data from the analytical curve is shown in Table 2.

Limits of detection (LD) and quantification (LQ)

The results of limit of detection (LD) and limit of quantification (LQ) were 1.45 and 4.38 µg mL⁻¹, respectively.

Table 2. Analysis of variance of absorbance values determined in the linearity parameter for cefazolin sodium

SOURCE	DF	SS	MS	F _{calcd.}	F _{crit.}
Model	1	0.875459433	0.875459433	1.16	4.12
Residues	16	0.000630844	3.94278E-05	22204.13*	4.49
Lack of fit	4	0.000123511	3.08778E-05	0.73	3.26
Pure error	12	0.000507333	4.22778E-05		
TOTAL	17	0.876090278			

* Significant at $p < 0.05$ %; DF = degrees of freedom; SS = sequential sum of squares; MS = adjusted mean squares

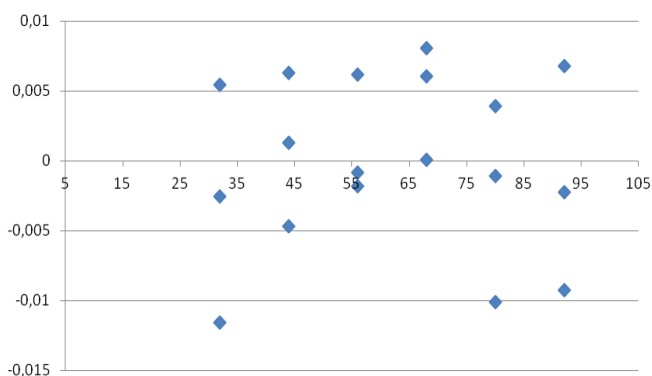
Table 3. Values determined for the precision parameter of cefazolin sodium by visible spectrophotometric method

	Absorbances						RSD (%)
Repeatability	0.578	0.588	0.591	0.574	0.582	0.590	1.19
Intermediate Precision	0.583	0.574	0.580	0.576	0.582	0.576	0.76
	0.581	0.589	0.579	0.574	0.577	0.582	

* RSD = relative standard deviation

Table 4. Results of the recovery test by visible spectrophotometric method

	Cefazolin sodium added (mL)	Cefazolin sodium recovered (mL)	Recovery (%)	Average Recovery (%)	RSD (%)
R1	0.6	0.60	99.79	100.58	0.69
R2	1.2	1.21	101.03		
R3	1.8	1.82	100.93		

**Figure 4.** Residue analysis for cefazolin sodium in lyophilized powder obtained by visible spectrophotometric method.

Precision, selectivity and accuracy

The results of precision are shown in Table 3.

The spectra analysis present that all reagents did not interfere in the visible spectrophotometric method, showing the selectivity of this procedure.

Table 4 shows the recovery values obtained for each concentration level tested in the accuracy parameter of visible spectrophotometric method for cefazolin sodium.

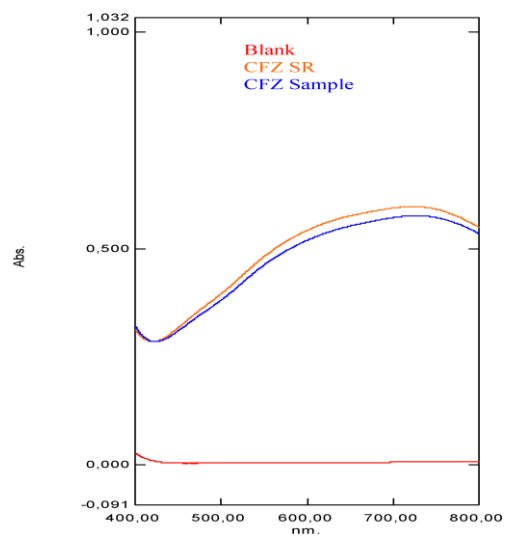
**Figure 5.** Overlap of the visible spectrophotometric spectra referring the solutions at a concentration of $56.0 \mu\text{g mL}^{-1}$ of blank, cefazolin sodium in lyophilized powder and cefazolin sodium reference.

Table 5. Evaluation of the robustness of the analytical method for analysis of cefazolin sodium by visible spectrophotometry.

Length of wave (nm)	Absorbance 1	Absorbance 2	Absorbance 3	Average absorbance	RSD (%)
767	0.571	0.583	0.564	0.573 ± 0.004	1.68
760	0.578	0.571	0.574	0.574 ± 0.010	0.61

Robustness

The changes in the wavelength of absorption are shown in Table 5.

The average variations in wavelength selected for the study to assess the robustness parameter were statistically analyzed, and the results are shown in Table 6.

Table 6. Statistical analysis of the variation of wavelength in the visible spectrophotometric method

	Statistical test			
	$F_{\text{calculated}}$	F_{critical}	$t_{\text{calculated}}$	T_{critical}
Wavelength 767 and 760 nm	1.42	5.05	-0.79	2.23

Determination of cefazolin sodium content

The assay was performed by comparing the absorbance obtained in analysis of cefazolin sodium standard and samples, both at a concentration of 56.0 $\mu\text{g mL}^{-1}$. The results are shown in Table 7.

Table 7. Values determined for the dosing of cefazolin sodium by visible spectrophotometric method

Day	Content of CFZ*		Average content, %	RSD (%)
	mg	%		
1	56.26	100.46	100.32	0.18
2	56.06	100.11		
3	56.22	100.40		

* Each value is the average of six determinations

Discussion

The reported methods for the determination of cefazolin sodium are complex, expensive, time-consuming or require the use of large amounts of organic solvents^[66]. In this research, a non-toxic solvent was chosen in order to obtain a low cost and environmentally friendly visible spectrophotometric method for quantification of cefazolin sodium in lyophilized powder.

Quantitative visible spectrophotometric analysis has as its principle the direct relationship between the amount of light absorbed and the concentration of the substances, also known as Lambert-Beer law.²¹ This region, in pharmaceutical analysis, is widely used for identification and assay of drug and medicines.²¹ All spectrophotometric techniques are

based on chemical interaction with a radiant energy and, in most cases, the effect of this interaction is the energy absorption by the material being analyzed.¹⁶

These features make spectrophotometric techniques particularly suitable for the determination of low concentrations of clinically important compounds.²⁴ The method has shorter analysis time, are economically most suitable and do not generate chemical waste too much.^{24, 60-65}

Proper wavelength selection of the methods depends upon the nature of sample, and its solubility.⁵⁶ Cefazolin sodium is completely soluble in water.²¹ Thus, purified water was chosen to be used as a solvent presenting appropriate features in the spectra, such as a good absorption intensity of the functional chromophore groups present on the molecule; besides easy acquisition, disposal, low cost and environmental advantages, since it does not generate toxic waste to the operator and the ecosystem.^{21, 56} The wavelength of 767 nm was chosen due to the adequate molar absorptivity of cefazolin sodium in this region.

Cefazolin sodium, in its chemical structure, presents moments of molecular resonance, allowing the intermediates to have electronic density close to the phenolic compounds. Spectrophotometric quantification of phenolic compounds is accomplished by a variety of techniques, however, the one utilizing Folin-Ciocalteu reagent is among the most extensively used. The reagent consists of a mixture of phosphomolybdic and phosphotungstic acids, in which molybdenum and tungsten are in the +6 oxidation state, but in the presence of certain reducing agents, such as phenolic compounds, they form the so-called blue molybdenum and blue tungsten.^{58, 59}

During the development of the visible spectrophotometric method for quantification of cefazolin sodium in the pharmaceutical form powder for injection solution, were tested concentrations that varied from 2.0 to 182.0 $\mu\text{g mL}^{-1}$. The concentrations from 32.0 to 92.0 $\mu\text{g mL}^{-1}$, since this group showed linearity of response.

The linearity of the method, we constructed a graph of concentration versus absorbance, which showed proportionality between both. Residue analysis indicated that the regression model used is appropriate. Each average value of absolute areas obtained in determining the analytical curve was plotted in relation to its concentration, observing linearity in the range of 32-92 $\mu\text{g mL}^{-1}$, as shown in Figure 4. The results for linearity were statistically analyzed using tests of variance (ANOVA); according to ANOVA there is no deviation from linearity in calibration curve and the regression model is appropriate.

The calculated values for the limits of detection and quantification of cefazolin sodium in lyophilized powder is an estimate (LD = 1.45 $\mu\text{g mL}^{-1}$ and LQ = 4.38 $\mu\text{g mL}^{-1}$).

These values indicate the ability of this method to reliably detect and quantify cefazolin sodium in its pharmaceutical dosage form.

The precision of the method was evaluated in two different ways: by repeatability (intraday precision) and intermediate precision (interday and inter-analyst precisions). The results are presented in Table 4. The intraday precision ($n = 6$) gave an RSD value of 1.19 %. The RSD values observed in intermediate precision ($n = 12$) was 0.76 %, demonstrating appropriate precision of the method.

The accuracy of the method was determined by measuring the reference standard recovery in triplicate at three levels (R1, R2 and R3), from 80 to 120 % of the method concentration ($56.0 \mu\text{g mL}^{-1}$), according to ICH recommendation.⁵⁴ The accuracy was determined using a recovery assay performed at three concentration levels (Table 5). The recovery test is an experimental design to verify the relationship between the amount of substance added and the amount quantified by this assay.⁵⁷ Thus, the data demonstrates adequate accuracy of the method, since the experimental concentrations were very close to the real values (close to 100 %).

Changes in the wavelength of absorption were performed to evaluate the robustness of the method. During the analysis of the pharmaceutical product, the levels found no significant difference and RSD were below 0.61 %, demonstrating the robustness of the proposed method, compared to the measured parameter, as shown in Tables 6 and 7.

The content of cefazolin sodium in lyophilized powder was 100.32 %. The proposed visible spectrophotometric method met all requirements required by the official codes agency guidelines,^{15,51,54-55} making it adequate, presenting linearity, precision, selectivity, accuracy and robustness, and can be used for assay of cefazolin sodium in lyophilized powder at quality control laboratories.

Conclusion

The validation of analytical methods is the way to ensure that the developed process is safe and meets the requirements of official compendia, demonstrating reliability and reproducibility of the results. Green chemistry is important for the development of methods that are less harmful to the environment, less costly, and have the same reliability and reproducibility of conventional methods.

All validation parameters found to be highly satisfactory, indicating selectivity, linearity, precision, accuracy, robustness and adequate detection and quantification limits, with no significant statistical difference. The method, therefore, can be applied in routine of quality control laboratories, due to its ease to execute, low cost, low generation of toxic waste and safety for analyst and environmental.

Acknowledgement

The authors are grateful to ABL™ to the supplied of the samples, CNPq (Brasília, Brazil) and FAPESP (São Paulo, Brazil) for their financial support.

References

- ¹El-Shaboury, S. R., Saleh, G. A., Mohamed, F. A., Rageh, A. H. Analysis of cephalosporin antibiotics. *J. Pharm. Biomed. Anal.*, **2007**, *45*, 1-19. <https://doi.org/10.1016/j.jpba.2007.06.002>
- ²Hardman, J. G., Limbird, L. E., Goodman & Gilman: *the pharmacological basis of therapeutics*. 11th. New York: McGraw-Hill, **2006**, p. 1206-1213.
- ³Neu, H. C. Cephalosporin antibiotics: molecules that respond to different needs. *Am. J. Surgery*, **1988**, *155*(1), p. 1-4, 1988. [https://doi.org/10.1016/S0002-9610\(88\)80204-6](https://doi.org/10.1016/S0002-9610(88)80204-6)
- ⁴Pichichero, M. E. Use of selected cephalosporins in penicillin-allergic patients: a paradigm shift. *Diagn. Microbiol. Infect. Disease*, **2007**, *57*(3), 3-8. <https://doi.org/10.1016/j.diagmicrobio.2006.12.004>
- ⁵Sweetman, S. C., Martindale: the complete drug reference. 36th. London: Pharmaceutical Press, **2009**. 3694 p.
- ⁶Ohannesian, S., *Handbook of Pharmaceutical Analysis*. New York: Informa Health Care, **2002**, 585 p.
- ⁷Watson, D., *Pharmaceutical Analysis: a textbook for pharmacy students and pharmaceuticals chemists*. London: Churchill Livingstone, **1999**, 337 p.
- ⁸Alekseev, V. D., Drug synthesis methods and manufacturing technology. *Pharm. Chem. J.*, **2010**, *44*(1), 16-26.
- ⁹Kristen, R., Levinson, M. E., Ksyse, D., Clinical and in vitro evaluation of cefazolin, a new cephalosporin antibiotic. *Antimicrobial Agents and Chemotherapy*, v. 3, n. 2, p. 168-174, 1973. <https://doi.org/10.1128/AAC.3.2.168>
- ¹⁰Tótolí, E. G., Salgado, H R. N., Development of an innovative, ecological and stability-indicating analytical method for semiquantitative analysis of ampicillin sodium for injection by thin-layer chromatography (TLC). *World J. Pharm. Pharm. Sci.*, **2014**, *3*(1), 1944-1957.
- ¹¹BP. BRITISH PHARMACOPEIA, London: The Stationary Office, **2010**, *1*, 396-398
- ¹²EP. EUROPEAN PHARMACOPEIA. Council of Europe, **2005**, *2*, 1220-1222.
- ¹³JP. JAPANESE PHARMACOPEIA, Tokyo: Society of Japanese Pharmacopeia, **2011**, 16th.
- ¹⁴FP. FARMACOPÉIA PORTUGUESA, Lisboa: Imprensa Nacional, **2005**, 6th, 166-168.
- ¹⁵USP. THE UNITED STATES PHARMACOPEIA., Rockville: The United States Pharmacopeia Convention, **2016**, 39th.
- ¹⁶Pedroso, T. M., Salgado, H. R. N., Methods for qualitative analysis of cefazolin sodium raw material and pharmaceutical product. *Phys. Chem.*, **2013**, *3*(9), 29-38,
- ¹⁷Ali, S. M., Elbashir, A. A., Aboul-Enein, H. Y., Spectroscopic methods for analysis of cephalosporins in pharmaceutical formulations. *World J. Anal. Chem.*, **2015**, *3*(1), 21-32.
- ¹⁸Saleh, G. A., Askal, H. F., Darwish, I. A., El-Shorbagi, A. N. A., Spectroscopic analytical study for the charge-transfer complexation of certain cephalosporins with chloranilic acid. *Anal. Sci.*, **2003**, *19*, 281-287. <https://doi.org/10.2116/analsci.19.281>

- ¹⁹Ayad, M. M., Shalaby, A. A., Abdellatef, H. E., El Said, H. M., Spectrophotometric and atomic absorption spectrometric determination of certain cephalosporins. *J. Pharm. Biomed. Anal.*, **1999**, *18*, 975-983. [https://doi.org/10.1016/S0731-7085\(98\)00106-X](https://doi.org/10.1016/S0731-7085(98)00106-X)
- ²⁰Saleh, G. A., Askal, H. F., Radwan, M. F., Omar, M. A., Use of charge-transfer complexation in the spectrophotometric analysis of certain cephalosporins. *Talanta*, **2001**, *54*, 1205-1215, 2001. [https://doi.org/10.1016/S0039-9140\(01\)00409-X](https://doi.org/10.1016/S0039-9140(01)00409-X)
- ²¹Pedroso, T. M., Salgado, H. R. N., Validation of cefazolin sodium in pharmaceutical dosage forms by UV-spectrophotometric method. *Phys. Chem.*, **2013**, *3*, 11-20, 2013.
- ²²Omar, M. A., Abdelmageed, O. H., Tamer, Z., Attia, T. Z., Kinetic spectrophotometric determination of certain cephalosporins in pharmaceutical formulations. *Int. J. Anal. Chem.*, **2009**, 1-12. <https://doi.org/10.1155/2009/596379>
- ²³Al-Momani, I. F., Spectrophotometric determination of selected cephalosporins in drug formulations using flow injection analysis. *J. Pharm. Biomed. Anal.*, **2001**, *25*, 751-757. [https://doi.org/10.1016/S0731-7085\(01\)00368-5](https://doi.org/10.1016/S0731-7085(01)00368-5)
- ²⁴Amin, A. S., Ragab, G. H., Spectrophotometric determination of certain cephalosporins in pure form and pharmaceutical formulations. *Spectrochim. Acta*, **2004**, *60*, 2831-2835. <https://doi.org/10.1016/j.saa.2003.12.049>
- ²⁵Agbaba, D., Eric, S.; Karlijkovic-Rajic, K., Zivanov, S., Stakic, D., Spectrophotometric determination of certain cephalosporins using ferric hydroxamate method. *Spectr. Lett.*, **1997**, *30*(2), 309-319. <https://doi.org/10.1080/00387019708006990>
- ²⁶Ogorevc, B., Hudnik, V., A spectroscopic and polarographic investigation of the complexation of cefazolin with copper (II) ions. *Inorg. Chim. Acta*, **1985**, *108*, L3-L6. [https://doi.org/10.1016/S0020-1693\(00\)84312-1](https://doi.org/10.1016/S0020-1693(00)84312-1)
- ²⁷Kalinkova, G. N., Ovcharova, G., Gagavzov, I., Kretev, V., Petrov, L., Comparative IR-spectral studies of different modifications of the antibiotic cefazolin Na. *J. Mol. Struct.*, **1990**, *219*, 329-334. [https://doi.org/10.1016/0022-2860\(90\)80077-W](https://doi.org/10.1016/0022-2860(90)80077-W)
- ²⁸Elizarova, T. E., Shtyleva, S. V., Pleteneva, T. V., Using near-infrared spectrophotometry for the identification of pharmaceutical and drugs. *Pharm. Chem. J.*, **2008**, *42*(7), 432-434. <https://doi.org/10.1007/s11094-008-0146-2>
- ²⁹Halaleh, M. I. H., Abu-Nameh, E. S. M., Jamhour, R. M. A. Q., Direct titration and indirect spectrophotometric determination of selected cephalosporins. *Acta Pol. Pharm.*, **1998**, *55*(2), 93-97.
- ³⁰Moore, C. M.; Sato, K., High-performance liquid chromatography determination of cephalosporin antibiotics using 0.3 mm I.D. columns. *J. Chromy. A*, **1991**, *539*, 215-220. [https://doi.org/10.1016/S0021-9673\(01\)95377-4](https://doi.org/10.1016/S0021-9673(01)95377-4)
- ³¹Tsai, T. H.; Chen, Y. F., Simultaneous determination of cefazolin in rat blood and brain by microdialysis and microbore liquid chromatography. *Biomed. Chromy.*, **2000**, *14*, 274-278. [https://doi.org/10.1002/1099-0801\(200006\)14:4<274::AID-BMC985>3.0.CO;2-H](https://doi.org/10.1002/1099-0801(200006)14:4<274::AID-BMC985>3.0.CO;2-H)
- ³²Sørensen, L. K.; Snor, L. K., Determination of cephalosporins in raw bovine milk by high-performance liquid chromatography. *J. Chromy. A*, **2000**, *882*, 145-151. [https://doi.org/10.1016/S0021-9673\(99\)01317-5](https://doi.org/10.1016/S0021-9673(99)01317-5)
- ³³Pedroso, T. M., Salgado, H. R. N., Validation of analytical methodology for quantification of cefazolin sodium pharmaceutical industry. *Braz. J. Pharm. Sci.*, **2013**, *50*, 213-223, 2013. <https://doi.org/10.1590/S1984-82502011000100022>
- ³⁴Samanidou, V. F., Hapeshi, E. A., Papadoyannis, I. N., Rapid and sensitive high-performance liquid chromatographic determination of four cephalosporins antibiotics in pharmaceuticals and body fluids. *J. Chromy. B*, **2003**, *788*, 147-158. [https://doi.org/10.1016/S1570-0232\(02\)01040-1](https://doi.org/10.1016/S1570-0232(02)01040-1)
- ³⁵Ohmori, T., Suzuki, A., Niwa, T., Ushikoshi, H., Shirai, K., Yoshida, S., Ogura, S., Itoh, Y., Simultaneous determination of eight β -lactam antibiotics in human serum by liquid chromatography-tandem mass spectrometry. *J. Chromy. B*, **2011**, *879*, 1038-1042. <https://doi.org/10.1016/j.jchromb.2011.03.001>
- ³⁶Liang, D., Chow, D., White, C. High-performance liquid chromatographic assay of cefazolin in rat tissues. *J. Chromy. B*, **1994**, *656*, 460-465. [https://doi.org/10.1016/S0378-4347\(94\)80109-6](https://doi.org/10.1016/S0378-4347(94)80109-6)
- ³⁷Chan, C. Y., Chan, K., French, G. L. Rapid high-performance liquid chromatographic assay of cephalosporins in biological fluids. *J. Antimicrob. Chemotherapy*, **1986**, *18*(4), 537-545. <https://doi.org/10.1093/jac/18.4.537>
- ³⁸Lalitha, N.; Sanjay, P. P. N.; Vyshak. M. G.; Kadri, U. Stability-indicating reverse phase HPLC method for the determination of cefazolin. *Tropical J. Pharm. Res.*, **2010**, *9*(1), 45-50. <https://doi.org/10.4314/tjpr.v9i1.52034>
- ³⁹Al-Rawithi, S., Hussein, R., Raines, D. A., Al-Showaier, I., Kurdi, W., Sensitive assay for determination of cefazolin or ceftriaxone in plasma utilizing LC. *J. Pharm. Biomed. Anal.*, **2000**, *22*, 281-286. [https://doi.org/10.1016/S0731-7085\(99\)00273-3](https://doi.org/10.1016/S0731-7085(99)00273-3)
- ⁴⁰Annesley, T., Wilkerson, K., Matz, K., Giacherio, D., Simultaneous determination of penicillin and cephalosporin antibiotics in serum by gradient liquid chromatography. *Clin. Chem.*, **1984**, *30*(6), 908-910.
- ⁴¹Arayne, M. S., Sultana, N., Bi, Z., Simultaneous determination of cefazolin or ceftizoxime in the presence of ascorbic acid from pharmaceutical formulation and human serum by RP-HPLC. *Pak. J. Pharm. Sci.*, **2007**, *1*, 56-61.
- ⁴²Baranowska, I., Markowski, P., Baranowski, J., Simultaneous determination of 11 drugs belonging to four different groups in human urine samples by reversed-phase high-performance liquid chromatography method. *Anal. Chim. Acta*, **2006**, *570*, 46-58. <https://doi.org/10.1016/j.aca.2006.04.002>
- ⁴³Bayomi, S. M., Vallner, J. J., Dipiro, J. T., Quantitative of cefazolin sodium in plasma and tissues by high-performance liquid chromatography. *Int. J. Pharm.*, **1986**, *30*, 57-61. [https://doi.org/10.1016/0378-5173\(86\)90135-3](https://doi.org/10.1016/0378-5173(86)90135-3)
- ⁴⁴Bompadre, S., Leone, F., Ferrante, L., Alo, F. P.; Ioannidis, G., Determination of cefazolin in human serum by high-performance liquid chromatography with on-line solid-phase extraction. *J. Liq. Chromy. Related Technol.*, **1998**, *21*(3), 417-426. <https://doi.org/10.1080/10826079808000500>
- ⁴⁵Brisson, A. M., Fortillan, J. B., Determination of cephalosporins in biological material by reversed-phase liquid column chromatography. *J. Chromy.*, **1981**, *223*, 393-399. [https://doi.org/10.1016/S0378-4347\(00\)80112-7](https://doi.org/10.1016/S0378-4347(00)80112-7)
- ⁴⁶Danzer, L. A., Liquid-chromatography determination of cephalosporins and chloramphenicol in serum. *Clin. Chem.*, **1983**, *29*(5), 856-858.
- ⁴⁷Farthing, C., Farthing, D., Brophy, D. F., Larus, T., Maynor, L., Fakhry, I., Gehr, T. W. B., High-performance liquid chromatography determination of cefepime and cefazolin in human plasma and dialysate. *Chromatographia*, **2008**, *67*(5-6), 441-447. <https://doi.org/10.1365/s10337-008-0529-2>
- ⁴⁸El-Desoky, H. S., Ghoneim, E. M., Ghoneim, M. M., Voltammetric behavior and assay of the antibiotic drug cefazolin sodium in bulk form and pharmaceutical formulation at a mercury electrode. *J. Pharm. Biomed. Anal.*, **2005**, *39*, 1051-1056. <https://doi.org/10.1016/j.jpba.2005.05.020>
- ⁴⁹Carioca, J. O. B., *Brazilian Network on Green Chemistry: Awareness, Responsibility and Action*. Universidade Estadual do Ceará: Fortaleza, **2008**.
- ⁵⁰Brito, N. M., Junior, O. P. A., Polese, L., Ribeiro, M. L., Validação de métodos analíticos: Estratégia e discussão. *Rev. Ecotoxicol. Meio Ambiente*, **2003**, *13*, 129-146. <https://doi.org/10.5380/pes.v13i0.3173>

- ⁵⁰BRASIL, Ministério da Saúde. Resolução RE 899, de 29 de maio de 2003. Determina a publicação do "Guia para validação de métodos analíticos e bioanalíticos". Diário Oficial da União, Brasília, 02 de junho 2003. Seção 1.
- ⁵¹ISO - INTERNATIONAL STANDARD ORGANIZATION; General Requirements for the Competence of Testing and Calibration Laboratories, ISO/IEC 17025, 1999.
- ⁵²INSTITUTO NACIONAL DE METROLOGIA, NORMALIZAÇÃO E QUALIDADE INDUSTRIAL (INMETRO). Orientação sobre validação de métodos de ensaios químicos, DOQ-CGCRE-008, 2011.
- ⁵³Int. Conf. Harmonization, (ICH). Validation of Analytical Procedures: Text and Methodology Q2(R1), Geneva, 2005.
- ⁵⁴Chierentin, L., Salgado, H. R. N., Performance characteristics of UV and visible spectrophotometry methods for quantitative determination norfloxacin in tablets. *J. Sci. Res.*, 2014, 6, 531-541. <https://doi.org/10.3329/jsr.v6i3.18381>
- ⁵⁵Marona, H. R. N., Schapoval, E. E. S., Spectrophotometric determination of sparfloracin in tablets. *J. Antimicrob. Chemotherapy*, 1999, 44(1), 136-137. <https://doi.org/10.1093/jac/44.1.136>
- ⁵⁶Furlan, C. M., Santos, K. P., Sedano-Partida, M. D., Motta, L. B., Santos, D. Y. A., Salatino, M. L. F., Negri, G., Berry, P. E., Van-Ee, B. W., Salatino, A., Flavonoids and antioxidant potential of nine Argentinian species of Croton (Euphorbiaceae). *Braz. J. Botany*, 2015, 38(4), 693-702. <https://doi.org/10.1007/s40415-014-0115-9>
- ⁵⁷Sousa, C. M. M., Silva, H. R., Vieira-Jr, G. M., Ayres, M. C. C., Costa, C. L. S., Araújo, D. S., Cavalcante, L. C. D., Barros, E. D. S., Araújo, P. B. M., Brandão, M. S., Chaves, M. H., Fenóis totais e atividade antioxidante de cinco plantas medicinais. *Quim. Nova*, 2007, 30(2), 351-355. <https://doi.org/10.1590/S0100-40422007000200021>
- ⁵⁸Moreno, A., Salgado, H. R. N., Spectrophotometric determination of ceftazidime in pharmaceutical preparations using neocuproin as a complexing agent. *Anal. Lett.*, 2008, 41(12), 2143-2152. <https://doi.org/10.1080/00032710802240818>
- ⁵⁹Marona, H. R. N., Schapoval, E. E. S. Spectrophotometric determination of sparfloracin in pharmaceutical formulation using bromothymol blue. *J. Pharm. Biomed. Anal.*, 2001, 26(3), 501-504. [https://doi.org/10.1016/S0731-7085\(01\)00429-0](https://doi.org/10.1016/S0731-7085(01)00429-0)
- ⁶⁰Silva, L. M., Almeida, A. E., Salgado, H. R. N., Thermal analysis and validation of UV and visible spectrophotometric methods for the determination of new antibiotic tigecycline in pharmaceutical product. *Adv. Anal. Chem.*, 2012, 2(1), 10-15.
- ⁶¹Kogawa, A. C., Salgado, H. R. N., Quantification of doxycycline hyclate in tablets by ultraviolet spectrophotometric method. *World Res. J. Pharm. Res.*, 2013, 1(2), 21-24.
- ⁶²Kogawa, A. C., Salgado, H. R. N., Quantification of rifaximin in tablets by spectrophotometric method ecofriendly in ultraviolet region. *Scientifica*, 2016, n. 3463405, 1-9. <https://doi.org/10.1155/2016/3463405>
- ⁶³Brbaklic, V., Kogawa, A. C., Salgado, H. R. N. Quantification of rifaximin in tablets by an environmentally friendly visible spectrophotometric method. *Current Pharm. Anal.*, 2016, 12, DOI 10.2174/1573412912666160906144024

Received: 15.05.2017.

Accepted: 28.06.2017.



SYNTHESIS OF THIENOPYRIMIDINE DERIVATIVES STARTING FROM THIOPHENE AND PYRIMIDINE RINGS

Abdelreheem A. Saddik,^{[a][b]*} Adel M. Kamal El-Dean,^[a] Khairy M. Hassan,^[a]
and Mohamed S. Abbady^[a]

Keywords: thieno[3,4-*d*]pyrimidines; thieno[3,2-*d*]pyrimidines; thieno[2,3-*d*]pyrimidines.

Thienopyrimidines derivatives continue to attract great interest due to the wide variety of interesting biological activities observed for compounds characterized by this heterocyclic system. This review results from the literature survey containing the synthesis of thieno[2,3-*d*]pyrimidines, thieno[3,2-*d*]pyrimidines and thieno[3,4-*d*]pyrimidines from thiophene ring then build pyrimidine ring and from pyrimidine ring then build thiophene ring.

* Corresponding Authors

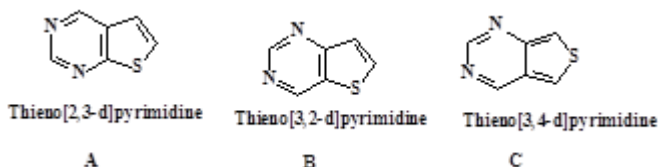
E-Mail: abdelraheemseddik@gmail.com

[a] Chemistry Department, Faculty of Science, Assiut University, Assiut 71516, Egypt

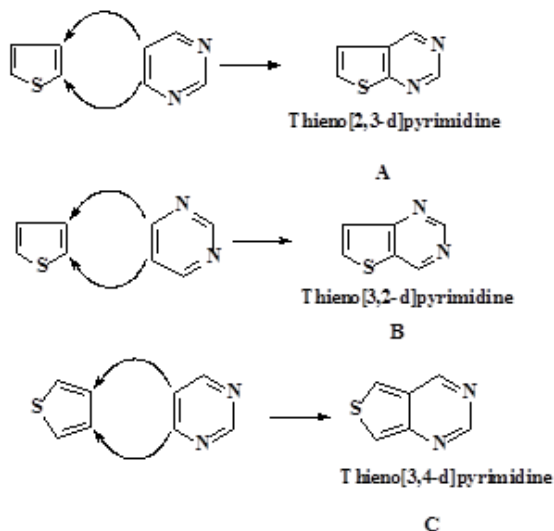
[b] Department of Materials Science and Engineering National Chiao Tung University Hsinchu, 300, Taiwan (Republic of China)

Introduction

Thienopyrimidine can be represented in three structures as shown below.¹



Synthesis of thienopyrimidines was accomplished either starting with thiophene moiety followed by construction of pyrimidine moiety on it or starting with pyrimidine nucleus followed by construction of thiophene block on it.



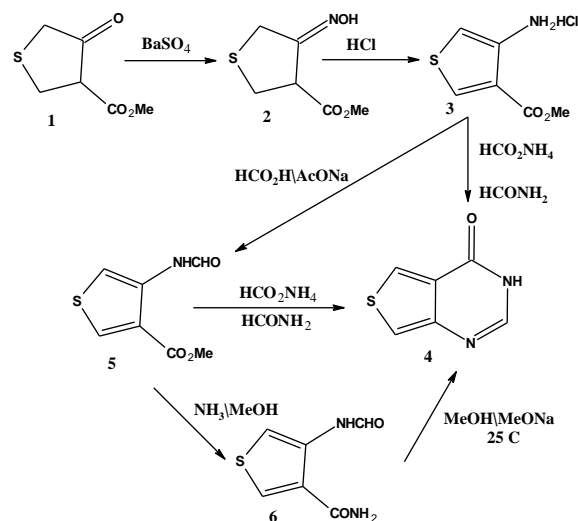
Synthesis

Preparation of thieno[3,4-*d*]pyrimidine

a) From 4-oxo-tetrahydrothiophene-3-carboxylate

3-Methyl 4-oxo-tetrahydrothiophene-3-carboxylate (**1**)² was converted to the oxime (**2**) by reacting with hydroxylamine hydrochloride in methanol and barium carbonate. The produced oxime was rearranged with hydrogen chloride in methanol at room temperature³ into 3-amino-4-carbomethoxythiophene (**3**). Methyl 4-amino thiophene-3-carboxylate (**4**) was converted into thieno[3,4-*d*]pyrimidin-4(3H)-one (**3**) by reacting with formamide at 175 °C in the presence of ammonium formate in 71 % yield.⁴

Application of these conditions in the case of the free base, compound (**3**) gave only traces of the desired (**4**) along with large amounts of tar. Since aminothiophene bases are notoriously unstable, the molecule was stabilized by formylation with formic acid in the presence of sodium acetate to give (**5**) in 59 % yield, which when treated with ammonium formate and formamide at 145 °C gave a 50 % yield of the thienopyrimidine (**4**).

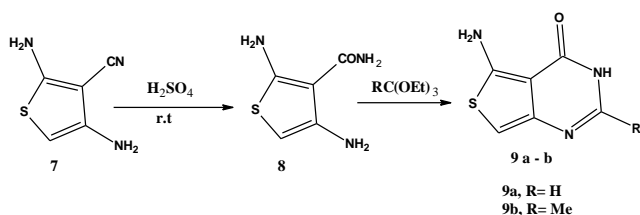


Scheme 1.

On the other hand, methyl 4-formamidothiophene-3-carboxylate (**5**) was converted into the corresponding 4-formamidothiophene-3-carboxamide (**6**) using methanolic ammonia solution which easily gave thienopyrimidine (**4**) with methanolic sodium methoxide in 93 % yield (Scheme 1).

b) From 4-amino-thiophene-3-carboxylic acid amide

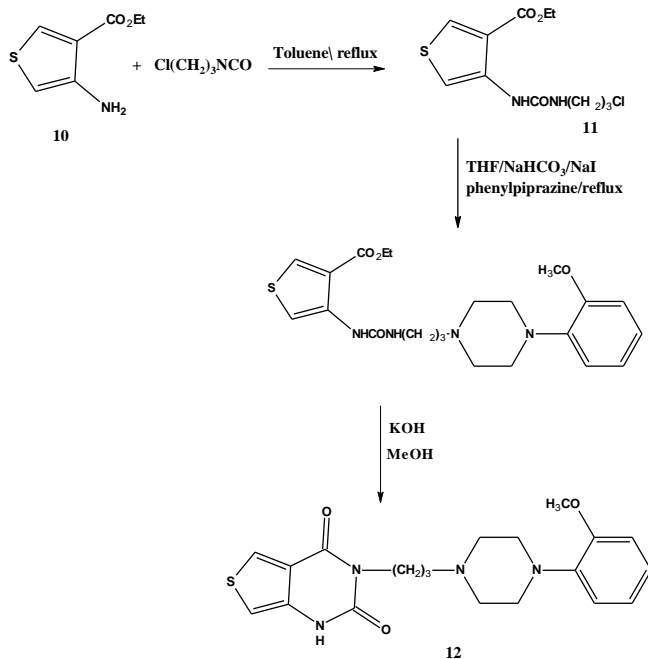
2,4-Diaminothiophene-3-carbonitrile (**7**) was converted to amide (**8**) by using sulfuric acid at room temperature cyclization by using triethyl orthoformate or triethyl orthoacetate gave thieno[3,4-*d*]pyrimidine (**9**) in 65 % yield (Scheme 2).⁵



Scheme 2.

c) From 3-aminothiophene-4-carboxylic ester

Thiophene amino esters (**10**) were reacted with 2-chloroethyl isocyanate in toluene and gave the 4-(2-chloroethyl)thiophene derivatives (**11**). Compounds (**11**) were then reacted with 2-methoxyphenylpiperazines in THF, 2-propanol or DMF to afford the thienopyrimidine-2,4-dione derivatives in 56 % yield (**12**) (Scheme 3).⁶

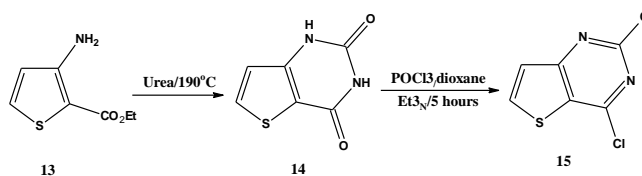


Scheme 3.

Thieno[3,2-*d*]pyrimidine

From ethyl or methyl 3-aminothiophene carboxylate derivatives

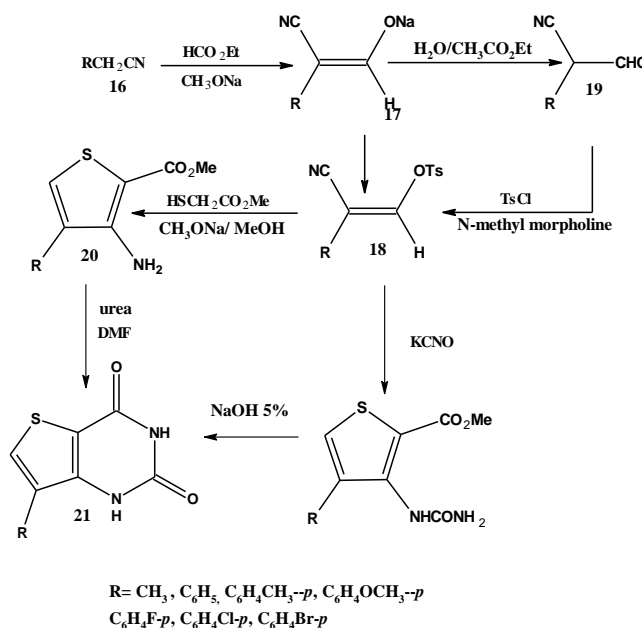
Ethyl 3-aminothiophene-2-carboxylate (**13**) was heated up to 190 °C with urea under neat condition followed by treatment with sodium hydroxide then acidified with sulfuric acid gave thieno[3,2-*d*]pyrimidine-2,4(1*H*,3*H*)-dione (**14**) in 84 % yield. The latest compound was converted into 2,4-dichlorothieno[3,2-*d*]pyrimidine (**15**) by the reaction with phosphorus oxychloride in dioxane in the presence of triethylamine in 81.4 % yield (Scheme 4).⁷



Scheme 4.

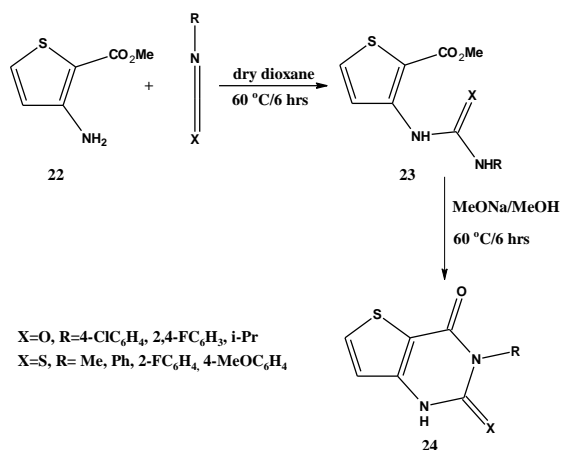
Aryl acetonitrile (**16**) reacted with ethyl formate in the presence of sodium methoxide to afford the corresponding sodium 2-cyano-2-arylethenolate (**17**) which was reacted with *p*-toluenesulfonyl chloride in DMF affording 2-aryl-3-(*p*-toluenesulfonato) acylonitriles (**18**).

The latter compound underwent acidic hydrolysis to give 2-formyl-2-arylacetonitriles (**19**) which reacted with *p*-toluenesulfonyl chloride in the presence of excess 4-methylmorpholine in dichloromethane to give 2-cyano-2-arylvinyl toluenesulfonate (**18**). The obtained compound, when treated with methyl thioglycolate, gave the thiophene (**20**). The thiophene **20** was cyclized either by potassium cyanate or urea to thieno[3,2-*d*]pyrimidine in 80 % yield (**21**) (Scheme 5).⁸



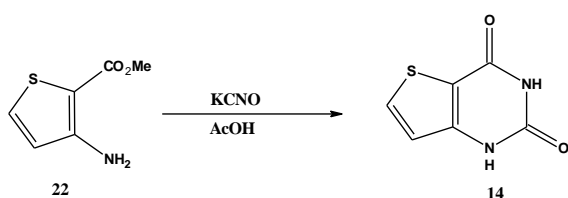
Scheme 5.

Shestakov A. S. *et al.*⁹ reported synthesis of thieno[3,2-*d*]pyrimidine by the reaction of methyl 3-aminothiophene-2-carboxylate (**22**) with isocyanates and isothiocyanates. Initially, carbamides or thiocarbamides (**23**) were formed, alkaline treatment of (**23**) led to the formation of pyrimidinediones or 2-thioxopyrimidin-4-ones in 95 % yield (**24**) (Scheme 6).



Scheme 6.

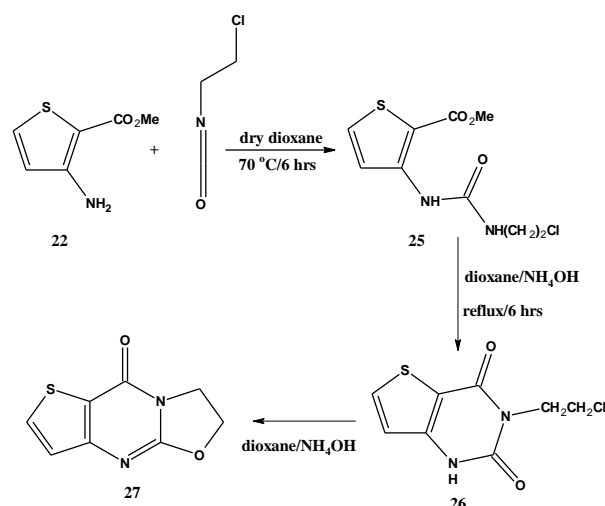
Thieno[3,2-*d*]pyrimidin-2,4(1*H*,3*H*)-dione (**14**) was prepared by Temburnikar *et al.*¹⁰ in the reaction of methyl-3-amino-2-thiophene carboxylate (**22**) with potassium cyanate in the presence of acetic acid as white solid in yield (71 %) (Scheme 7).



Scheme 7.

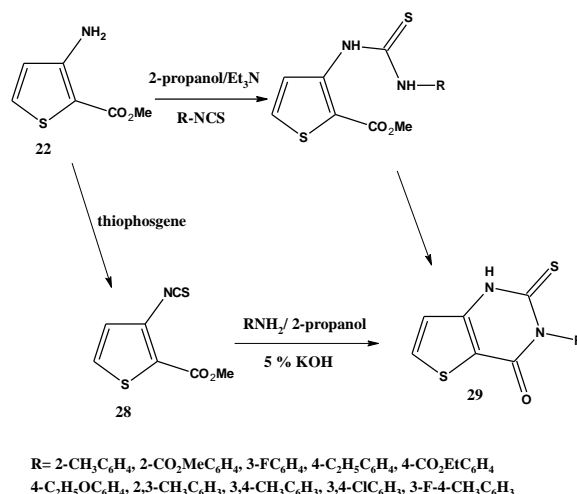
The interaction of methyl 3-aminothiophene-2-carboxylate (**22**) and 2-chloroethylisocyanates gave methyl 3-(3-(2-chloroethyl)ureido)thiophene-2-carboxylate (**25**) with potential antihypertensive activity.¹¹ The attempts to obtain 3-(2-chloroethyl)thieno[3,2-*d*]pyrimidine-2,4(1*H*,3*H*)-dione (**26**) led to a very slow reaction. In more complicated conditions (two-days boiling ammonia-dioxane solution) led to a tricyclic compound in 78 % yield (**27**) (Scheme 8).

A. Ivachtchenko *et al.*¹¹ reported that the amino-thiophene ester (**22**) was reacted with thiophosgene to generate isothiocyanate (**28**).



Scheme 8.

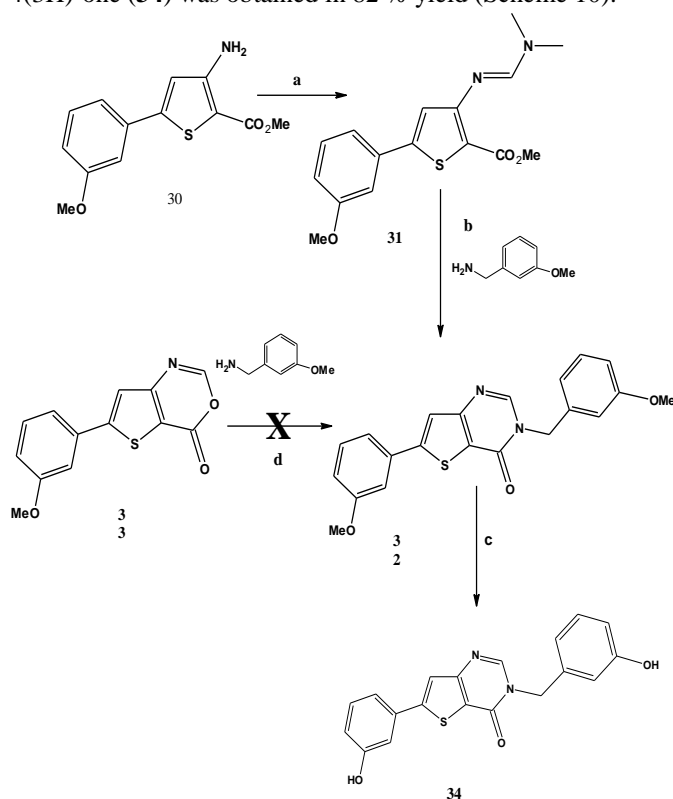
Further condensation of this reactive isothiocyanate intermediate with various primary amines in a mixture of 2-propanol and 5 % aqueous KOH under reflux smoothly afford thieno[3,2-*d*]pyrimidines (**29**). On the other hand compound (**29**) was prepared directly by reacting of aminothiophene ester (**22**) with isothiocyanate derivatives in the presence of 2-propanol and triethylamine in 75 % yield (Scheme 9).



Scheme 9.

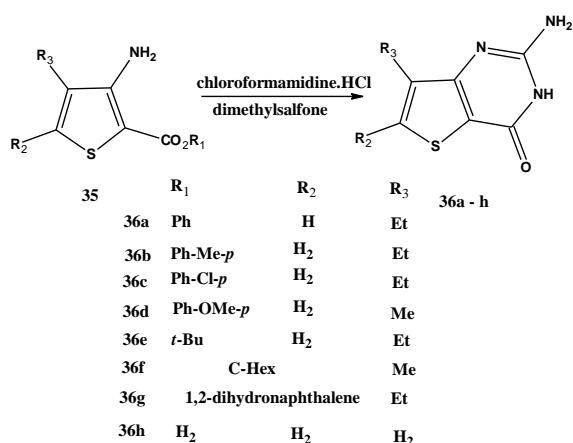
Thieno[3,2-*d*]pyrimidines were synthesized by E. Perspicace *et al.*¹² in a two- or a three-step procedure, respectively, as depicted in the following Scheme, starting from compound (**30**). The starting materials methyl 3-amino-5-(3-methoxyphenyl)-thiophene-2-carboxylate (**30**) was synthesized using the multi-step procedure well described in the literature.¹³ The condensation of molecule (**30**) with *N,N*-dimethylformamide dimethyl acetal (DMF-DMA) gave methyl 3-dimethylaminomethylideneamino-5-(3-methoxy-phenyl)thiophene-2-carboxylate (**31**) in very good yield¹⁴ which were used directly in the next step without purification to afford compound (**32**). The condensation of 6-(3-methoxyphenyl)-4*H*-thieno[3,2-*d*][1,3]oxazin-4-one (**33**) with 3-methoxybenzyl amine as an alternative route to produce (**32**) was failed.

After *O*-demethylation using boron trifluoride methyl sulfide complex $\text{BF}_3 \cdot \text{SMe}_2$, the thieno[3,2-*d*]pyrimidin-4(3*H*)-one (**34**) was obtained in 82 % yield (Scheme 10).



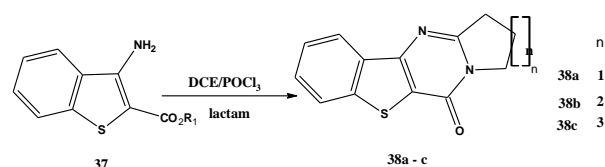
Scheme 10. Reagents and conditions: (a) DMF-DMA, EtOH, microwave irradiation (100 °C, 80 W, 15 min), 98%; (b) DMF, microwave irradiation (100 °C, 80 W, 15 min), 31%; (c) $\text{BF}_3 \cdot \text{SMe}_2$, CH_2Cl_2 , rt, 82 %; (d) MeOH, reflux.

The reaction of 3-aminothiophene derivatives with chloroform amidine hydrochloride in dimethylsulfone gave thieno[3,2-*d*]pyrimidine derivatives in yield from 40 to 90 % according to the Scheme 11.¹⁵



Scheme 11.

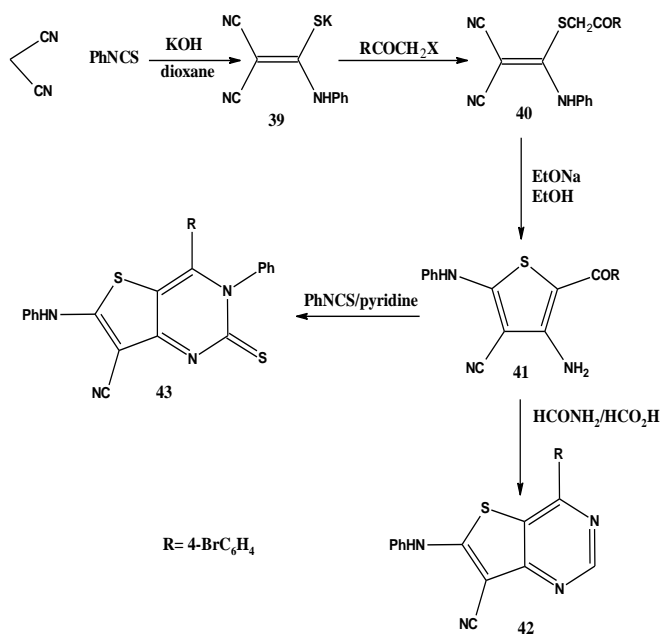
Reaction of methyl 3-aminobenzothiophene-2-carboxylate (**37**) with lactams in the presence of dichloroethane and POCl_3 gave benzothieno[3,2-*d*]pyrimidinone derivatives (**38a-c**) in yield 88, 60 and 93 %, respectively (Scheme 12).¹⁶



Scheme 12.

From *o*-ketoaminothiophene

The reaction of malononitrile with phenyl isothiocyanate in the presence of potassium hydroxide afford the potassium salt of ketene N,S-acetal (**39**). Compound (**39**) was allowed to react with *p*-bromophenacyl bromide or chloroacetone to afford the *S*-alkylated derivatives (**40**) which underwent cyclization in the presence of sodium ethoxide into compound (**41**). The reaction of (**41**) with formamide and formic acid under refluxing temperature gave 4-(4-bromophenyl)-6-(phenylamino)thieno[3,2-*d*]pyrimidine-7-carbonitrile (**42**) in 60 % yield. Also, compound (**41**) was allowed to react with phenyl isothiocyanate in pyridine when the corresponding 4-(4-bromophenyl)-3-phenyl-6-(phenylamino)-2-thioxo-2,3-dihydrothieno[3,2-*d*]pyrimidine-7-carbonitrile (**43**) was formed in 74 % yield (Scheme 13).¹⁷



Scheme 13.

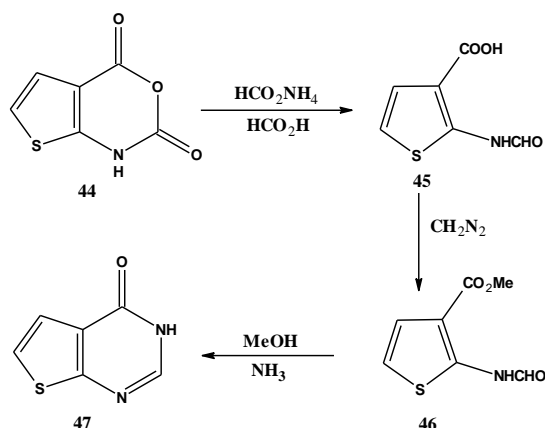
Thieno[2,3-*d*]pyrimidines

A-Starting from thiophene ring and building pyrimidine ring on it

1*H*-Thieno[2,3-*d*][1,3]oxazin-2,4-dione

Thieno[2,3-*d*]pyrimidine was first synthesized by Baker *et al.*¹⁸ when thieno[2,3-*d*][1,3]oxazine-2,4-dione (**44**) was treated with ammonium formate in 89 % formic acid at 100 °C to initiate ring opening and formylation with formation of 2-formylamino-thiophene-3-carboxylic acid (**45**).

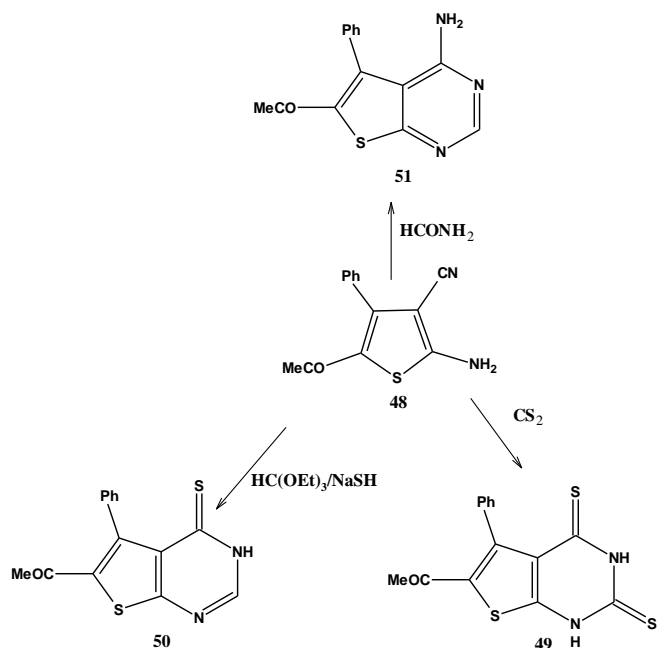
The compound (**45**) then was reacted with diazomethane to give methyl ester (**46**), the methyl ester (**46**) was treated with methanolic ammonia to give 3H-thieno[2,3-*d*]pyrimidin-4-one (**47**) in 4 % yield (Scheme 14).



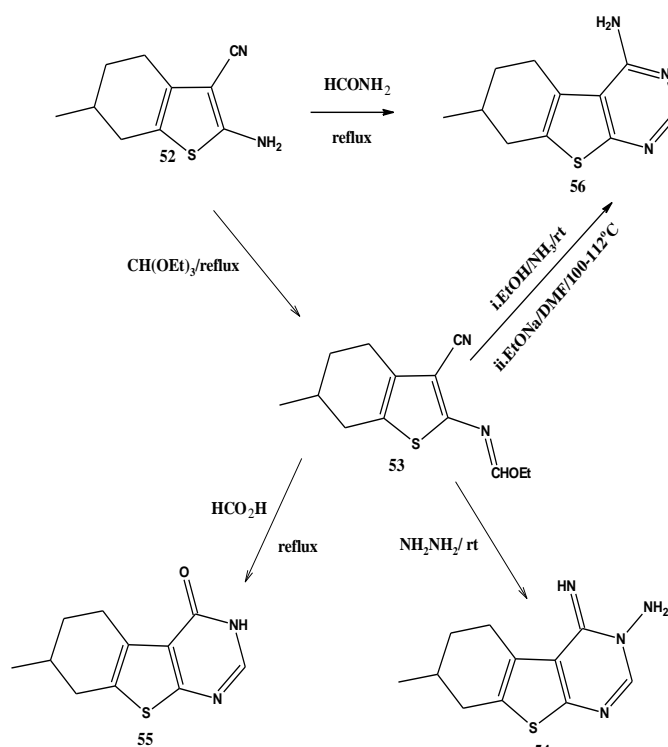
Scheme 14.

2-Amino-thiophene-3-carbonitrile from 5-acetyl-2-amino-4-phenyl-thiophene-3-carbonitrile

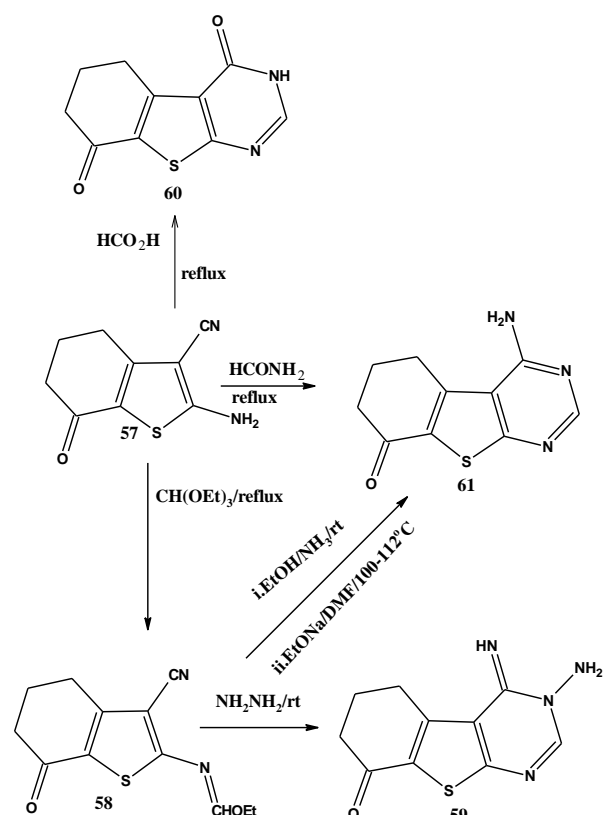
5-Acetyl-2-amino-4-phenyl-thiophene-3-carbonitrile (**48**)¹⁹ was reacted with carbon disulfide in pyridine to afford the thieno[2,3-*d*]pyrimidine dithione derivative (**49**) in 45 % yield.²⁰ When compound (**48**) was reacted with triethyl orthoformate followed by sodium hydrogen sulfide treatment according to Taylor *et al.*²¹, the thieno[2,3-*d*]pyrimidine thione derivative (**50**)²⁰ was formed in 67% yield. Compound (**48**) was underwent cyclocondensation during refluxing in formamide²² to afford the aminothiopyrimidine derivatives (**51**) in 78 % yield (Scheme 15).²⁰



Scheme 15.



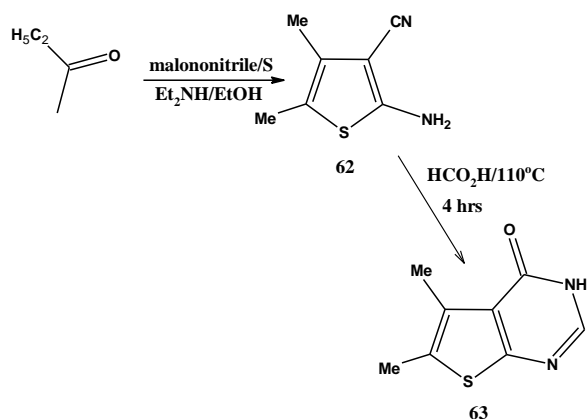
Scheme 16.



Scheme 17.

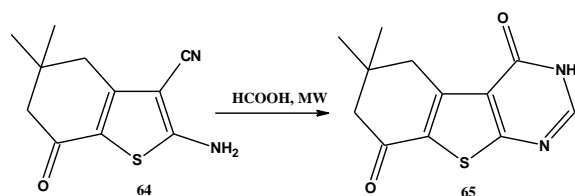
Imidoformates (**53**, **58**) were prepared in excellent yield by treatment of 2-amino-6-methyl-4,5,6,7-tetrahydro-1-benzothiophene-3-carbonitrile (**52**) prepared by Gewald reaction as reported in the literature²³ and 2-amino-7-oxo-4,5,6,7-tetrahydro-1-benzothiophene-3-carbonitrile (**57**) prepared from 1,3-cyclohexanedione²⁴ with triethyl orthoformate at reflux temperature. Reactions of imidoformates (**53**, **58**) with hydrazine hydrate afford the thienopyrimidines (**54**, **59**) in 77 % and 64 % yields, respectively. Similarly, the reaction of imidoformates (**53**, **58**) with ethanolic ammonia followed by the cyclization of intermediates with sodium ethoxide in refluxed dimethylformamide, the formation of aminothiopyrimidines (**56**, **61**) in 80 % and 75 % yields, respectively. The reaction of compounds (**52**, **57**) with formic acid gave thienopyrimidinone derivatives (**55**, **60**) in 80 % yield (Scheme 16 and Scheme 17).

The compounds (**56**, **61**) were prepared by refluxing 2-amino-3-cyanothiophenes (**52**, **57**) with formamide. Also, M. I. Hossain *et al.*²⁵ used the 2-aminothiophene-3-carbonitrile (**62**) which prepared by Gewald method from 2-butanone with sulfur and malononitrile to synthesize thieno[2,3-*d*]pyrimidine (**63**) in 85 % yield (Scheme 18).



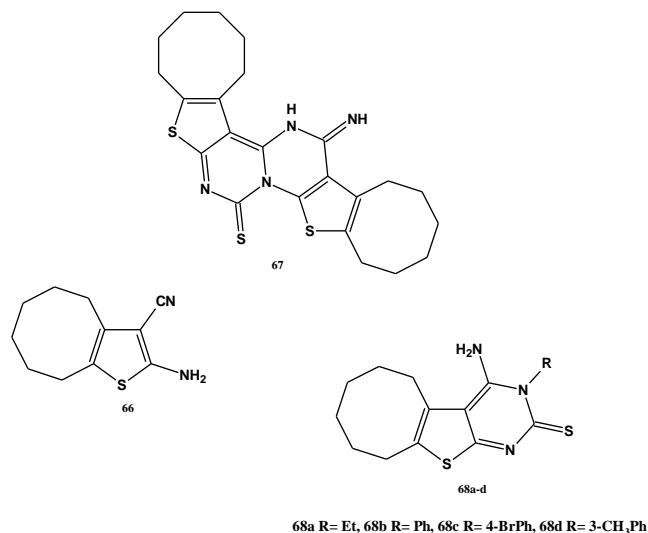
Scheme 18.

Nitinkumar S. Shetty *et al.*²⁶ used microwave irradiation to synthesize thieno[2,3-*d*]pyrimidine from α -aminothiophene carbonitriles.^{23,27} The precursor 2-amino-5,5-dimethyl-7-oxo-4,5,6,7-tetrahydro-1-benzothiophene-3-carbonitrile (**64**) was prepared by the reaction of 1,3-dimedone under conditions reported by K. Gewald.^{22,24} Thienopyrimidin-4-one (**65**) was prepared by the microwave irradiation of 2-amino-3-cyanothiophene (**64**) in the presence of formic acid in 80 % yield (Scheme 19).



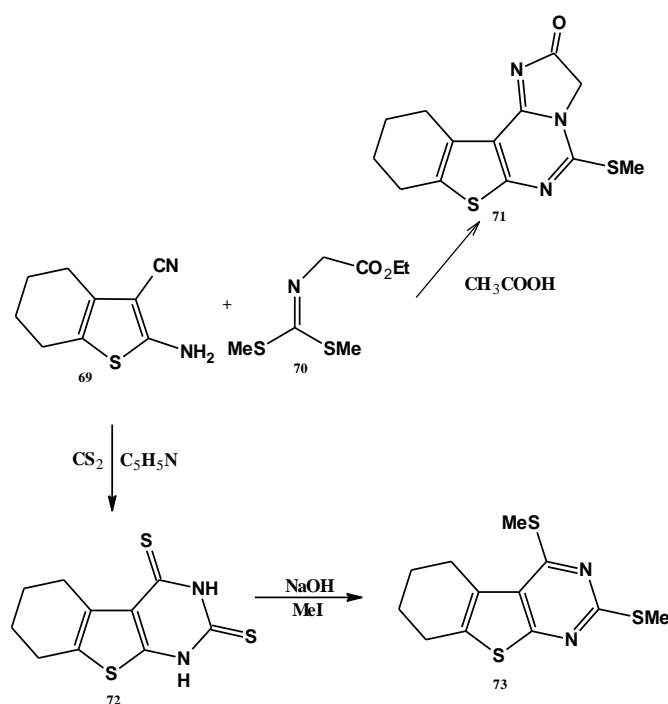
Scheme 19.

Compounds (**68a-d**) were obtained by reacting the aminocyano derivative (**66**) with the aromatic isothiocyanates in ethanol in the presence of a catalytic amount of triethylamine. Using phenyl isothiocyanate, hexacyclothienopyrimidine (**76**) was produced in 50 % yield (Scheme 20).²⁸



Scheme 20.

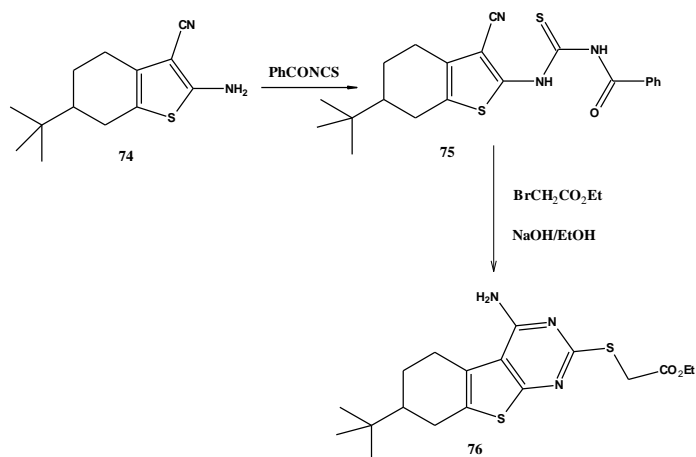
Reaction of heteroaromatic 2-aminothiophene-3-carbonitrile (**69**) with ethyl *N*-bis(methylthio)methyleneamino acetate (**70**) gave thieno[2,3-*d*]pyrimidine (**71**) in a one-step process in 75 % yield.²⁹ Compound (**69**) reacted with carbon disulfide in pyridine to afford thieno[2,3-*d*]pyrimidin-2,4-dithione (**72**) which could be alkylated with methyl iodide in the presence of sodium hydroxide and gave compound (**73**) in 81 % yield (Scheme 21).



Scheme 21.

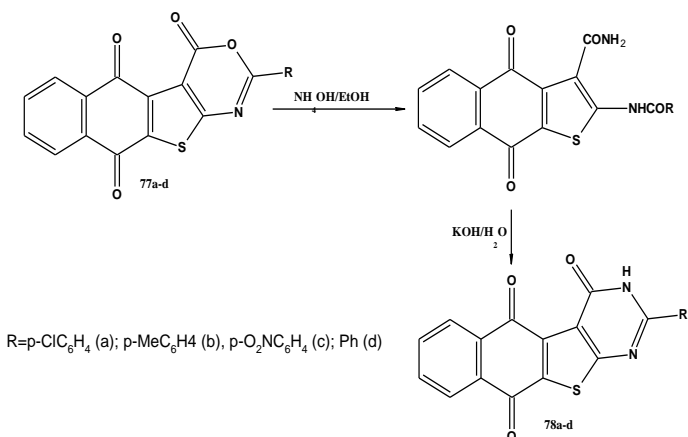
From ethyl 2-aminothiophene-3-carboxylate

Li *et al.*³⁰ prepared thieno[2,3-*d*]pyrimidine derivative (**74**) by reaction of 2-aminobenzo[*b*]thiophene-3-carbonitrile (**75**) with benzoyl isothiocyanate to give *N*-((6-(tert-butyl)-3-cyano-4,5,6,7-tetrahydrobenzo[*b*]thiophen-2-yl)carbamoyl)benzamide (**76**) which reacted with ethyl bromoacetate in ethanol in the presence of sodium hydroxide as white crystal in yield 57 % (Scheme 22).



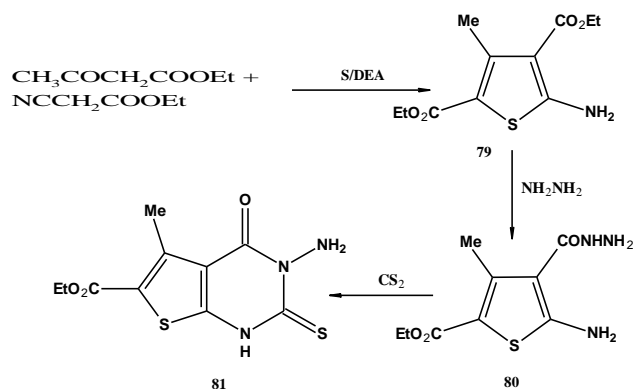
Scheme 22.

2-Aryl-4H-naphtho[2',3':4,5]thieno[2,3-*d*][1,3]oxazine-4,5,10-triones (**77a-d**) allowed to get 2-aryl-naphtho[2',3':4,5]thieno[2,3-*d*][1,3]pyrimidine-4,5,10(3*H*)-triones (**78a-d**) easily. Pyrimidine triones were obtained in 78 % yield in the reaction of oxazinetriones with ammonium hydroxide in ethanol without the isolation of intermediate compounds which were transformed by 5 % solution KOH during 1 h (Scheme 23).



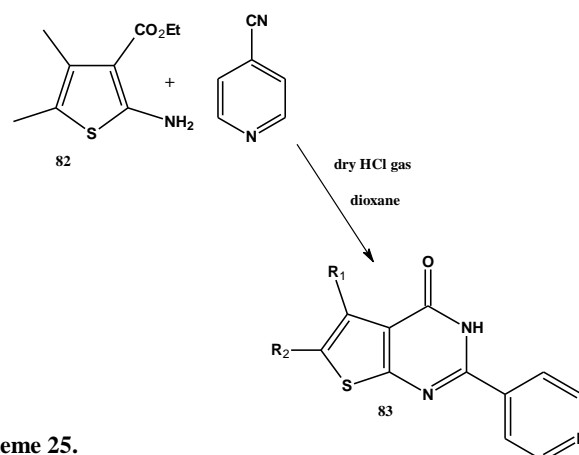
Scheme 23.

The interaction of ethyl acetoacetate with ethyl cyanoacetate and elementary sulfur in ethanol medium and in the presence of diethylamine led to diethyl 5-amino-3-methylthiophene-2,4-dicarboxylate.²⁹ The hydrazide (**80**) obtained by refluxing of ethyl carboxylate (**79**) with hydrazine hydrate in ethanol compound (**80**) was treated with carbon disulfide to afford the 3-amino-6-carboxyethyl-5-methyl-2-thioxo-thieno[2,3-*d*]pyrimidin-4-one (**81**) in 68 % yield (Scheme 24).³¹



Scheme 24.

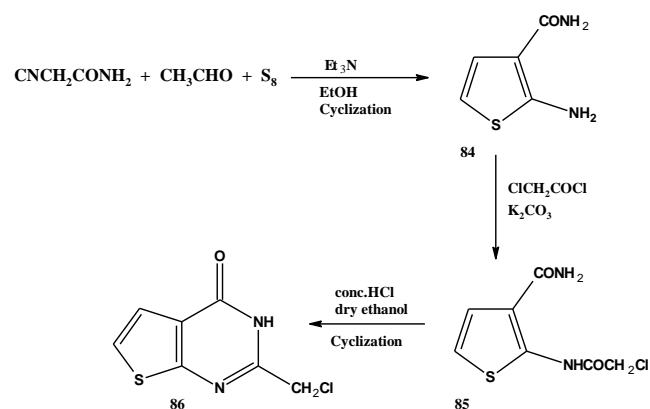
Nitin G. Haswani *et al.*³² reported the synthesis of 2-aminothiophene-3-carboxylate (**82**) according to Gewald method and the product was subjected to react with nitriles in the presence of HCl gas to afford thienopyrimidine (**83**) in 98 % yield (Scheme 25).



Scheme 25.

From 2-aminoindeno[2,1-*b*]thiophene-3-carboxylic amide

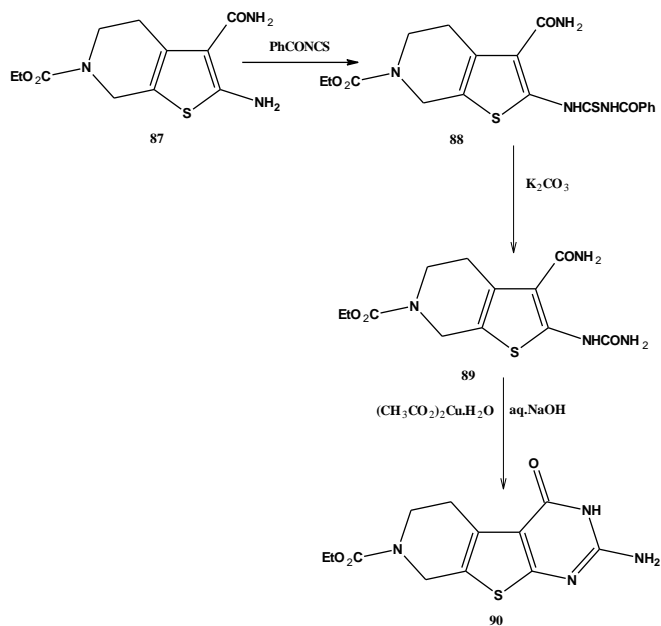
Cyano acetamide was reacted with acetaldehyde in the presence of sulfur and triethylamine according to Gewald method in ethanol to give 2-aminothiophene-3-carboxamide (**84**) which reacted with chloroacetyl chloride to give the intermediate chloroacetyl derivative (**85**).



Scheme 26.

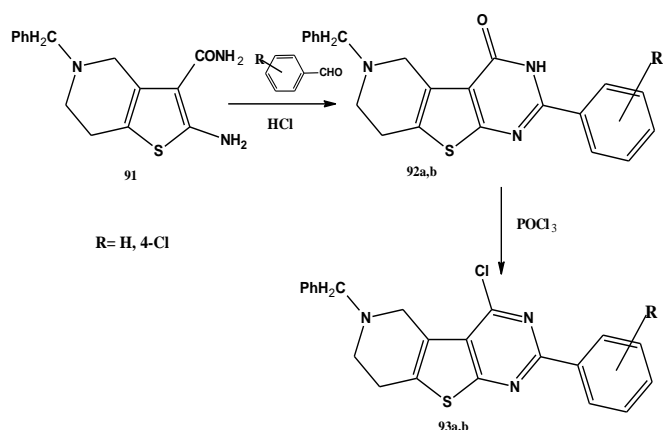
The chloroacetyl derivative was cyclized with concd. HCl in ethanol producing thieno[2,3-*d*]pyrimidine (**86**) in 78 % yield (Scheme 26).³³

The reaction of 2-aminothiophene-3-carboxamide (**87**) with benzoyl isothiocyanate in acetone afforded the corresponding [*N*-benzoyl(thiocarbamoyl)]-aminothiophene derivative (**88**) in 67 % yield. The isolated compound (**88**) was hydrolyzed to yield the corresponding thiourea (**89**). In the accomplishment of the cyclodesulfurization by use of a heavy metal salt, compound (**89**) was added to a suspension of a slight excess of the metal salt in aqueous sodium hydroxide to give thieno[2,3-*d*]pyrimidine (**90**) in 97 % yield (Scheme 27).³⁴



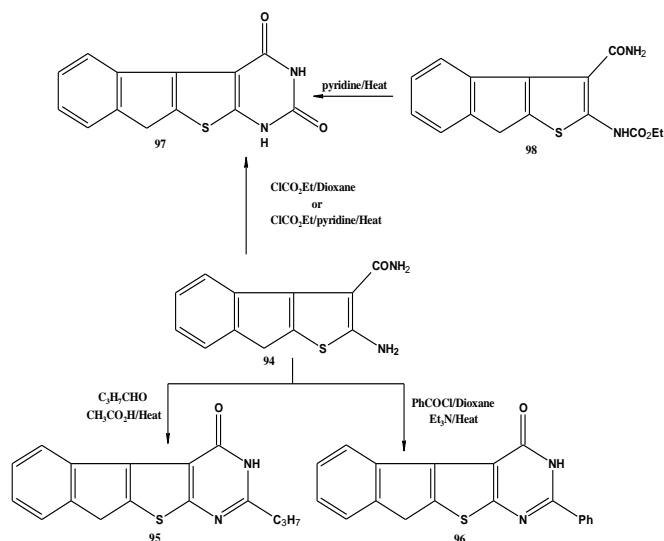
Scheme 27.

On the other hand, 2-amino-5-benzyl-4,5,6,7-tetrahydrothieno[3,2-*c*]pyridine-3-carboxamide (**91**) was condensed with aromatic aldehydes in ethanol in the presence of concd. HCl affording 6-benzyl-2-phenyl(or 4-chlorophenyl)-5,6,7,8-tetrahydropyridothieno[2,3-*d*]pyrimidine-4(4*H*)-ones (**92a-b**) in 70 % and 78 % yield, respectively.³⁵ Compounds **92a-b** were reacted with phosphorus oxychloride to give 4-chloro derivatives (**93a-b**) in 90 % and 70 % yields, respectively (Scheme 28).



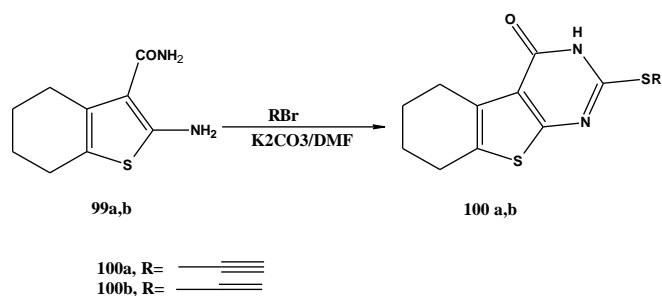
Scheme 28.

2-Aminoindeno[2,1-*b*]thiophene-3-carboxylic acid amide (**94**)³⁶ was cyclized with butyraldehyde and benzoyl chloride to afford 2-propyl-3,9-dihydroindeno[1',2':4,5]thieno[2,3-*d*]pyrimidin-4-one (**95**) and 2-phenyl-3,9-dihydroindeno[1',2':4,5]thieno[2,3-*d*]pyrimidin-4-one (**96**) in 85 % yield and 62 % yields, respectively. Moreover, treatment of compound **94** with ethyl chloroformate in dry dioxane under reflux afforded not only to the cyclized thieno[2,3-*d*]pyrimidindione derivative (**97**) but also gave (3-carbamoyl-8*H*-indeno[2,1-*b*]thiophen-2-yl)carbamic acid ethyl ester (**98**) as well. Refluxing compound **98** in dry pyridine or compound **94** with ethyl chloroformate in dry pyridine gave in both cases the same product, 1,3,9-trihydroindeno[1',2':4,5]thieno[2,3-*d*]pyrimidine-2,4-dione (**97**) in 69 % yield. The pyrimidinedione (**97**) could be formed *via* the formation of compound **98**, which was isolated and cyclized by refluxing that in pyridine to thieno[2,3-*d*]pyrimidinedione (**97**) (Scheme 29).



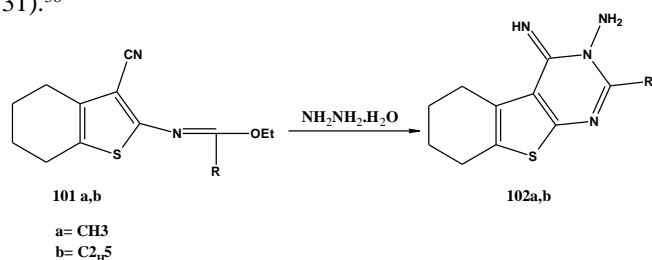
Scheme 29.

2-Aminobenzo[*b*]thiophene-3-carboxamide (**99a-b**) reacted with propargyl bromide or with allyl bromide in DMF in the presence of K₂CO₃ to give 2-(prop-2-yn-1-ylthio)benzothieno[2,3-*d*]pyrimidinone (**100a**) or 2-(allylthio)benzothieno[2,3-*d*]pyrimidinone derivatives (**100b**) in yield 60 % and 64 %, respectively (Scheme 30).³⁷



Scheme 30.

N-(3-Cyano-4,5,6,7-tetrahydro-benzo[b]thiophen-2-yl)-acetimidic acid ethyl ester and (Z)-ethyl N-3-cyano-4,5,6,7-tetrahydrobenzo[b]thiophen-2-ylpropionimidate (**101a,b**) were reacted with hydrazine hydrate in ethanol to give 4-aminobenzothieno[2,3-d]pyrimidin-3[4H]-amine and 2-ethyl-4-aminobenzothieno[2,3-d]pyrimidin-3[4H]-amine (**102a,b**) in 77 % and 65 % yield, respectively (Scheme 31).³⁸

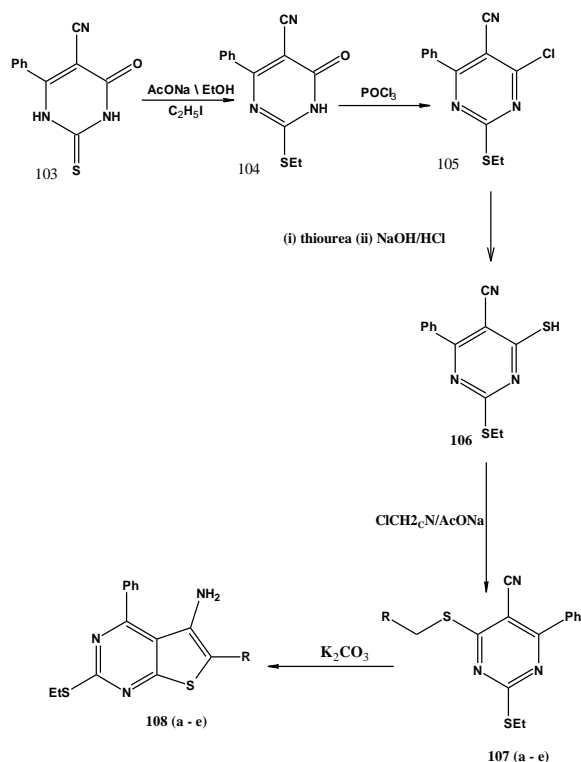


Scheme 31.

B) Starting from pyrimidine ring and building thiophene ring on it

From 4-Oxo-6-phenyl-2-thioxo-1,2,3,4-tetrahydro pyrimidine-5-carbonitrile

4-Oxo-6-phenyl-2-thioxo-1,2,3,4-tetrahydropyrimidine-5-carbonitrile (**103**)³⁹ was alkylated and gave 2-ethylmercapto-4-oxo-6-phenyl-3,4-dihydropyrimidine-5-carbonitrile (**104**). Compound **104** was converted into 2-ethylmercapto-4-chloro-6-phenyl-3,4-dihydropyrimidine-5-carbonitrile (**105**) using phosphorus oxychloride.



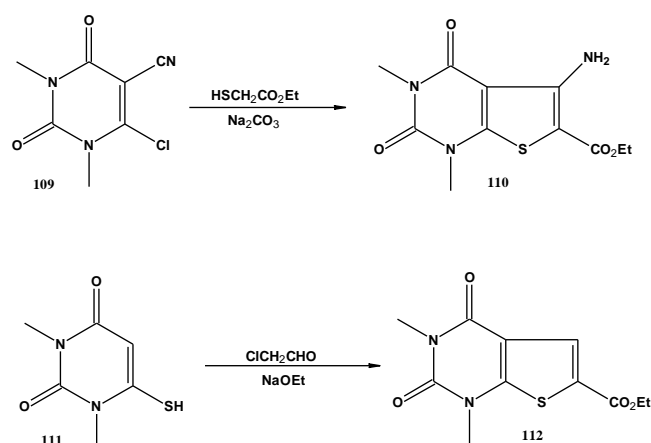
108a: R= CONH₂, 108b: R= CN, 108c: R= CO₂Et, 108d: R= CONHPh-Cl-p, 108e: R= CONHPh-OMe-p

Scheme 32.

Compound **105** was converted into 2-ethylmercapto-4-mercapto-6-phenylpyrimidine-5-carbonitrile (**106**) via reaction with thiourea in refluxed ethanol followed by treatment with sodium hydroxide solution and then acidified with dilute HCl. When compound **106** reacted with α -halo carbonyl compounds in ethanol in the presence of sodium acetate, alkylation of mercapto group was occurred to afford compounds **107a-e**. Compounds **107a-e** were undergone *Thorpe-Ziegler* cyclization reaction in ethanol in the presence of potassium carbonate and afforded compounds **108a-e** in 62 %, 65 %, 70 %, 50 % and 40 % yield, respectively (Scheme 32).^{40,41}

From 1,3-dimethyluracil derivatives

6-Chloro-5-cyano-1,3-dimethyluracil (**109**) prepared from the formyluracil in two steps,⁴² was cyclized to 5-aminothieno[2,3-d]pyrimidine (**110**) on heating with ethyl 2-mercaptoacetate in the presence of sodium carbonate. 6-Mercapto-uracil (**111**)⁴³ was allowed to react with chloroacetaldehyde in the presence of sodium acetate at room temperature to give the thieno[2,3-d]pyrimidine (**112**) (Scheme 33).⁴⁴

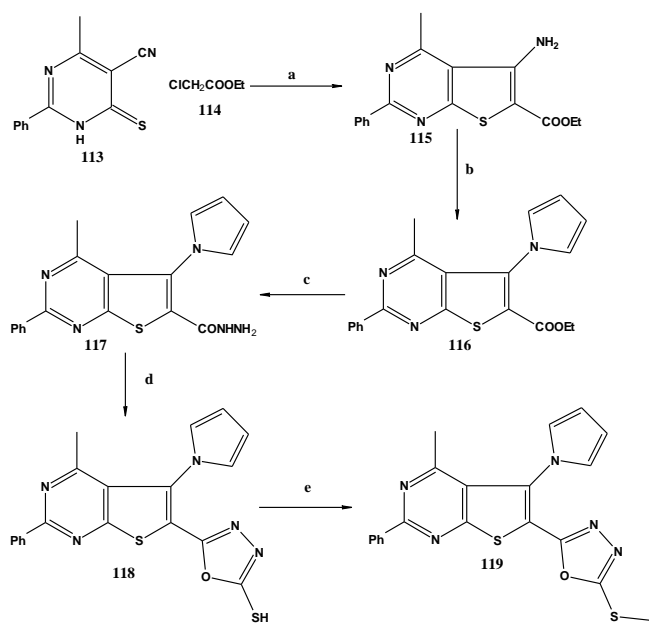


Scheme 33.

From 5-cyano-1,6-dihydro-4-methyl-2-phenyl-6-thioxopyrimidine

5-Cyano-1,6-dihydro-4-methyl-2-phenyl-6-thioxopyrimidine (**113**) was prepared by treating benzoyl isothiocyanate with 3-aminocrotonitrile in refluxing dioxane.^{45,46} Cyclization of thioxopyrimidine (**113**) with ethyl chloroacetate (**114**) in DMF in the presence of excess anhydrous potassium carbonate at room temperature gave the ethyl 5-amino-4-methyl-2-phenylthieno[2,3-d]pyrimidine-6-carboxylate (**115**) in 92 % yield (Scheme 34).

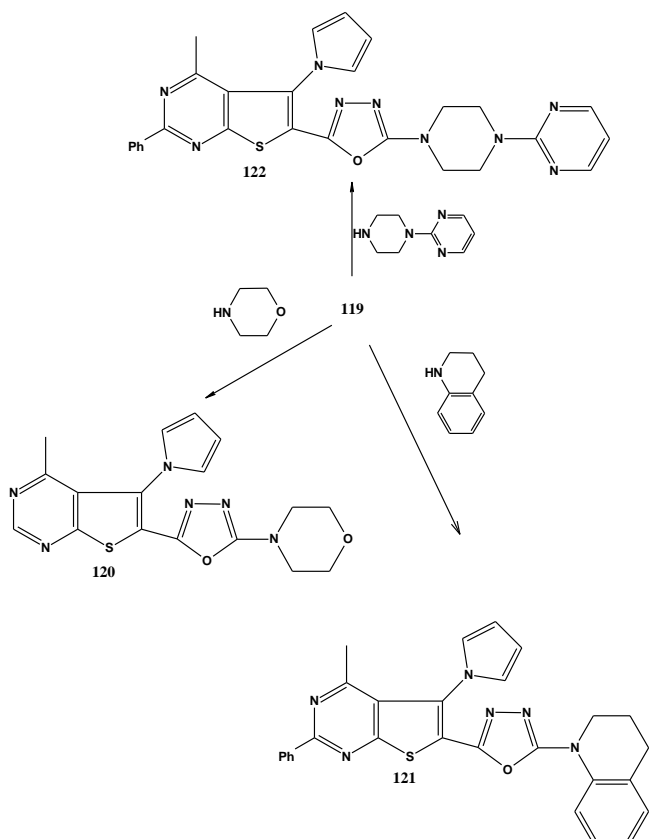
Treatment of compound **115** with 2,5-dimethoxytetrahydrofuran in glacial acetic acid produced the ethyl 5-(1-pyrrolyl)-4-methyl-2-phenylthieno[2,3-d]pyrimidine-6-carboxylate (**116**), which reacted with an excess of 85 % hydrazine hydrate in refluxing ethanol to give the corresponding 5-(1-pyrrolyl)-4-methyl-2-phenylthieno[2,3-d]pyrimidine carbohydrazide (**117**).



Reagents: (a) DMF/K₂CO₃; (b) 2,5-(MeO)₂-tetrahydrofuran, glacial acetic acid; (c) hydrazine hydrate; (d) CS₂/pyridine; (e) MeI

Scheme 34.

The carbohydrazide (**117**) was used as a key intermediate for the synthesis of novel 1,3,4-oxadiazole-thieno[2,3-*d*]pyrimidine derivatives. Cyclization of carbohydrazide (**117**) with CS₂ in the presence of pyridine afforded the 6-(2,3-dihydro-2-mercapto-1,3,4-oxadiazol-5-yl)-4-methyl-5-(1-pyrrolyl)-2-phenylthieno[2,3-*d*]pyrimidine (**118**).

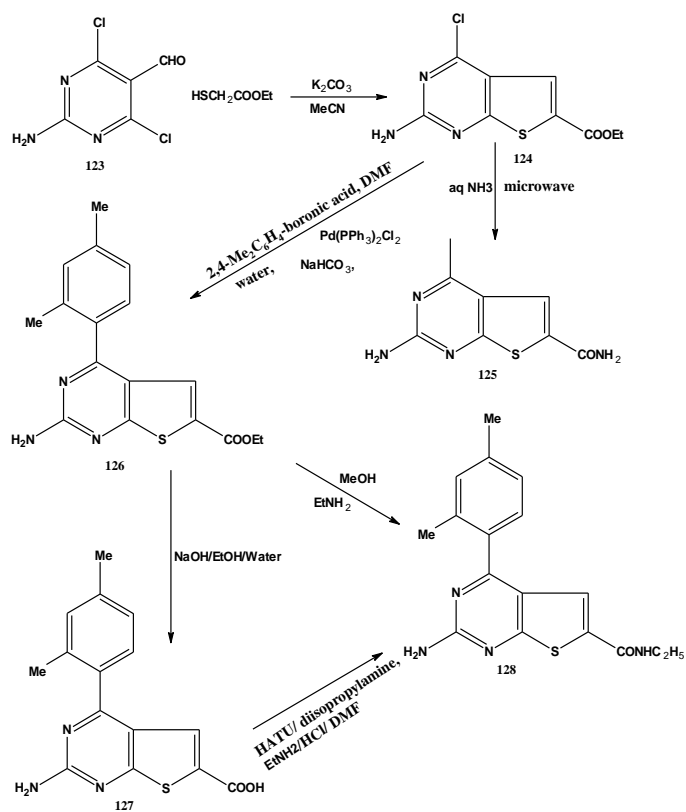


Scheme 35.

Its reaction with iodomethane in the presence of sodium methoxide yielded the 6-(2-methylthio-1,3,4-oxadiazol-5-yl)-4-methyl-5-(1-pyrrolyl)-2-phenylthieno[2,3-*d*]pyrimidine (**119**) (84 % yield) (Scheme 34). On the other hand, some novel 6-(2-substituted-1,3,4-oxadiazol-5-yl)-4-methyl-5-(1-pyrrolyl)-2-phenylthieno[2,3-*d*]pyrimidine derivatives (**120**, **121** and **122**) were also obtained by the condensation reaction of compound (**119**) with morpholine, 1,2,3,4-tetrahydro quinoline and 1-(2-pyrimidyl) piperazine in 90, 56 and 58 % yield, respectively (Scheme 35).⁴⁷

From 4,6-dichloro-5-formyl pyrimidine

The reaction of ethyl-2-mercaptoacetate with 4,6-dichloro-5-formyl pyrimidine (**123**) gave the compound **124** in 22 % yield, which was reacted with aqueous ammonia at high temperature to afford 2,4-diaminothiopyrimidine (**125**) in 82 % yield.⁴⁸ The Suzuki cross-coupling reaction of compound **124** with commercially available boronic acid derivatives gave 4-aryl-2-aminopyrimidines.⁴⁹ Saponification of the ethyl ester (**126**) gave the corresponding acid **127**, which was coupled with ethylamine hydrochloride in the presence of HATU to give ethyl amide (**128**) in 72 % yield (Scheme 36).⁵⁰



Scheme 36.

CONCLUSION

From the literature survey, thienopyrimidine derivatives were proved to be very important compounds with extensive biological activities which can use in treatment of many diseases.

On the other hand, thienopyrimidines derivatives have a lot of synthesis methods starting from thiophene ring but only several methods from pyrimidine ring containing compounds.

ACKNOWLEDGMENTS

I would like thanks to all authors worked in this review to can get it in this form.

REFERENCES

- ¹Liuyu, D., Houying, G., Qiuming, Z., Xinming, H., Shaoyong, G., *Wuhan J. Nat. Sci.*, **2012**, 17(2), 177-184.
- ²Woodward, R. B., Eastman, R. H., *J. Am. Chem. Soc.*, **1946**, 68, 2229-2234. <https://doi.org/10.1021/ja01215a034>
- ³Cheney, L. C., Piening, J. R., *J. Am. Chem. Soc.*, **1945**, 67, 731-735. <https://doi.org/10.1021/ja01221a011>
- ⁴Baker, B. R., Schaub, R. E., Joseph, J. P., McEroy, F. J., Wiims, J. H., *J. Org. Chem.*, **1953**, 18, 138-152. <https://doi.org/10.1021/jo01130a004>
- ⁵El Azab, I. H., Kenzy, N. A., *Synth. Commun.*, **2014**, 44, 2692-2714. <https://doi.org/10.1080/00397911.2014.916301>
- ⁶Russell, K. R., Press, J. B., Rampulla, R. A., McNally, J. J., Falotico, R., Keiser, J. A., Bright, D. A., Tobia, A., *J. Med. Chem.*, **1988**, 31, 1786-1793. <https://doi.org/10.1021/jm00117a019>
- ⁷Ziegler, D., Brossmer, R., *Tetrahedron*, **1973**, 23, 2055-2058. [https://doi.org/10.1016/S0040-4039\(01\)86805-2](https://doi.org/10.1016/S0040-4039(01)86805-2)
- ⁸Jourdan, F., Laaurée, D., Robba, M., *J. Heterocycl. Chem.*, **1994**, 31, 305-312. <https://doi.org/10.1002/jhet.5570310208>
- ⁹Shestakov, A. S., Present, M. A., Kartsev, V. G., Shikhaliev, K. S., *Eur. Chem. Bull.*, **2014**, 3(7), 713-718. DOI: 10.17628/ecb.2014.3.713-718.
- ¹⁰Temburnikar, K. W., Zimmermann, S. C., Kim, N. T., Ross, C. R., Gelbmann, C., Salomon, C. E., Wilson, G. M., Balzarini, J., Seley-Radtke, K. L., *Bioorg. Med. Chem.*, **2014**, 22, 2113-2122. <https://doi.org/10.1016/j.bmc.2014.02.033>
- ¹¹Ivachtchenko, A., Kovalenko, S., Tkachenko, O. V., Parkhomenko, O., *J. Comb. Chem.*, **2004**, 6, 573-583. <https://doi.org/10.1021/cc0499461>
- ¹²Perspicace, E., Oberwinkler, S. M., Hartmann, R. W., *Molecules*, **2013**, 18, 4487-4509. <https://doi.org/10.3390/molecules18044487>
- ¹³Migianu E., Kirsch, G., *Synthesis*, **2002**, 8, 1096-1100. <https://doi.org/10.1055/s-2002-31963>
- ¹⁴Hertzog, D. L., Al-Barazanji, K. A., Bigham, E. C., Bishop, M. J., Britt, C. S., Carlton, D. L., Cooper, J. P., Daniels, A. J., Garrido, D. M., Goetz, A. S., *Bioorg. Med. Chem. Lett.*, **2006**, 16, 4723-4727. <https://doi.org/10.1016/j.bmcl.2006.07.008>
- ¹⁵Kirsch, G., Abdillahi I., *Synthesis*, **2010**, 9, 1428-1430. <https://doi.org/10.1055/s-0029-1218697>
- ¹⁶Kirsch, G., Abdillahi I., *Synthesis*, **2011**, 8, 1314-1318. <https://doi.org/10.1055/s-0030-1258469>
- ¹⁷El-Saghier, A. M. M., Matough, F. S., Farhat, M. F., Saleh, N. A., Kredan, K. M., El-Tier S. O., B. Hussien, H., *Jordan J. Chem.*, **2008**, 3(3), 223-232.
- ¹⁸Baker, B. R., Schaub, R. E., Joseph, J. P., McEroy F. J., Wiims, J. H., *J. Org. Chem.*, **1953**, 18, 138-152. <https://doi.org/10.1021/jo01130a004>
- ¹⁹Gewald, K., *Chem. Ber.*, **1965**, 98, 3571-3577. <https://doi.org/10.1002/cber.19650981120>
- ²⁰Abdelrazek F. M., Ead, H., *J. Prakt. Chemie.*, **1988**, 8, 585-589. <https://doi.org/10.1002/prac.19883300412>
- ²¹Taylor, E. C., McKillop A., Vromen, S., *Tetrahedron*, **1967**, 23, 885-889. [https://doi.org/10.1016/0040-4020\(67\)85037-3](https://doi.org/10.1016/0040-4020(67)85037-3)
- ²²Ried W., Giesse, P., *Angew. Chem. Int. Ed.*, **1968**, 7, 136. <https://doi.org/10.1002/anie.196801361>
- ²³Sebnis, R. W., Ragnekar, D. W., Sonawane, N. D., *J. Heterocycl. Chem.*, **1999**, 36, 333-345. <https://doi.org/10.1002/jhet.5570360203>
- ²⁴Gewald, A. K., Schinke, E., Bottcher, H., *Chem. Ber.*, **1966**, 99, 94-100. <https://doi.org/10.1002/cber.19660990116>
- ²⁵Hossain M. I., Bhuiyan, M. M. H., *J. Sci. Res.*, **2009**, 1(1), 317-325.
- ²⁶Shetty, N. S., *Int. J. Adv. Chem. Eng. Biol. Sci.*, **2014**, 1(1), 80-84.
- ²⁷Dave, C. G., Shah, R. D., *J. Heterocycl. Chem.*, **1998**, 35, 1295-1300. <https://doi.org/10.1002/jhet.5570350609>
- ²⁸Kandeel, M. M., Mounir, A. A., Refaat, H. M., Kassab, A. E., *J. Chem. Res.*, **2012**, 2, 105-110. <https://doi.org/10.3184/174751912X13282020691270>
- ²⁹Bhuiyan, M. H., Rahman, K. M., Abdur Rahim, K. H., Abu Naser, M. I. H. M., *Acta Pharm.*, **2006**, 56, 441-450.
- ³⁰Li, S. G., Vilchèze, C., Chakraborty, S., Wang, X., Kim, H., Anisetti, M., Ekins, S., Rhee, K. Y., Jacobs, W. R., Freundlich, J. S., *Tetrahedron Lett.*, **2015**, 56, 3246-3250. <https://doi.org/10.1016/j.tetlet.2015.02.129>
- ³¹Abu-Hashem, A. A., El-shehry, M. F., Badria, F. A., *Acta Pharm.*, **2010**, 60, 311-323. <https://doi.org/10.2478/v10007-010-0027-6>
- ³²Haswani, N. G., Bari, S. B., *Turk. J. Chem.*, **2011**, 35, 915-924.
- ³³Bhadane, M. R., Chandra, J. N. N. S., Nargund, L. V. G., *Der Pharma Chemica*, **2011**, 3(4), 238-244.
- ³⁴Ameen, M. A., *Z. Naturforsch*, **2006**, 61b, 1234-1238.
- ³⁵Salahuddin, M., Singh, S., Shantakumar, S. M., *Rasayan J. Chem.*, **2009**, 2(1), 167-173.
- ³⁶Hegab, M. I., Hassan, N. A., Rashad, A. E., Fahmy, A. A., Abdel-Megeid, F. M., *Phosphorus Sulfur Silicon Relat. Elem.*, **2007**, 182, 1535-1556. <https://doi.org/10.1080/10426500701247151>
- ³⁷Haggam, R. A., Moustafa, A. H., *AFINIDAD LXXI 565 Enero – Marzo*, **2014**, 68-73.
- ³⁸Mulla, J. A. S., Khazi, M. I. A., Pancharukhi, S. I., Gong, Y. D., Khazi, I. A. M., *Med. Chem. Res.*, **2014**, 23, 3235-3243. <https://doi.org/10.1007/s00044-013-0900-1>
- ³⁹Kambe, S., Saito, K., Kishi, H., *Synthesis*, **1979**, 4, 287-289. <https://doi.org/10.1055/s-1979-28650>

- ⁴⁰Saddik, A. A., Hassan, Kh. M., Kamal El-Dean, A. M., Abbady, M. S., *Eur. Chem. Bull.*, **2015**, 4(9), 436-441. DOI: [10.17628/ecb.2015.4.436-441](https://doi.org/10.17628/ecb.2015.4.436-441).
- ⁴¹Saddik, A. A., Kamal El-Dean, A. M., El-Sokary, G. H., Hassan, Kh. M., Abbady, M. S., Ismail, I. A., Saber, S. H., *J. Chin. Chem. Soc.*, **2017**, 64, 87-93. <https://doi.org/10.1002/jccs.201600279>
- ⁴²Senda, S., Hirota, K., Asso, T., *Chem. Pharm. Bull.*, **1978**, 26, 3208-3211. <https://doi.org/10.1248/cpb.26.3208>
- ⁴³Ogura, H., Sakaguchi, M., Takeda, K., *Chem. Pharm. Bull.*, **1972**, 20(2), 404-408. <https://doi.org/10.1248/cpb.20.404>
- ⁴⁴Hirota, K., Shirahashi, M., Senda, S., Yogo, M., *J. Heterocycl. Chem.*, **1990**, 27, 717-721. <https://doi.org/10.1002/jhet.5570270345>
- ⁴⁵Ho, Y. W., Yao, C. T., *J. Chin. Chem. Soc.*, **2003**, 50, 283-296. <https://doi.org/10.1002/jccs.200300043>
- ⁴⁶Elnagdi, M. H., Abdelrazek, F. M., Ibrahim, N. S., Erian, A. W., *Tetrahedron*, **1989**, 45, 3597-3604. [https://doi.org/10.1016/S0040-4020\(01\)81038-3](https://doi.org/10.1016/S0040-4020(01)81038-3)
- ⁴⁷Ho Y.W., Suen, M.C., *J. Chin. Chem. Soc.*, **2009**, 56, 408-415. <https://doi.org/10.1002/jccs.200900060>
- ⁴⁸Clark, J., Shahhet, M. S., Korakas, D., Varvounis, G., *J. Heterocycl. Chem.*, **1993**, 30, 1065-1072 .
- ⁴⁹Zhu, L., Duquette, J., Zhang, M., *J. Org. Chem.*, **2003**, 68, 3729-3732 .<https://doi.org/10.1021/jo0269114>
- ⁵⁰Brough, P. A., Barril, X., Borgognoni, J., Chene, P., Davies, N. G. M., Davis, B., Drysdale, M. J., Dymock, B., Eccles, S. A., Echeverria, C. G., Fromont, C., Hayes, A., Hubbard, R. E., Jordan, A. M., Jensen, M. R., Massey, A., Merrett, A., Padfield, A., Parsons, R., Radimerski, T., Raynaud, F. I., Robertson, A., Roughley, S. D., Schoepfer, J., Simmonite, H., Sharp, S. Y., Surgenor, A., Valenti, M., Walls, S., Webb, P., Wood, M., Workman P., Wright, L., *J. Med. Chem.*, **2009**, 52, 4794-4809.

Received: 25.05.2017.
Accepted: 02.07.2017.



DEVELOPING ETHYLENE-PROPYLENE-DIENE BLENDS FOR INDUSTRIAL APPLICATIONS

Ebtesam E. Ateia,^[a] D. E. El-Nashar,^[b] E. Takla^[a] M. Abd Alla Mahmoud^[a]

Keywords: Black filler; white filler; swelling measurements; mechanical properties; physico-chemical properties.

Different contents of high abrasion furnace black filler [HAF] and white filler [silica] are mixed with ethylene-propylene-diene monomer rubber [EPDM] cured by the conventional sulfur system. The thermogravimetric analysis (TGA) characteristics, physico-mechanical properties and swelling measurements of the prepared samples have been investigated. EDAX analyses were done to define the chemical composition of the investigated samples and to locate the dispersion of the fillers and their intensity. Comparison of the black and white fillers was performed and it was found that filler incorporation into the rubber matrix was one of the major parameters that enhanced the tensile strength and swelling resistance. The hardness of the investigated samples increased with increasing the filler concentration up to 40/60 phr (part per hundred parts of rubber). This increase can be attributed to greater and more uniform dispersion of filler into the rubber system. Carbon/silica are extensively used in the industry as cheapening filler with high reinforcing effect. Finally, the addition of precipitated silica at the expense of toxic carbon black (CB) is the main step in decreasing the health risk associated with the presence of CB-filled EPDM composites.

* Corresponding Authors

Fax: No Fax

E-Mail: drebtesam2000@yahoo.com

[a] Physics Department, Faculty of Science, Cairo University, Giza, Egypt

[b] Department of Polymers and Pigments, National Research Centre, Dokki, Cairo, Egypt.

% and 200 % were determined using a Zwick tensile machine (model 1425).⁷ Hardness was measured using the Shore A, durometer according to D2240-07; Equilibrium swelling of the investigated samples was carried out in toluene. The swelling percentage (Q %) of the samples was calculated by using the following equation.⁸

$$Q(\%) = 100 \frac{W - W'}{W'} \quad (1)$$

where W and W' represent the weights of the samples after swelling and free from dissolved matter respectively.

The swelling data were utilized to determine the molecular weight between cross-links M_C by applying Flory–Rehner relation.^{9,10} The degree of cross-linking density (ν) is given as:⁹

$$\nu = \frac{1}{2M_C} \quad (2)$$

Introduction

Ethylene-propylene-diene rubber (EPDM) is one of the most widely used synthetic elastomer, having both special and general-purpose applications. Fillers are incorporated into ethylene-propylene-diene polymer mainly to enhance service properties and in many cases to decrease the material cost. In most applications, carbon black (CB) and silica have been used as the main reinforcing fillers that increase the effectiveness of rubber. When carbon black (CB) is added into rubber, the tensile strength, tear strength, modulus and abrasion resistance are increased.¹ However, silica provides a unique combination of tear strength, abrasion resistance, aging resistance and adhesion properties.^{2,3} Since silica and carbon black have unique advantages, the utilization of hybrid filler of silica and carbon black in rubber should give the benefits of both fillers. The addition of precipitated silica in CB-filled rubber can be applied to tire treads, wire and fabric coating, hoses, rubber-covered belts, engine mounts and cable jackets.^{4,5} The effect of filler ratio on the physico-chemical and mechanical properties of EPDM has been studied to develop and characterize an applicable rubber with good mechanical properties and low cost.

Experimental

All rubber ingredients were mixed with each other as that was mentioned in our previous work.⁶ The tensile strength, elongation at break, Young's modulus and modulus at 100

Results and Discussion

The TGA curves obtained for the investigated samples made with using carbon black and silica can be seen in Figure 1 and the calculated parameters are given in Table 1. The obtained TGA curves indicate three stages of degradation process. In the temperature range from room temperature to 250 °C there was no observed change in the weight of samples while above 250 °C a slow degradation could be observed up to ≈ 350 °C. Above 350 °C, the decomposition rate is high, which shows the decomposition of organic polymeric materials.

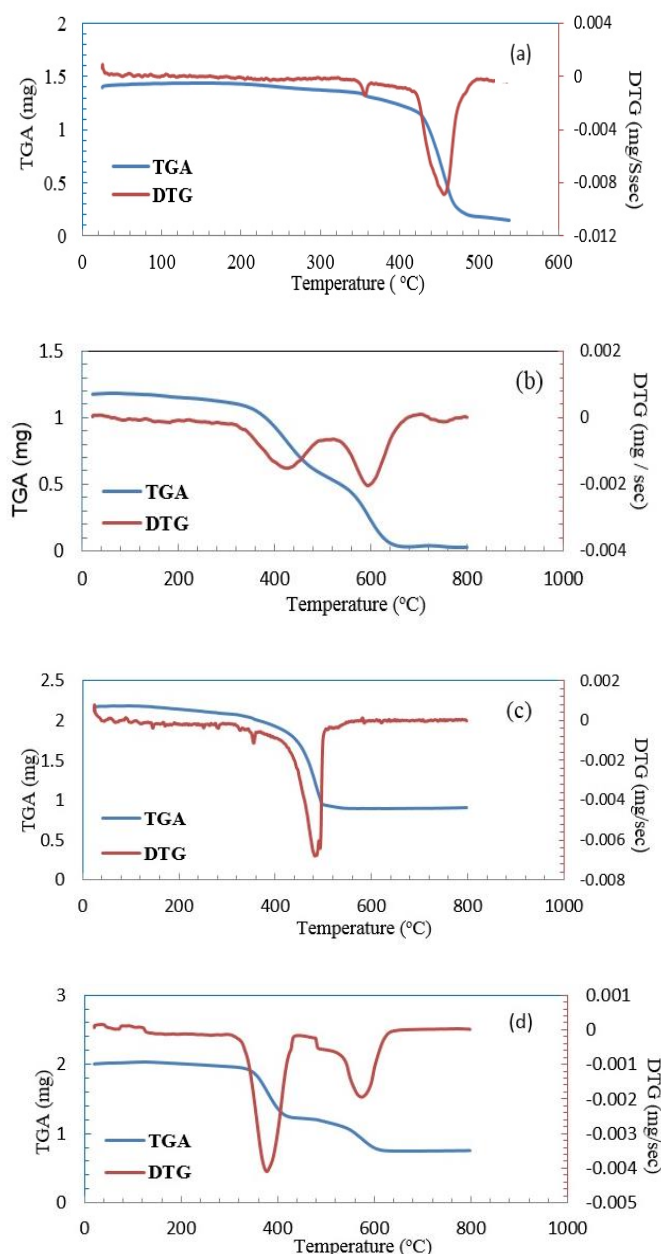


Figure 1. Thermogravimetric analysis curves for (a) EPDM without filler (b) 100 carbon / zero silica (c) zero Carbon/100 silica (d) 40 carbon / 60 silica

It is clear that the thermal stability of EPDM samples increased with increasing filler loading especially in the case of carbon black (CB). This can be due to the existence of C-C bonds with high binding energy. This approves the ability of CB in retarding the heat diffusion into EPDM matrix. However, the lowest thermal stability is obtained for EPDM loaded with 100 phr (phr: part per hundred parts of rubber), silica. This can be attributed to the lower binding energy of Si-C bonds compare to binding energy of C-C bond (346 kJ mol^{-1}).¹¹

The DTG curves have only one degradation peak, corresponding to maximum weight losses of the investigated samples. The obtained data agrees well with the previous discussion.

DSC data (Table 1) provided information concerning the change of enthalpy associated with a physical or chemical change within a material.

The conventional Field Emission Scanning Electron Microscopy (FESEM) was used to provide information about the morphology of the investigated samples. This method provided detailed information about the size and distribution of fillers and then the filler-rubber interactions as well.¹² Figure 2. represents the FESEM for the EPDM without filler, 100CB/0 silica and the samples loaded with the optimum concentrations of carbon black and white silica of 40/60 phr respectively. It is clear that the cracks and vicinity were the main features of the EPDM without filler as shown in Fig.2a. Heavy agglomerations of carbon black were observed for EPDM loaded with 100CB/0 silica (Fig. 2b), which could be attributed to filler-filler interaction networking. The surface of 40 CB/60 silica containing samples was improved and became smoother due to the uniform dispersion of optimum filler concentration as shown in Fig.2c. A good dispersion of the silica filler in the rubber matrix¹³ reduced the filler-filler interaction and increased the rubber-filler interaction.¹⁴

EDAX analyses were done to define the chemical composition of the investigated samples and to locate the dispersion of the filler and its intensity. EDAX analyses of the typical samples are given as inset in Fig. 2.

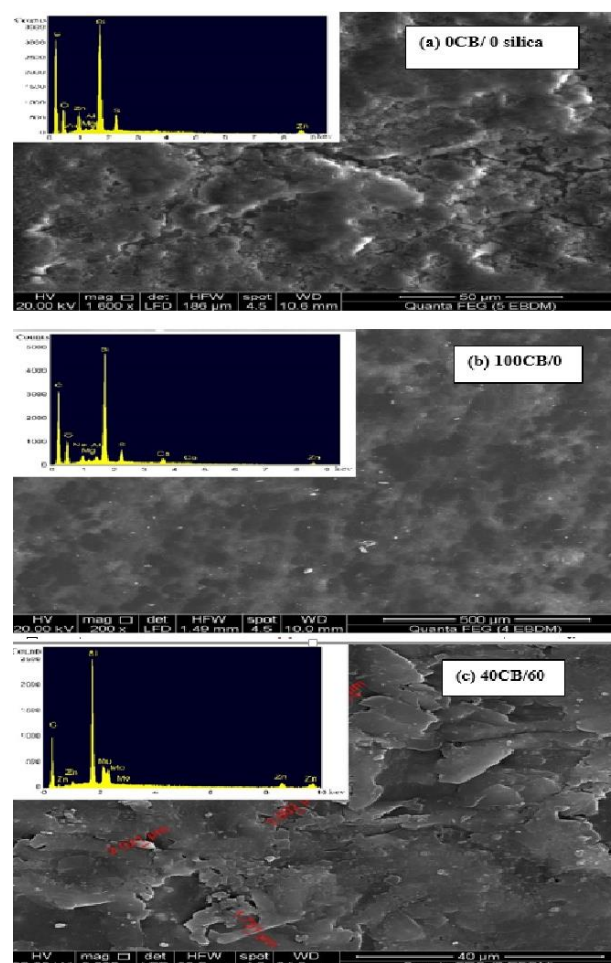


Figure 2. The FESEM images of (a) EPDM without filler (b) 100 carbon / zero silica (c) EPDM loaded with the optimum concentrations of carbon black and white silica respectively. Inset figures show EDAX analyses of the investigated samples.

Table 1. DSC and TGA parameters for the investigated samples.

Samples	Weight loss	DTG peak temp., °C	$\Delta H \text{ J g}^{-1}$	Thermal stability temp, °C	T_g , °C
0 CB /0 silica	%	448	4.066	461	-19.8
100CB /zero silica	49.44 %	586	0.2557	766	-69.2
0 CB / 100silica	47.866 %	475	3.260	496	-57.29
40 CB /60 silica	37.815%	507	0.9721	604	-70.5

Table 2. Rheological parameters of EPDM filled with different concentrations of carbon black and silica.

CB/silica content	Properties						
	M_L (1b.in)	M_H (1b.in)	t_{C90} (min)	t_{S2} (min)	CRI (min ⁻¹)	$\Delta t=(M_H-M_L)(1b.in)$	α_f
0/0	5	41	7	3	25	36	0.0
100/0	8	59	9	6	33.33	51	0.44
80/20	11	71	11	8.5	40	60	0.73
60/40	13	85	14	12	50	72	1.07
40/60	16	90	16	14.5	66.67	74	1.20
20/80	11	86	13	10	33.33	73	1.09
0/100	10	83	10	6.5	28.58	73	1.02

Table 3. Swelling characteristics of EPDM filled with HAF black and Silica.

CB/silica content	Soluble fraction, $\Delta M\%$	The crosslink density, $\nu_{EANC} \times 10^{20}$	$1/Q$	Q_f/Q_g
0/0	203.7	1.454	0.441	0
100/0	101.2	6.087	0.901	0.489
80/20	86.8	11.836	1.318	0.334
60/40	96.6	17.471	1.686	0.261
40/60	95.8	38.323	3.003	0.147
20/80	103.8	23.573	2.070	0.213
0/100	135.8	18.640	1.761	0.250

The rheological features of the EPDM filled with HAF and silica are given in Table 2. The minimum torque M_L , which reflects minimum viscosity of the blends can be taken as a measuring tool of filler-filler interaggregate formation.¹⁵ M_H is the maximum torque which reveals the cross-linking density of the loaded samples. The table shows that M_L values were gradually increased with increasing silica content (decreasing carbon black) up to a ratio of 40/60 phr of carbon black and silica respectively. On the other hand, M_H values were increased with larger rates than M_L values up to the same ratio of 40/60 phr then the values were decreased. This behavior was observed due to the presence of the fillers in the investigated samples which reduced the mobility of macromolecules and accordingly increased the torque of the vulcanizates up to optimum content.¹⁶ This increase was the consequence of the creation of hydrogen bonds induced strong interactions between rubber and filler materials.¹⁷ The difference between M_H and M_L was a rough estimation possibility of the crosslinking density of the prepared samples and it was identified as Δt . It nearly increased with increasing filler content. However, among the EPDM filled samples, the carbon/silica filler ratio 40/60 showed the highest Δt . This was an indication of the enhancement in the filler- filler interaction. The obtained data showed that the scorch time T_{S2} of the samples increased with increasing silica content up to the optimum ratio of 40/60 phr of filler content. This was because of the absorption of the accelerator by silanol groups on the silica

surface. The change in rheometric torque with filler content was used to distinguish the filler-matrix interaction or reinforcement. The reinforcement factor α_f is determined from the following relation:¹⁸

$$\alpha_f = \frac{[\Delta L_{\max}(\text{filled}) - \Delta L_{\max}(\text{gum})]}{\Delta L_{\max}(\text{gum})} \quad (3)$$

where $\Delta L_{\max}(\text{filled})$ and $\Delta L_{\max}(\text{gum})$ are the variations in maximum torque through vulcanization for the filled and gum samples, respectively.

From the α_f values listed in Table 2, it is clear that the values of α_f for both HAF and silica are continuously increasing with the addition of both white and black fillers.

The effect of carbon black and white silica filler on mechanical parameters such as tensile strength σ (MPa), elongation at break $\epsilon_{\text{break}}\%$, Young's modulus E (MPa) and the hardness shore (A), modulus at 100% and 200 % of ethylene-propylene-diene (EPDM) polymers are shown in Figure 3.

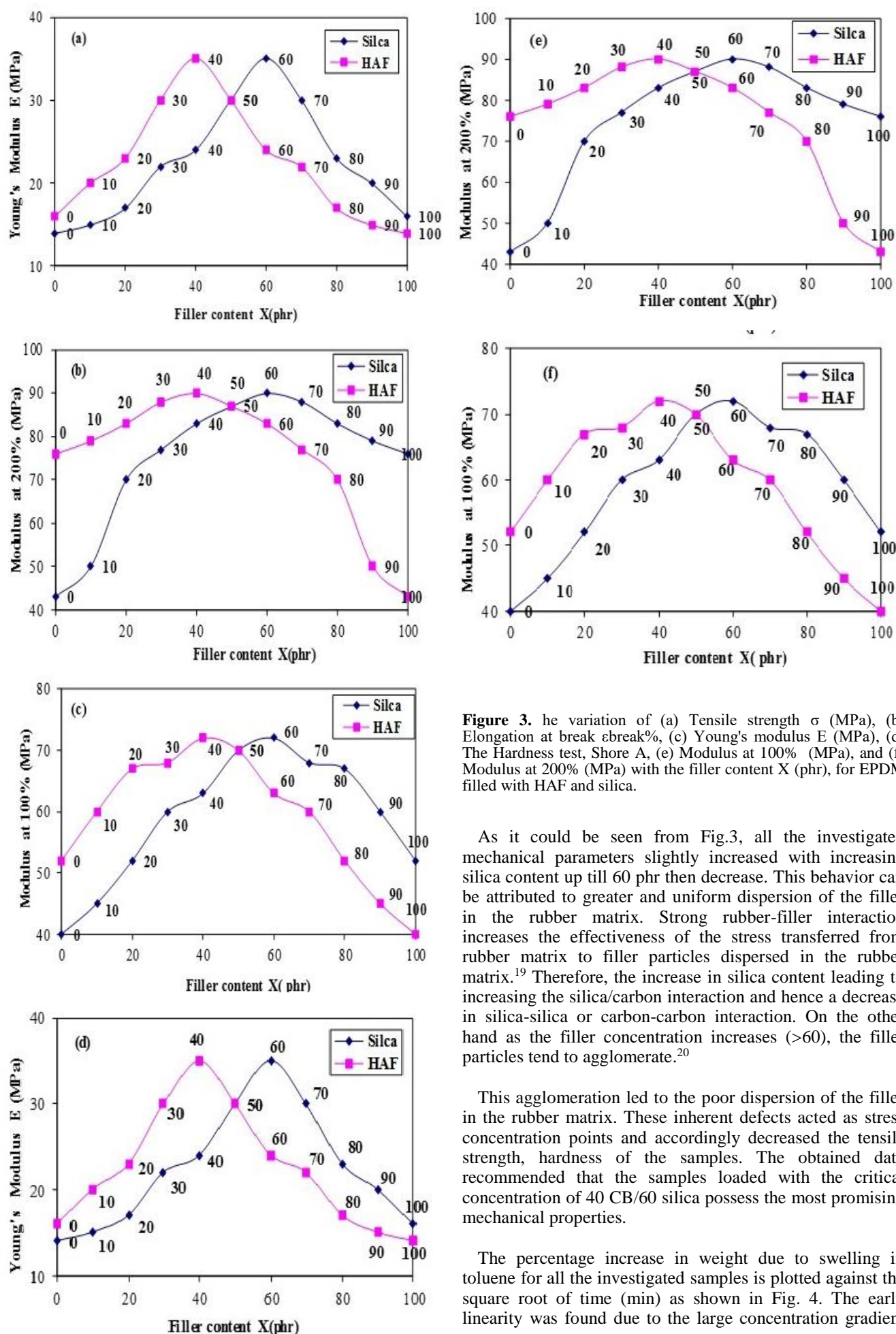


Figure 3. The variation of (a) Tensile strength σ (MPa), (b) Elongation at break $\epsilon_{\text{break}}\%$, (c) Young's modulus E (MPa), (d) The Hardness test, Shore A, (e) Modulus at 100% (MPa), and (f) Modulus at 200% (MPa) with the filler content X (phr), for EPDM filled with HAF and silica.

As it could be seen from Fig.3, all the investigated mechanical parameters slightly increased with increasing silica content up till 60 phr then decrease. This behavior can be attributed to greater and uniform dispersion of the filler in the rubber matrix. Strong rubber-filler interaction increases the effectiveness of the stress transferred from rubber matrix to filler particles dispersed in the rubber matrix.¹⁹ Therefore, the increase in silica content leading to increasing the silica/carbon interaction and hence a decrease in silica-silica or carbon-carbon interaction. On the other hand as the filler concentration increases (>60), the filler particles tend to agglomerate.²⁰

This agglomeration led to the poor dispersion of the filler in the rubber matrix. These inherent defects acted as stress concentration points and accordingly decreased the tensile strength, hardness of the samples. The obtained data recommended that the samples loaded with the critical concentration of 40 CB/60 silica possess the most promising mechanical properties.

The percentage increase in weight due to swelling in toluene for all the investigated samples is plotted against the square root of time (min) as shown in Fig. 4. The early linearity was found due to the large concentration gradient

of solvent in the samples. The stability of the curve meant that the rubber samples extraction or degradation of its soluble ingredients was extremely small. It was obvious that the swelling rate of CB filled EPDM samples were decreased higher than in case of the silica filled system.

The increase of the swelling rate in silica filled samples was the consequence of the filler aggregate formation in the rubber matrix. The precipitated silica possessing many hydroxyl groups on its surface and as a result, the intermolecular hydrogen bonds between hydroxyl groups were very strong. Hence it aggregated tightly as that was confirmed by FESEM results.

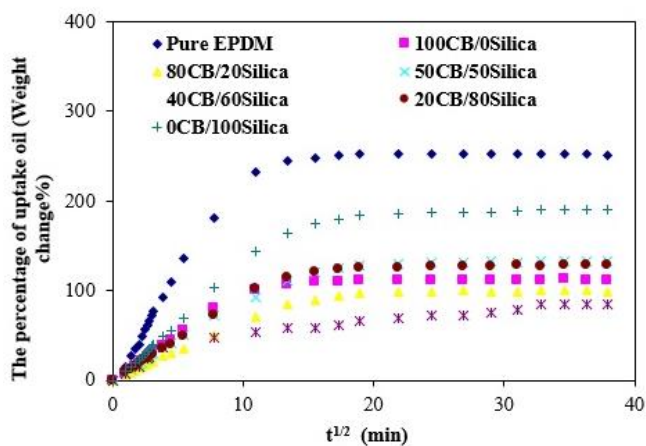


Figure 4. Solvent uptake percent versus square root of time for EPDM filled with HAF black and silica.

In general, the rubber swelling is influenced by numerous factors, such as density and crosslinking type, amount and type of elastomer and type of filler. The effect of interaction between rubber and the filler blend can be investigated and calculated using Lorenz and Parks equation^{21,22}.

$$\frac{Q_f}{Q_g} = ae^{-z} + b \quad (4)$$

The subscripts f and g in Eq. 4 denote to the filled and unfilled rubber vulcanizates respectively, z is the ratio by weight of filler in the vulcanizate, while a and b are constants.

The obtained values of Q_f/Q_g and $1/Q$ are presented in Table 3. The obtained data shows that the values of Q_f/Q_g decrease while the values of $1/Q$ increase with the increasing carbon black content up to the optimum concentration 40/60 phr. Moreover, the lowest values of Q_f/Q_g and the highest ones for $1/Q$ designate that, the higher the filler content, the stronger the rubber-filler interaction²³. Finally, the obtained data indicates that 40 CB/ 60 silica was capable of producing greater rubber-filler interaction compared to each of CB and silica separately. This was due to the more homogeneous dispersion of 40 CB/60 silica within the rubber matrix as confirmed by the morphological study. The calculated cross-links density ν (as shown in Table 3) confirmed the previous discussion.²⁴

The dependence of maximum weight change and cross-linking density with filler concentration for the investigated samples can be seen in Fig.5. As it can be seen from the figure, the lowest swelling rate is obtained for samples loaded with the optimum filler concentration 40 CB/60 silica, which agreed well with the calculated data gave in Table 3.

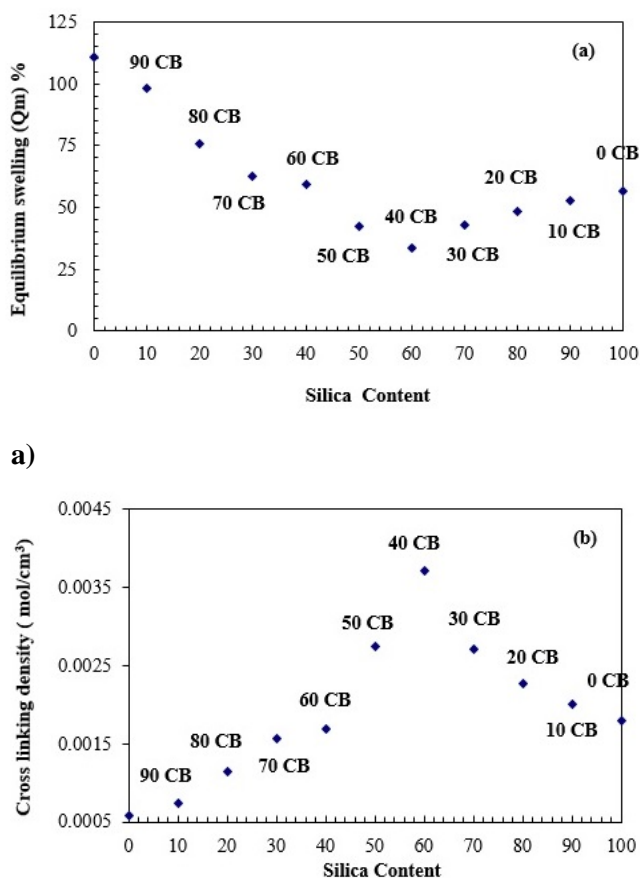


Figure 5. The dependence of maximum weight change(a) and cross linking density (b) with filler concentration for the investigated samples.

Conclusion

A significant enhancement of the property of the investigated EPDM samples by the addition of fillers could be achieved. Comparison of silica and carbon black additives demonstrated that carbon enhanced the thermal stability of EPDM. TGA studies revealed that the thermal stability of the investigated samples increased due to the incorporation of carbon black into the EDPM. The filler ratio 40 CB/60 silica appeared to be an excellent candidate for thread application to accomplish an overall good mechanical and physicochemical properties.

References

- Mahapatra, S. P. Tripathy, D. K., *Cell. Polym.*, **2005**, *24*, 209-222.
- Laube, S. and Shell, J., *Meeting of the Rubber Division*, American Chemical Society, Savanna, **2002**.

- ³Ismail, M. N. El-Sabbagh S. H. and Yehia, A. A., *J. Elastom. Plast.*, **1999**, *31*, 255-270.
- ⁴Saad, A. G. El-Sabbagh, S. H., *J. Appl. Polym. Sci.*, **2001**, *79(1)*, 60-71.
- ⁵Guy, L. Daudey, S. Cochet P. and Bomal, Y., *Raw Mater. Appl.*, **2009**, *62*, 383-391.
- ⁶Hassan, H. H., Ateia, E., Darwish, N. A., Halim, S. F., Abd El-Aziz, A. K., *Mater. Des.*, **2012**, *34*, 533-540. <https://doi.org/10.1016/j.matdes.2011.05.005>
- ⁷Leblanc, J. L., *Prog. Polym. Sci.*, **2002**, *27*, 627-687. [https://doi.org/10.1016/S0079-6700\(01\)00040-5](https://doi.org/10.1016/S0079-6700(01)00040-5)
- ⁸Julve, D., Pérez, J., Ramos J. and Menéndez, M., *Rubber Chem. Technol.*, **2011**, *84(1)*, 74-87. <https://doi.org/10.5254/1.3544676>
- ⁹De, S., Panda, P. K., Bhunia S, and Roy, M., *Polym. Plast. Technol. Eng.*, **2014**, *53(11)*, 1131-1141. <https://doi.org/10.1080/03602559.2014.886117>
- ¹⁰Zhag, G. Q. Zhou, M. H., Ma, J. H. Liang, B. R., *J. Appl. Polym. Sci.*, **2003**, *90*, 2241-2245. <https://doi.org/10.1002/app.12888>
- ¹¹Clarson S. J. and Semlyen, J. A., "Siloxane Polymers," PTR Prentice Hall, New Jersey, **1993**, 567-615.
- ¹²Yin, D., Zhang, Y., Peng, Z., Zhang, Y., *J. Appl. Polym. Sci.*, **2003**, *88*, 775-82. <https://doi.org/10.1002/app.11604>
- ¹³Ichazo, M. N. Albano, C., Hernandez, M., Gonzalez J. and Carta, A., *Adv. Mat. Res.*, **2008**, *47-50*, 113-116. <https://doi.org/10.4028/www.scientific.net/AMR.47-50.113>
- ¹⁴Wolff, S., Gori, U. Wang, M. J. and Wolff, W., *ERJ*, **1994**, *16*, 16-19.
- ¹⁵Yan, H., Sun, K., Zhang Y. and Zhang, Y., *Polym. Test.*, **2005**, *24*, 32-38. <https://doi.org/10.1016/j.polymertesting.2004.07.011>
- ¹⁶Li, Y., Wang, M. J., Zhang, T., Zhang F. and Fu, X., *Rubber Chem. Technol.*, **1994**, *67*, 693. <https://doi.org/10.5254/1.3538704>
- ¹⁷Kaushik, P., Rajasekar, R., Dong Jin, K., Zhen Xiu, Z., Samir, K. P., Chapal, K. D., Jin, K. K., *Mater. Des.*, **2010**, *31*, 677. <https://doi.org/10.1016/j.matdes.2009.08.014>
- ¹⁸Trakarnpruk, W., Porntangjitlikit, S., *Renew. Energy*, **2008**, *33*, 1558-1563. <https://doi.org/10.1016/j.renene.2007.08.003>
- ¹⁹Leblanc, J. L., *Prog. Polym. Sci.*, **2002**, *27*, 627-687. [https://doi.org/10.1016/S0079-6700\(01\)00040-5](https://doi.org/10.1016/S0079-6700(01)00040-5)
- ²⁰Wolff, S., *Rubber Chem. Technol.*, **1996**, *69*, 325-346. <https://doi.org/10.5254/1.3538376>
- ²¹Ismail, H., Ramly, A. F., Othman, N., *J. Appl. Polym. Sci.*, **2013**, *128*, 2433-2438. <https://doi.org/10.1002/app.38298>
- ²²Ward, A. A., Khalif, A. L., *J. Elastom. Plast.*, **2007**, *60*, 623-630.
- ²³Roy, K., Alam, Md. N., Mandal, S. K., Debnath, S. C., *J. Nanostruct. Chem.*, **2016**, *6*, 15-24. <https://doi.org/10.1007/s40097-015-0174-x>
- ²⁴Yatsuyanagi, F., Suzuki, N., Ito, M., Kaidou, H., *Polymer*, **2001**, *42*, 9523-9529. [https://doi.org/10.1016/S0032-3861\(01\)00472-4](https://doi.org/10.1016/S0032-3861(01)00472-4)

Received: 20.05.2017.

Accepted: 02.07.2017.



ENERGY CHARACTERISTICS OF HYDROCARBON - WATER FUEL MIXTURES

G. A. Korablev^[a] and N. V. Khokhriakov^[a]

Keywords: Spatial-energy parameter, cluster water nanostructures, high energy bonds.

The consistent calculations of bond energy in cluster water nanostructures have been performed following the *P*-parameter methodology and quantum-mechanical methods. The formation of high energy bonds in the process of hydrocarbon hydrogen containing fuel preparation has been explained.

* Corresponding Authors

E-Mail: korablevga@mail.ru

[a] Izhevsk State Agricultural Academy, 426069, Russia, Izhevsk, Studencheskaya St., 11,

Introduction

Water plays an ambiguous role in of hydrocarbon fuels of internal combustion engines. On the one hand, simple dilution of petroleum or diesel fuel with water can significantly deteriorate fuel characteristics of the mixture. The water containing fuels¹ can have the potential energy of 1/3 from energy unit of petroleum, and nevertheless the engines produce the same power as with the additional amount of petroleum by the mass equal to the mass of water added.. Specificity of technological processes is ultimately defined by the mechanism of physic-chemical transformations occurring on the atom-molecular level. In this investigation, their possible evaluations are studied based on the concept of spatial energy parameter (*P*-parameter).

Formation of high energy bonds in fuel mixtures

Practical use of hydrogen containing fuel is possible only if a number of conditions are fulfilled:

The introduction of complex additives into the fuel, with alcohols such as ethanol and so-called “hydrogen catalyst” content having the primary meaning.¹ Such additives are mixed following the special technique – first, by separate fractions, and in the end, all the mixture is intensively stirred by a hydraulic cutting pump (hydraulic shears). “Hydrogen catalyst” contributes to active dissociation of water molecules with the formation of hydrogen and oxygen which burn in the engine chamber afterward.

But is not clear how during such a short combustion time of the given amount of mixture introduced into the chamber, water dissociation in this volume and burning of its products

can take place. Moreover, as a result of water dissociation by the reaction $\text{H}_2\text{O}=\text{H}^++\text{OH}^-$ the direct oxygen release is not observed. Obviously, other important mechanisms of physico-chemical transformation of energy are involved. For instance, whose potential energy increases due to the formation of special high energy bonds. It is possible that similar processes take place during the formation of burning mixture. This is aided by the introduction of alcohols (up to 20 %) into the fuel mixture that results in the formation of fullerene, for example, $\text{C}_{60}(\text{OH})_{10}$. High energy bonds formed in the systems $\text{C}_{60}(\text{OH})-n(\text{H}_2\text{O})$ due to the introduction of “hydrogen catalyst” into the mixture.

Similar to ATP hydrolysis which is accompanied by the release of chemical bond energy, the breakage of high energy bonds releases heat in containing fuel when it is burning in the engine chamber. The physico-chemical mechanism of the formation of energy saturated bonds in this system is given below.

Investigation technique

The value of the relative difference of *P*-parameters of interacting atom-components – coefficient of structural interaction α was used as the main numerical characteristic of structural interactions in condensed media:²

$$\alpha = 100 \frac{P_1 - P_2}{(P_1 + P_2) / 2} \quad (1)$$

Applying the reliable experimental data, we obtain the nomogram of the dependence degree of structural interactions upon coefficient α – unified for the wide range of structures. This approach allows evaluating the degree and of structural interactions of phase formation, isomorphism and solubility processes in multiple systems, including molecular ones. In particular, the features of cluster formation in the system $\text{CaSO}_4 - \text{H}_2\text{O}$ have been investigated.³

Table 1. P-parameters of atoms calculated via the electron bond energy

Atom	Valence electrons	W, eV	r_i , Å	q^2 , eV Å	P_0 , eV Å	R, Å	$P_E=P_0/R$, eV
H	1S ¹	13.595	0.5295	14.394	4.7985	0.5295	9.0624
H	1S ¹					0.28	17.137
C	2P ¹	11.792	0.596	35.395	5.8680	0.77	7.6208
C	2P ¹					0.69	8.5043
C	2P ²	11.792	0.596	35.395	10.061	0.77	13.066
C	2S ¹	19.201	0.620	37.240	9.0209	0.77	11.715
C	2S ²				14.524	0.77	18.862
C	2S ² +2P ²				24.585	0.77	31.929
C	1/2(2S ² +2P ²)						15.964
O	2P ¹	17.195	0.4135	71.383	4.663	0.66	9.7979
O	2P ²	17.195	0.4135	71.383	11.858	0.66	17.967
O	2P ²					0.59	20.048
O	2P ⁴	17.195	0.4135	71.383	20.338	0.66	30.815

To evaluate the directness and degree of phase formation processes¹ the following equations are used:

$$\frac{1}{q_2 / r_i} + \frac{1}{W_i / n_i} = \frac{1}{P_E} \quad (21)$$

Initial values of P-parameters:

$$r_E = \frac{1}{r_0 P_0} = \frac{1}{q^2} = \frac{1}{(W r n)_i} \quad (3)$$

$$P_E = \frac{P_0}{r_i} \quad (4)$$

where:

W_i – electron orbital energy;⁴

r_i – orbital radius of i orbital;⁵

$q = Z/n$ – by^{6,7}

n_i – number of electrons in the given orbital,

Z^* and n^* – effective nucleus charge and effective main quantum number.

P_0 is called as spatial energy parameter, and

P_E – effective P-parameter.

The calculation results by equations^{2,3,4} for a number of elements are given in Table 1, from which it is seen that for hydrogen atom the values of P_E – parameters substantially differ at the distance of orbital (r_i) and covalent (R) radii. The hybridization of valence orbitals of carbon atom is evaluated as the averaged value of P-parameters of 2S² and 2P²- orbitals.

Values of P_c -parameter in binary and complex structures:

$$\frac{1}{P_c} = \frac{1}{N_1 P_1} + \frac{1}{N_2 P_2} + \dots \quad (5)$$

where N – number of homogeneous atoms in each subsystem.

The results of such calculations for some systems are given in Table 2.

Bond energy (E) in binary and more complex systems:

$$\frac{1}{E} \approx \frac{1}{P_E} = \frac{1}{P_1(N/k)_1} + \frac{1}{P_2(N/k)_2} \dots \quad (6)$$

where (as applicable to cluster systems) k_1 and k_2 – number of subsystems forming the cluster system; N_1 and N_2 – number of homogeneous clusters.⁷ So for C₆₀(OH)₁₀ $k_1 = 60$, $k_2 = 10$.

Calculations and comparisons

It was assumed that structural-stable water cluster could have the same static number of subsystems (k) as the number of subsystems in the system interacting with it.⁸ For example, the water cluster (H₂O)₁₀ is interacting with fullerene [C₆OH]₁₀.

Similarly with cluster [C₆OH]₁₀ the formation of the cluster [(C₂H₅OH)₆ – H₂O]₁₀ is apparently possible, which corresponds to the system (C₂H₅OH)₆₀ – (H₂O)₁₀. The interaction of water clusters was considered as the interaction of subsystems (H₂O)₆₀ – N(H₂O)₆₀.

Based on such concepts, the bond energies in these systems are calculated by equation 6, the results are given in Table 3. To compare, the calculation data obtained by Khokhriakov N.V. with quantum-chemical techniques¹⁰ are also given.

Both techniques produce consistent values of bond energy (in eV). Besides, the methodology of P-parameter allows explaining why the energy of cluster bonds of water molecules with fullerene C₆₀(OH)₁₀ 2 times exceed the bond energy of the molecules of cluster water (Table 3).

Table 2. Structural P_c-parameters

Radicals, molecules	P ₁ , eV	P ₂ , eV	P ₃ , eV	P ₄ , eV	P _c , eV	Orbitals of oxygen atom
OH	17.967	17.137			8.7712	2P ²
OH	9.7979	9.0624			4.7080	2P ¹
H ₂ O	2 × 17.138	17.967			11.788	2P ²
H ₂ O	2 × 9.0624	17.967			9.0226	2P ²
C ₂ H ₅ OH	2 × 15.964	2 × 9.0624	9.7979	9.0624	3.7622	2P ¹

Table 3. Calculation of bond energy – E, eV

System	C ₆₀ P ₁ /k ₁	(OH) ₁₀ P ₂ /k ₂	(H ₂ O) ₁₀ P ₃ /k ₃	n ₃	P _E , eV From eqn. (6)	E, eV From quantum-mechanical calcn.
C ₆₀ (OH) ₁₀ –N(H ₂ O) ₁₀	15.964/60	8.7712/10	11.788/10	1	0.174	0.176
				2	0.188	0.209
				3	0.193	0.218
				4	0.196	0.212
				5	0.197	0.204
(H ₂ O) ₆₀ –N(H ₂ O) ₆₀	9.0226/60	9.0226/60		n ₂		
				1	0.0768	0.0863
				2	0.1020	0.1032
				3	0.1128	0.1101
				4 5	0.1203	0.1110
(C ₂ H ₅ OH) ₆₀ –(H ₂ O) ₁₀	3.7622/60	9.0226/10			0.1274	0.115
(C ₂ H ₅ OH) ₁₀ –(H ₂ O) ₆₀	3.7622/10	9.0226/60			0.0586	0.0607
					0.1074	≈ 0.116

Table 4. Spatial-energy interactions in the system H-R, where R= C, (OH), H₂O

System	P ₁ , eV	P ₂ , eV	α=100ΔP/<P>	Spatial bond type
H-C	17.137	15.964	7.09	Covalent
H-OH	9.0624	8.7712	3.27	Orbital
H-H ₂ O	9.0624	9.0226	0.44	Orbital

In accordance with the nomogram, the phase formation of structures can take place only if the relative difference of their P-parameters (α) is under 25-30 %, and the most stable structures are formed when α < 6-7 %.

In Table 4 different values of coefficient α in systems H-C, H-OH and H-H₂O are given, which are within 0.44 – 7.09 (%). The interactions at the distances of covalent radii have been taken into account in the system H-C for carbon and hydrogen atoms, while for other systems – at the distance of orbital radius.

The interaction in system H-C at the distances of covalent radius plays a role of fermentative action, which results in the transition of dimensional characteristics in water molecules from the orbital radius to the covalent one and formation of system C₆₀(OH)₁₀ – N(H₂O)₁₀ with bond energy between the main components 2 times greater than between the water molecules (high energy bonds).

Thus, broad capabilities of water clusters to change their spatial-energy characteristics apparently explain all the diversity of structural properties of water in its different modifications, including the formation of high energy bonds in water containing fuel for internal combustion engines.

Conclusions

Results of bond energy calculations in water cluster nanostructures following the P-parameter methodology agree with quantum-mechanical methods.

Changes which can take place in spatial-energy characteristics of water clusters explain the formation of high energy bonds in the process of hydrocarbon fuel preparation.

The breaking of these bonds with the release of an additional amount of heat energy occurs in the combustion chamber.

References

- ¹Gupperman. R. V., USA Patent *US5156114*; **1995**.
- ²Korablev G. A., *Spatial-Energy Principles of Complex Structures Formation*, Leiden, the Netherlands, Brill Academic Publishers and VSP, **2005**, 426 pages (Monograph).
- ³Korablev G. A., Yakovlev G. I., Kodolov V. I., Some features of cluster formation in the system CaSO₄-H₂O. *Chem. Phys. Mesoscopy*, **2002**, 4(2), 188-196.
- ⁴Fischer C. F., Average-Energy of Configuration Hartree-Fock Results for the Atoms Helium to Radon, *Atomic Data*, **1972**, 4, 301-399.
- ⁵Waber J. T., Cromer D. T., Orbital Radii of Atoms and Ions, *J. Chem. Phys.* **1965**, 42(12), 4116-4123. <https://doi.org/10.1063/1.1695904>
- ⁶Clementi E., Raimondi D. L. Atomic Screening Constants from S.C.F. Functions 1., *J. Chem. Phys.*, **1963**, 38(11), 2686-2689. <https://doi.org/10.1063/1.1733573>
- ⁷Clementi E., Raimondi D. L. Atomic Screening Constants from S.C.F. Functions 2. *J. Chem. Phys.*, **1967**, 47(4), 1300-1307. <https://doi.org/10.1063/1.1712084>
- ⁸Korablev G. A., Zaikov G. E. Energy of the chemical bond and spatial-energy principles of hybridization of atom orbitals, *J. Appl. Polym. Sci.*, **2006**, 101(3), 2101-2107. <https://doi.org/10.1002/app.24213>
- ⁹Hodges M. P., Wales D. J., Global minima of protonated water clusters. *Chem. Phys. Lett.*, **2000**, 324, 279-288. [https://doi.org/10.1016/s0009-2614\(00\)00584-4](https://doi.org/10.1016/s0009-2614(00)00584-4)
- ¹⁰Khokhriakov N. V., Ferrers, M., Electronic properties of contacts of ideal carbon nanotubes, *Chem. Phys. Mesoscopy*, **2002**, 4(2), 261-263.

Received: 02.04.2017.

Accepted: 07.07.2017.



PHOTOCATALYTIC ACTIVITY OF CdS-ZnS COMPOSITE AND THEIR COMPONENTS

Taruna Dangi,^[a] Basant Menariya,^[a] Rakshit Ameta^[a] and Suresh C. Ameta^[a]

Keywords: ZnS; CdS; composite; photocatalytic activity; Evan's blue.

A composite of CdS and ZnS was prepared by simple solid state mechanochemical method and it was used for photocatalytic degradation of Evan's blue. The photocatalytic efficiency of CdS-ZnS composite was compared with pure CdS and ZnS. The effect of various parameters such as pH, the concentration of dye, amount of semiconductor and light intensity was observed. The optimum conditions obtained for this degradation were: Evan's blue = 1.3×10^{-5} M, pH = 5.5, amount of composite = 0.12 g and light intensity = 50.0 mWcm⁻². It was found that coupled chalcogenide CdS - ZnS shows better photocatalytic activity as compared with pure CdS and ZnS for the degradation of Evan's blue in the presence of visible light.

* Corresponding Authors

E-Mail: t1991dangi@gmail.com

[a] Department of Chemistry, PAHER University, UDAIPUR – 313003 (Raj.) INDIA

Introduction

Industrial activities have introduced large quantities of chemicals in the environment causing potential harm to the ecosystem. Among pollutants, dyes are one of the major sources of environmental contamination. As the international environmental standards are becoming more stringent, many research studies have focused their attention on the treatment of waste water. Although there are various techniques available to remove or degrade these pollutants like adsorption, air stripping, biological methods, various oxidation processes, etc., each one has its advantage and limitations. Recently, photocatalytic treatment of waste water has gained much attention, because it provides an eco-friendly pathway for removal of such pollutants.

Beydoun et al.¹ reported that photocatalysis (an advanced oxidation process) provides a highly improved, eco-friendly, efficient, sustainable, and affordable solution to wastewater treatment to get fresh water demands of the future generation. Gaya and Abdullah² reported that heterogeneous photocatalysis via various metal oxides was found to be an effective way which adequately addresses many of the water quality issues. ZnS is an important II-VI semiconductor with wide band gap 3.7 eV. The wide band gap semiconductors are ideal as photocatalysts due to rapid electron-hole pair generation by photo-excitation^{3,4}. ZnS also attracted attention in fields of photoconductors, photocatalysts, optical sensors and electroluminescent materials⁵

Patil et al.⁶ prepared ZnS-graphene composite by microwave irradiation method. The composite is used as a photocatalyst in degradation of methylene blue with irradiation by 663 nm light. Under the same conditions, the photocatalytic activity of the pure ZnS was also studied. The ZnS-GNS composite was found to enhance the rate of photodegradation of methylene blue as compared to ZnS alone.

Degradation of dyes is a popular method to check the photocatalytic activity of different type of photocatalyst. Sharma et al.⁷ reported that Bromophenol blue, Crystal violet and Reactive red were successfully photo-reduced using thioglycerol capped and uncapped ZnS nanoparticles after 3.0 h of irradiation. Since the photocatalytic activity depends on the generation of electron-hole pairs and the existence of different phases, they have tried to correlate the optical and morphological studies with these results to understand the phenomenon of photocatalytic activity at the nanoscale. Though the Ultra-violet irradiation can efficiently degrade the dyes, naturally abundant solar radiation is also very useful in the mineralization of dyes.

Eyasu et al.⁸ synthesized the chromium doped ZnS nanoparticles, with (0.05, 0.1, 0.2 and 0.3 mol % of Cr) using incipient wetness impregnation method. As-synthesized Cr-ZnS composite was used in dye degradation of Methyl orange (MO) was studied under UV and visible radiation and effect of parameters such as concentration, pH, and initial dye concentration were studied on the photocatalytic degradation of MO dye. It was observed that photocatalytic degradation decreased with increasing dye initial concentration.

CdS is a well-known photocatalyst that has been used as a visible-light photocatalyst. CdS has a narrow direct band gap (2.4 eV), so it is also used as a photosensitizer of various wide band gap semiconductor photoanodes in photoelectrochemical cell⁹⁻¹¹. Ahluwalia et al.¹² synthesized Se-ZnS nanocomposites of different wt% were impregnated onto ZnS by calcination at 200°C. The specific surface area notably increased from 54 m² g⁻¹ (ZnS) to 75 m² g⁻¹ with different wt% of Se loading. The band edge absorption at 330 nm (3.77 eV) of bare ZnS significantly red-shifted to 357 nm (3.30 eV), after 1 wt% Se loading. 1 wt% Se-ZnSNCs exhibited the highest photodegradation efficiency (95%) of Methyl orange dye as compared to ZnS (55%) under 160 min UV light irradiation.

Soltani et al.¹³ prepared ZnS and CdS nanoparticles by a simple microwave irradiation method under mild conditions. The band gap energies of ZnS and CdS nanoparticles were

estimated using UV-visible absorption spectra as 4.22 and 2.64 eV, respectively. Photocatalytic degradation of Methylene blue was carried out using mixtures of ZnS and CdS nanoparticles under a 500W halogen lamp of visible light irradiation. The study of the variation in the composite of ZnS-CdS, a composition of 1:4 (by weight) was found to be very efficient in degradation of Methylene blue. Higher degradation efficiency and reaction rate were achieved by increasing the amount of ZnS-CdS composite and initial pH of the solution.

Urchin-like ZnS/CdS semiconductor composites were successfully prepared by combining solvothermal route with homogeneous precipitation process. The optical properties and photocatalytic activities of the as-prepared ZnS/CdS composites toward such organic dyes as Methyl orange, Pyronine B, Rhodamine B and Methylene blue were separately investigated. It was found that the ZnS/CdS composites exhibit excellent photocatalytic degradation activity for the above mentioned dyes under UV irradiation, as compared to corresponding pure ZnS and commercial anatase TiO₂ (P-25). This enhanced activity may be related to the modification of CdS nanoparticles on the surfaces of thorns of ZnS urchins and a tentative mechanism for the enhanced photocatalytic degradation activities of the ZnS/CdS composite catalyst was proposed¹⁴.

Ivetic et al.¹⁵ synthesized ternary and coupled binary zinc oxide/tin oxide nanocrystalline powders by a simple solid-state mechanochemical method. The degradation of alprazolam, a short-acting anxiolytic of the benzodiazepine class of psychoactive drugs by ternary (Zn₂SnO₄ and ZnSnO₃) and coupled binary (ZnO/SnO₂) oxides under UV irradiation were observed and compared with pure ZnO and SnO₂. In the present work, the composite of cadmium sulfide with zinc sulfide was prepared by simple solid state mechanochemical method and it was used for photocatalytic degradation of Evan's blue.

Experimental

Preparation of composite

A composite of CdS and ZnS was prepared by simple solid state mechanochemical method. Composite (CdS – ZnS) was prepared by mixing the same amount of CdS and ZnS (in ratio 1:1) and then ground with pestle and mortar. It was then used for photocatalytic degradation of Evan's blue.

Characterization of composite

X-rays diffraction pattern of the pure CdS-ZnS composite samples recorded in X-ray diffractometer (XPRT-PRO model) is shown in Fig. 1. Average particle size of the crystalline composite powder was calculated by Debye Scherrer's equation and it was found to be 39.98 nm.

The surface morphology and elemental composition were observed by scanning electron microscope equipped with an energy-dispersive X-ray spectrophotometer (SEM JEOL Japan make, 5610V model).

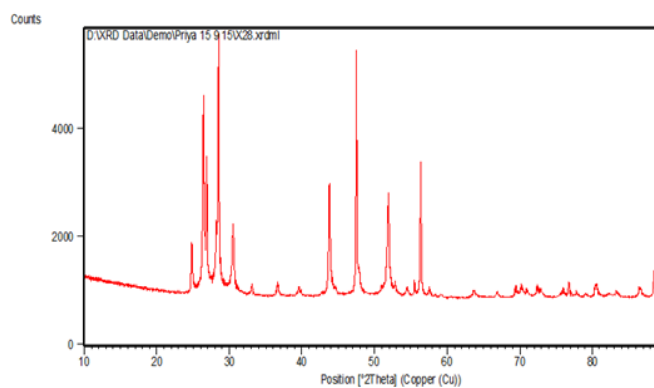


Figure 1. X-ray diffraction spectrum of composite

The SEM image of CdS-ZnS composite is shown in Fig. 2. It shows that particles have a rough surface with irregular size.

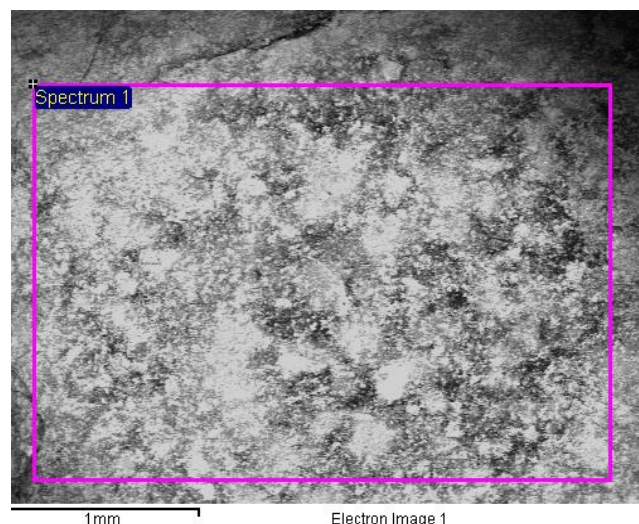


Figure 2. SEM of composite

Photocatalytic degradation

0.0960 g of Evan's blue was dissolved in 100.0 mL of doubly distilled water so that the concentration of dye solution was 1.0×10^{-3} M. It was used as a stock solution and further diluted to working solutions as and when required. The absorbance of Evan's blue solution was observed with the help of spectrophotometer (Systronic Model 106) at $\lambda_{\text{max}} = 610$ nm. It was irradiated with a 200 W tungsten lamp. The reaction solution was exposed to visible light.

A water filter was used between light source and solution to cut off thermal radiations. The dye solution was placed in equal amounts in four beakers.

- The first beaker containing Evan's blue solution was kept in dark
- The second beaker containing Evan's blue solution was exposed to light

- The third beaker containing solution Evan's blue and 0.12 g CdS-ZnS composite was kept in dark
- The fourth beaker containing Evan's blue solution and 0.12 g CdS-ZnS composite was exposed to light

After exposing these beakers for 3 hours, the absorbance of the solution in each beaker was measured with the help of a spectrophotometer. The absorbance of the solution of first three beakers was found almost constant, but the solution of the fourth beaker absorbance had a decrease as compared to the initial value of absorbance. It is clear from all these observations that the degradation required both; light and semiconductor composite.

A solution of 1.3×10^{-5} M Evan's blue was prepared in doubly distilled water and 0.12 g of ZnS, CdS and CdS-ZnS composite was added to it in separate beakers. The pH of reaction mixture was adjusted to 8.5 and then this mixture was exposed to a 200 W tungsten lamp (50.0 mWcm^{-2}). The absorbance was measured with increasing the time of exposure. Here, a linear plot between $1 + \log A$ and time was found, which shows that Evan's blue degradation followed pseudo-first order kinetics. The rate constant was calculated with the help of given formula –

$$k = 2.303 \times \text{slope} \quad (1)$$

Results and discussion

The results of a typical run of optimum condition is shown in Table 1.

Table 1. A typical run

Time (min.)	Absorbance (A)	1+logA
0.0	0.693	0.8407
10.0	0.652	0.8142
20.0	0.604	0.7810
30.0	0.553	0.7427
40.0	0.519	0.7152
50.0	0.493	0.6928
60.0	0.543	0.7348
70.0	0.505	0.7033
80.0	0.470	0.6721
90.0	0.418	0.6212
Rate constant (k) with CdS = $6.91 \times 10^{-5} \text{ sec}^{-1}$		
Rate constant (k) with ZnS = $4.11 \times 10^{-5} \text{ sec}^{-1}$		
Rate constant (k) with CdS-ZnS = $8.91 \times 10^{-5} \text{ sec}^{-1}$		

[Evan's blue] = 1.3×10^{-5} M; amount of composite = 0.12 g; pH = 5.5; light intensity = 50.0 mW cm^{-2}

Effect of pH

It has been observed that the rate of photocatalytic degradation of Evan's blue increases with increase in pH up to 5.5. Further increase in pH above 5.5 resulted in a decrease in the rate of reaction.

An electron from conduction band is abstracted by dissolved oxygen to generate $\text{O}_2^{\cdot-}$. This anion radical is unstable in acidic medium and will form HO_2^{\cdot} radical by reacting with protons of the medium. An increase in the rate of photocatalytic degradation of dye with the increase in pH may be due to the availability of more HO_2^{\cdot} radicals. A decrease in the rate of photocatalytic degradation of the dye may be due to the fact that Evan's blue is present in its anionic form, which will experience a force of repulsion with the negatively charged surface of the semiconductor due to absorption of more OH^- ions on the surface of the photocatalyst.

Table 2. Effect of pH

pH	Rate constant, $k \times 10^5 \text{ s}^{-1}$
5.0	7.12
5.5	8.90
6.0	7.10
6.5	5.68
7.0	4.02
7.5	3.33
8.0	2.59
8.5	2.31
9.0	2.00
9.5	1.2

[Evan's blue] = 1.3×10^{-5} M; amount of composite = 0.12 g; light intensity = 50.0 mW cm^{-2}

Effect of dye concentration

The effect of dye concentration on the photocatalytic degradation of Evan's Blue was observed in the range of 0.7×10^{-5} to 2.1×10^{-5} M and results are reported in Table 3. As the concentration of the dye was increased, it was observed that the dye degradation increases but after 1.3×10^{-5} M (optimum condition), the efficiency of the photocatalytic degradation showed a declining behavior. Here, the dye will start acting as an internal filter and it will not allow the desired light intensity to reach the surface of the semiconductor present at the bottom of the reaction vessel.

Table 3. Effect of dye concentration

[Evan's Blue] $\times 10^5 \text{ M}$	Rate constant, $k \times 10^5 \text{ s}^{-1}$
0.7	3.30
0.9	5.09
1.1	6.72
1.3	8.90
1.5	7.61
1.7	6.38
1.9	5.32
2.1	4.40

Amount of composite = 0.12 g; pH = 5.5; Light intensity = 50.0 mW cm^{-2}

Effect of amount of composite

The amount of semiconductor is also likely to affect the degradation of dye and therefore, different amounts of semiconductor were used. The results are reported in Table 4. When the semiconductor amount was kept low, the rate of degradation of dye was also less. It was observed that as the amount of photocatalyst was increased, the rate of photocatalytic activity increases. The rate of degradation was optimum at 0.12 g of the semiconductor. Beyond 0.12 g, the rate constant decreases slightly. Because after this value, an increase in the amount of photocatalyst will only increase the thickness of the photocatalyst layer and not the exposed the surface area. This was confirmed by taking reaction vessels of different dimensions. This slight decline may be due to the fact that excessive amount of photocatalyst may create hindrance and blocks light penetration.

Table 4. Effect of composite photocatalyst

Amount of composite (g)	Rate constant, $k \times 10^5 \text{ s}^{-1}$
0.02	3.90
0.04	4.87
0.06	5.91
0.08	6.82
0.10	7.38
0.12	8.90
0.14	7.70
0.16	6.92

[Evan's blue] = 1.3×10^{-5} M; pH = 5.5; light intensity = 50.0 mWcm^{-2}

Effect of light intensity

The distance between the light source and exposed surface area of photocatalyst was varied to determine the effect of light intensity on the photocatalytic degradation of Evan's blue. The results are summarized in Table 5. The results show that photocatalytic degradation of Evan's blue was more on increasing the intensity of light as this increases the number of photons striking per unit area of photocatalyst surface per unit time. The maximum rate was observed at 50.0 mW cm^{-2} for degradation of Evan's blue. On further increasing the intensity above 50.0 mWcm^{-2} , there was a slight decrease in the rate of photodegradation. This may be due to some thermal effects or side reactions.

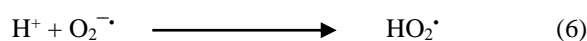
Table 5. Effect of light intensity

Light intensity (mW cm^{-2})	Rate constant, $k \times 10^5 \text{ s}^{-1}$
20.0	5.98
30.0	7.12
40.0	7.93
50.0	8.90
60.0	7.99
70.0	7.21

[Evan's blue] = 1.3×10^{-5} M; amount of composite = 0.12 g; pH = 5.5

Mechanism

On the basis of all these observations, a tentative mechanism for degradation of dye is proposed as:



Evan's blue dye (EB) absorbs suitable wavelength and gives its first excited singlet state. Then it undergoes intersystem crossing (ISC) to give the triplet state of the dye. On the other hand, the semiconducting composite CdS-ZnS also uses the radiant energy to excite its electron from valence band to the conduction band. This electron will be abstracted by oxygen molecule (dissolved oxygen) generating superoxide anion radical ($\text{O}_2^{\cdot -}$). This anion radical will be converted to HO_2^{\cdot} radical as the medium is acidic, where it is unstable and reacts with H^+ . This HO_2^{\cdot} radical converts the dye to its leuco form, which is degraded in final products. $\cdot\text{OH}$ radical does not participate as an active oxidizing species in this degradation reaction. This was confirmed by the fact that the rate of photodegradation was not affected appreciably by the presence of hydroxyl radical scavenger, isopropanol.

Conclusion

A comparative study has been carried out between the photocatalytic activity of pure CdS, ZnS and their composite. Evan's blue dye has been used as a model system to compare their photocatalytic performances. The rate constants for photocatalytic degradation of Evan's blue using CdS, ZnS and CdS-ZnS were 6.91×10^{-5} , 4.11×10^{-5} and $8.91 \times 10^{-5} \text{ sec}^{-1}$, respectively. These results indicate that the composite CdS-ZnS show better results as compared to CdS and ZnS alone. The observation of present work will explore the use of composites for better photocatalytic performance.

Acknowledgements

One of the authors Taruna Dangi is thankful to Head Department of Chemistry, PAHER University, Udaipur for providing laboratory facilities.

References

- ¹Beydoun, D., Amal, R., Low, G., and McEvoy, S., *Nanopart, J. Res.*, **1999**, *1*, 439–1,458.
- ²Gaya, U. I. and Abdullah, A. H., *J. Photochem. Photobiol., C*, **2008**, *9(1)*, 1-12.
- ³Pan, S. and Liu X., *J. Solid State Chem.*, **2012**, *191*, 51-56. <https://doi.org/10.1016/j.jssc.2012.02.048>
- ⁴Hu, J. S., Ren, L. L., Guo, Y. G., Liang, P. H., Cao and A. M., *Angew. Chem. Int. Ed.*, **2005**, *44*, 1269-1273. <https://doi.org/10.1002/anie.200462057>
- ⁵Yan J., Fang, X. S., Zhang, L. D., Bando, Y., Gautam U. and K., Dierre B., *Nano Lett.*, **2008**, *8*, 2794–2799. <https://doi.org/10.1021/nl801353c>
- ⁶Patil, B. N. and Acharya S. A., *Adv. Mat. Lett.*, **2014**, *5(3)*, 113-116. <https://doi.org/10.5185/amlett.2013.fdm.16>
- ⁷Sharma, M., Jain, T., Singh, S. and Pandey, O. P., *Solar Energy*, **2012**, *86 (1)*, 626–633. <https://doi.org/10.1016/j.solener.2011.11.006>
- ⁸Eyasu, A., Yadav O. P. and Bachheti, R. K., *Int. J. Chem. Tech Res.*, **2013**, *5(4)*, 1452-1461.
- ⁹Gao, X. F., Sun, W. T., Hu, Z. D., Ai, G., Zhang, Y. L., Feng, S., Li, F. and Peng, L.-M., *J. Phys. Chem. C*, **2009**, *113*, 20481-20485. <https://doi.org/10.1021/jp904320d>
- ¹⁰Wu, Y., Tamaki, T., Volotinen, T., Belova L., and Rao, K. V., *J. Phys. Chem. Lett.*, **2010**, *1*, 89-92. <https://doi.org/10.1021/jz900008y>
- ¹¹Xu, F., Volkov, V., Zhu, Y., Bai, H. Y., Rea, A., Valappil, N. V., Su, W., Gao, X., Kuskovsky, I. L. and Matsui, H., *J. Phys. Chem. C*, **2009**, *113*, 19419-19423. <https://doi.org/10.1021/jp903813h>
- ¹²Ahluwalia, S., Prakash, N. T., Prakash, R. and Pal, B., *Chem. Eng. J.*, **2016**, *306*, 1041–1048. <https://doi.org/10.1016/j.cej.2016.08.028>
- ¹³Soltani, N., Saion, E., Hussein, M. Z., Erfani, M., Abedini, A., Bahmanrokh G., Bahmanrokh, G., Manizheh, N. and Vaziri, P., *Int. J. Mol. Sci.*, **2012**, *13(10)*, 12242-12258. <https://doi.org/10.3390/ijms131012242>
- ¹⁴Liu, S. Li H. and Yan, L., *Mat. Res. Bull.*, **2013**, *48(9)*, 3328–3334. <https://doi.org/10.1016/j.materresbull.2013.05.055>
- ¹⁵Ivetic, T. B., Fincur, N. L., Dacanin, L. R., Abramovic, B. F. and Lukic-Petrovic, S.R., *Mater. Res. Bull.*, **2015**, *62*, 114-121. <https://doi.org/10.1016/j.materresbull.2014.11.001>

Received: 27.05.2017.

Accepted: 07.07.2017.